

**POLYMERIC TEMPLATING AND ALIGNMENT  
OF FULLERENES**

A Dissertation  
Presented to  
The Academic Faculty

by

Matthew Ryan Kincer

In Partial Fulfillment  
of the Requirements for the Degree  
Doctor of Philosophy in the  
School of Materials Science and Engineering

Georgia Institute of Technology  
December 2011

Copyright 2011 by Matthew R. Kincer

**POLYMERIC TEMPLATING AND ALIGNMENT  
OF FULLERENES**

Approved by:

Dr. Haskell W. Beckham, Advisor  
School of Material Science and  
Engineering  
*Georgia Institute of Technology*

Dr. David G. Bucknall  
School of Material Science and  
Engineering  
*Georgia Institute of Technology*

Dr. Mohan Srinivasarao  
School of Material Science and  
Engineering  
*Georgia Institute of Technology*

Dr. Yonathan Thio  
School of Material Science and  
Engineering  
*Georgia Institute of Technology*

Dr. Andrew Lyon  
School of Chemistry and Biochemistry  
*Georgia Institute of Technology*

Date Approved: Nov. 3<sup>rd</sup>, 2011

This work is dedicated to my parents, who have always supported me in every endeavor.

Without your love and support, I would not be the man I am today.

## ACKNOWLEDGEMENTS

I am very thankful for the academic support that I have received during my studies at Georgia Tech. My advisor, Dr. Haskell Beckham has been the key behind my development as a scientific researcher and I am very appreciative of all the support, guidance, and criticisms he has provided me through the years.

I would also like to thank my fellow lab mates in the Beckham Research Lab who have provided great friendships. Drs. Sunghyun Nam, Marcus Foston, and Chris Hubbell helped me get started in my studies here at Tech and I am thankful for the time they provided in helping me get situated. I would also like to thank Dr. Bo Xu, Ipek Yucelen, and Doh-Yeon Park for being there to provide assistance and fellowship during the final years of my studies. I have also been fortunate in receiving research assistance from Melissa Wilson, Brandon Lewis, and Amanda Nummy who served as undergraduate researchers and Tommy Giordano who worked with me as part of a high school internship. I am very thankful for their time devoted to some of the tedious studies that corresponded to the work contained within this thesis.

I would also like to thank Dr. David Bucknall for his role as unofficial co-adviser on my project. He has provided countless discussions and advice aiding my research efforts. Those who also provided fruitful discussions were my other committee members, Drs. Mohan Srinivasarao, Yonathan Thio, and Andrew Lyon, of whom I am very thankful for their time and thoughts.

I am also very gracious of the individuals who have helped analyze my materials with techniques of which I needed assistance. I want to thank Dr. Fernandez-Nieves and John Hyatt for their help and discussions with the light scattering and viscometry

measurements. I am thankful for Drs. Johannes Leisen and Rudra Choudhury for their expertise in running the solid-state NMR on my fullerene:PMMA complex materials. I would also like to thank Drs. Bilge Gurun, Katie Campbell, and David Bucknall for their work on the scattering measurements of my materials. I am grateful for training and friendship of Michael Kempf who visited our lab to help setup the anionic polymerization techniques.

I would also like to thank the people at Everlube Products in Peachtree City, GA, especially Charles Beall and Lenny Fultz, for allowing me to work as a student intern during my years at Georgia Tech. This has allowed me to learn the industrial side of the research work which will better enable me to make career choices in the future.

Without the laughter and friendship I received from numerous people within my life during the past few years I believe getting through my studies here at Tech would have been unbearable. I am very thankful for the friendships I have developed with those I have become close to in MSE. I would particularly like to thank Michelle Schlea whom not only helped me with capturing the SEM images but has only become my closest friend during my time here at Tech. I will always be grateful for the support she has provided and I look forward to what the future has in store for our relationship.

Lastly, I would like to thank my loving family who has always been my biggest supporters in all my endeavors. Without the love and care from my parents, I would not be in the position I am today. I will be forever indebted to them for being there whenever I needed them in my life.

# TABLE OF CONTENTS

	Page
ACKNOWLEDGEMENTS	iv
LIST OF TABLES	ix
LIST OF FIGURES	x
LIST OF SYMBOLS AND ABBREVIATIONS	xv
SUMMARY	xvii
 <u>CHAPTER</u>	
1 INTRODUCTION	1
2 BACKGROUND	
2.1 Introduction to Fullerenes	4
2.1.1 Formation and Isolation of Buckyballs	4
2.1.2 Structure of Fullerenes	6
2.1.3 Chemical Properties	7
2.1.4 Physical Properties	9
2.1.5 Endohedral Fullerenes	10
2.2 Potential Applications for Aligned Fullerenes	13
2.2.1 Quantum Computing	13
2.2.2 Photovoltaic Devices	15
2.3 Previous Methods of Templating Fullerenes	16
2.3.1 Fullerene Polymers	16
2.3.2 Carbon Nanotubes	17
2.3.3 Liquid Crystalline Systems	19
3 ELECTROSPINNING OF FULLERENE ENCAPSULATED FIBERS	
3.1 Introduction	20
3.1.1 Pendant Fullerenes Attached to Helix	20
3.1.2 Encapsulation of Fullerenes in Helix	22
3.2 Materials	24
3.3 Experimental	25
3.3.1 Synthetic Procedures	25
3.3.2 Processing Conditions	27
3.3.2.1 Polymer Solution Parameters	28
3.3.2.2 Process Parameters	30

3.3.2.3 Aligned Fibers	31
3.3.3 Instrumentation	34
3.4 Results and Discussion	36
3.5 Conclusions	46
4 SUPRAMOLCULAR FULLERENE:CYCLODEXTRIN COMPLEX	
4.1 Introduction	47
4.2 Materials	55
4.3 Experimental	55
4.3.1 Synthetic Procedures	55
4.3.2 Instrumentation	57
4.4 Results and Discussion	58
4.5 Conclusions	66
5 SYNTHESIS AND INCLUSION OF FULLERENE STARS INTO A POLYMER MATIX	
5.1 Introduction	67
5.2 Materials	70
5.3 Experimental	71
5.3.1 Synthetic Procedures	71
5.3.2 Instrumentation	72
5.4 Results and Discussion	74
5.5 Conclusions	89
6 ESR STUDIES ON ENDOHEDRAL FULLERENES USING TEMPLATING METHODS	
6.1 Introduction	90
6.2 Materials	92
6.3 Experimental	92
6.3.1 Synthetic Procedures	92
6.3.2 Instrumentation	95
6.4 Results and Discussion	95
6.5 Conclusions	102
7 CONCLUSIONS AND FUTURE WORK	
7.1 Conclusions	103
7.1.1 Electrospinning of Fullerene Encapsulated Fibers	103
7.1.2 Supramolecular Fullerene:Cyclodextrin Complex	104
7.1.3 Synthesis and Inclusion of Fullerene Stars into a Polymer Matrix	105
7.1.4 ESR Studies on Endohedral Fullerenes Using Templating Methods	106
7.2 Recommendations for Future Work	107
7.2.1 Electrospinning of Fullerene Encapsulated Fibers	107
7.2.2 Supramolecular Fullerene:Cyclodextrin Complex	107

7.2.3 Synthesis and Inclusion of Fullerene Stars into a Polymer Matrix	108
7.1.4 ESR Studies on Endohedral Fullerenes Using Templating Methods	109
APPENDIX A: s-PMMA:Fullerene Complex Calculations	110
APPENDIX B: <sup>1</sup> H NMR Spectra of Cyclodextrin Intermediates	114
APPENDIX C: Mass Spectra of Cyclodextrin Intermediates	116
APPENDIX D: Experimental Use of Different Gauge Needles During Electrospinning	119
APPENDIX E: Dilute Solution Viscometry of Cyclodextrin:Fullerene Complex during Formation	121
APPENDIX F: Calculation of Fullerene Stars R <sub>g</sub> 's	122
APPENDIX G: Diffusion NMR of Fullerene Stars	123
APPENDIX H: Further Light Scattering Analysis of Fullerene Stars	125
REFERENCES	130

## LIST OF TABLES

	Page
Table 2.1: Solubility of C <sub>60</sub> and C <sub>70</sub> in various solvents. The shaded boxes indicate solvents used in experiments in this dissertation [24-27].	9
Table 2.2: Periodic table with shading around elements that have been experimentally shown to be included within a fullerene cage. As noted with the green shading, the work in this dissertation involves endohedral fullerenes containing a nitrogen atom [45].	12
Table 3.1: Constants for various solvents with the solvents used in the experimental procedure shaded [102, 103].	31
Table 4.1: Association constants of host molecules interacting with C <sub>60</sub> . The shaded β-CD is the molecule chosen for studies.	50
Table 4.2: Dilute solution viscometry data showing drastic increase in the flow of the complex solution through a capillary.	65
Table 5.1: Neutron reflectivity ideal scattering length densities (SLD) for relevant compounds.	77
Table 5.2: Characterization data of the fullerene stars synthesized.	80
Table E1: Dilute solution viscometry data from two-solvent mixture studies.	121

## LIST OF FIGURES

	Page
Figure 2.1: Illustration of the various fullerene molecules structure including C <sub>60</sub> (a), C <sub>70</sub> (b), and C <sub>84</sub> (c).	4
Figure 2.2: Schematic diagram of the conventionally used extraction process of fullerenes from the carbon soot produced from the arc discharge.	6
Figure 2.3: Proposed structure for a solid-state spin quantum computer based on linear chains of endohedral fullerenes.	15
Figure 2.4: Different types of polymeric C <sub>60</sub> derivatives: (a) main-chain fullerene polymer; (b) immobilization of fullerenes on solid surface; (c) star-shaped fullerene polymers; (d) fullerene-end-capped polymers; (e) crosslinked polymeric fullerene derivatives; (f) side-chain fullerene polymers; (g) fullerodendrimer.	17
Figure 2.5: Carbon nanotubes provide excellent host for encapsulation of fullerene molecules creating a 1-D tube of aligned molecules.	18
Figure 3.1: Illustration of the encapsulation of free C <sub>60</sub> within helix of s-PMMA forming unaligned gel. The gel can then be processed by electrospinning the solution resulting in aligned fibers.	24
Figure 3.2: Electrospinning setup containing heated jacket for syringe and needle which is needed in order to keep solution above gelling point during electrospinning process. Split electrode collection plates provide uniaxially aligned fibers across gap allowing for method to align fibers.	29
Figure 3.3: Split electrode collector plates which induce the fibers to align within the void.	35
Figure 3.4: Comb designed collector plate increases the amount of obtained aligned fibers.	36
Figure 3.5: SANS of s-PMMA:C <sub>60</sub> gel at various temperatures. A solution of s-PMMA:C <sub>60</sub> was mixed together at elevated temperatures and the scattering behavior was analyzed as the solution cooled. The transition between 71 and 63°C can be attributed the gelation of the solution.	39

Figure 3.6:	SEM images of fullerene encapsulated s-PMMA electrospun fibers including a) randomly aligned fibers, b) uniaxially aligned fibers, c) fibers collected with porous surface, and d) fibers with varying diameters due to bead formation.	40
Figure 3.7:	DSC curves of s-PMMA powder and electrospun fibers which shows $T_g$ and melting transitions. The s-PMMA powder shows a characteristic $T_g$ at 130°C and no melting transition. When the s-PMMA is electrospun a new melting transition around 120°C is seen due to the induced chain orientation achieved during the process. An additional melting transition around that begins at 180°C is seen when $C_{60}$ is added to the s-PMMA and electrospinning is used to orient the fibers. As expected, the fiber orientation and inclusion complex is broken down once the sample is heated above 250°C as shown in the second heating of the fibers.	42
Figure 3.8:	1D averaged WAXS diffraction pattern from sPMMA+ $C_{60}$ radially averaged over all azimuthal angles. Inset shows the raw 2D scattering data, clearly showing the high degree of anisotropy and therefore alignment of the fibers.	43
Figure 3.9:	Plot of the azimuthal angle data obtained from the $2\theta = 25^\circ$ peak (open circles) with fit using the Hermann's orientation equations.	45
Figure 3.10:	(1) The full CP/MAS spectra of (a) the physical mixture of s-PMMA and $C_{60}$ (b) unwashed gel of s-PMMA- $C_{60}$ and (c) s-PMMA- $C_{60}$ fiber. (2) The enlarge region (142.5 – 145.5 ppm) of the respective spectrum, where the resonance responsible for fullerenes is observed. The spinning side bands are marked with *.	46
Figure 4.1:	Absorbance data plotted with use of Benesi-Hildebrand equation.	53
Figure 4.2:	Synthetic procedure used to make bis- $\beta$ -cyclodextrin used in supramolecular studies.	56
Figure 4.3:	Addition of fullerene to bis- $\beta$ -cyclodextrin results in supramolecular complex formation.	57
Figure 4.4:	Mass spectrum of the $\beta$ -CD dimer.	62
Figure 4.5:	$^1H$ NMR spectrum of the $\beta$ -CD dimer.	63
Figure 4.6:	Evident color changes in $C_{60}$ /bis- $\beta$ -cyclodextrin solution over time.	64
Figure 4.7:	Dynamic light scattering of the $\beta$ -CD dimer: $C_{60}$ complex.	66

Figure 4.8	TEM images of the $\beta$ -CD dimer. Image a) shows the clustering occurring between the particles while image b) taken at higher magnification shows the relative uniformity of the size of the particles forming the clusters. Image c) shows a cartoon of the proposed association occurring between the $\beta$ -CD dimer molecules resulting in the formation of the aggregates.	67
Figure 4.9:	TEM images of the $\beta$ -CD dimer: $C_{60}$ complex. Image a) shows the high degree of variation in the length of the fibers formed while image b) shows the relative uniformity of the width maintained throughout the length of a fiber. Image c) shows cartoon of the potential inclusion complex formation and potential bundling of chains.	68
Figure 5.1:	Fullerene stars with number of polystyrene chains grafted X, from 1-6	71
Figure 5.2:	Increased incorporation of fullerene molecules within the cylindrical phase due to polymeric grafts.	73
Figure 5.3:	GPC chromatograms showing retention differences seen between the 6.5 kg/mol PS and 40 kg/mol $C_{60}$ star.	78
Figure 5.4:	GPC chromatograms showing retention differences between the 1.8 kg/mol PS and 12 kg/mol $C_{60}$ star.	79
Figure 5.5:	GPC chromatograms showing retention differences between the 0.8 kg/mol PS and 5.5 kg/mol $C_{60}$ star. Due to the close MW of the parent PS and the fullerene star, complete removal of the unreacted PS was not achieved.	79
Figure 5.6:	$^{13}C$ NMR of the 12 kg/mol $C_{60}PS_6$ stars	81
Figure 5.7:	$^{13}C$ NMR of the 5.5 kg/mol $C_{60}PS_6$ star.	82
Figure 5.8:	HSQC of the 5.5 kg/mol $C_{60}PS_6$ star.	83
Figure 5.9:	Glass transition temperature comparison between PS standards(●) and $C_{60}PS_6$ stars. The $C_{60}PS_6$ stars were plotted twice according to their single-arm $M_n$ (▲) and total $M_n$ (■) of the star.	84
Figure 5.10:	Dynamic light scattering results of the 40 kg/mol $C_{60}PS_6$ stars after dialysis.	86
Figure 5.11:	Wide angle x-ray scattering results for the 12 kg/mol $C_{60}PS_6$ star blended with linear PS.	87

Figure 5.12: Reflectivity profiles for dPS-PMMA films. The concentration was varied with respect to the dPS block for a.) 12 kg/mol and b.) 40 kg/mol fullerene star.	89
Figure 5.13: NR Profile of the 3 wt% C <sub>60</sub> PS <sub>6</sub> 2 film including a modeled fit that determined the SLD profile as shown in the inset.	90
Figure 5.14: Illustration of the structure of the thin films at a.) lower star concentration and b.) high concentrations.	91
Figure 5.15: SLD profile using model fit for 17 wt% C <sub>60</sub> PS <sub>6</sub> in dPS-PMMA. The dips in SLD are due to the formation of layers of fullerene stars within the dPS layer.	92
Figure 6.1: ESR spectrum of pure <sup>14</sup> N@C <sub>60</sub> dissolved in toluene.	99
Figure 6.2: GPC of the N@C <sub>60</sub> product after attachment of PS arms to cage.	100
Figure 6.3: Method of maintaining the alignment achieved by a) collecting the electrospun fibers on a piece of tape and b) rolling up the tape and orienting the sample with respect to the magnetic field.	101
Figure 6.4: ESR spectrum of s-PMMA electrospun fibers containing <sup>14</sup> N@C <sub>60</sub> vertically aligned within quartz tube.	102
Figure 6.5: ESR spectrum of s-PMMA electrospun fibers containing <sup>14</sup> N@C <sub>60</sub> horizontally aligned within quartz tube.	103
Figure 6.6: ESR spectrum of s-PMMA electrospun fibers containing <sup>14</sup> N@C <sub>70</sub> vertically aligned within quartz tube.	104
Figure B1: <sup>1</sup> H NMR of mono-tos-β-CD.	114
Figure B2: <sup>1</sup> H NMR of mono-amino-β-CD.	115
Figure C1: Mass spectrum of β-CD.	116
Figure C2: Mass spectrum of mono-tos-β-CD.	117
Figure C3: Mass spectrum of mono-amino-β-CD.	118
Figure G1: Diffusion coefficients of PS standards (●) and fullerene stars (■).	124
Figure H1: Dynamic light scattering of 12 kg/mol fullerene star in THF.	126
Figure H2: Dynamic light scattering of 5.5 kg/mol fullerene star in THF.	127
Figure H3: Hydrodynamic radius analysis obtained from CONTIN analysis of light scattering data.	128

Figure H4: Polydispersity analysis obtained from CONTIN analysis of light scattering data.

129

## LIST OF SYMBOLS AND ABBREVIATIONS

$\alpha$ -CD	alpha-cyclodextrin
$\beta$ -CD	beta-cyclodextrin
C <sub>60</sub>	[60]fullerene
C <sub>70</sub>	[70]fullerene
C <sub>84</sub>	[84]fullerene
CP	cross polarization
D	diffusion coefficient
DCB	dichlorobenzene
DMF	dimethylformamide
DSC	differential scanning calorimeter
ESR	electron spin resonance
F	Hermann's orientation factor
FWHM	full width at half maximum
$\gamma$ -CD	gamma-cyclodextrin
GPC	gel permeation chromatography
HSQC	heteronuclear single quantum coherence
I <sub>h</sub>	icosahedron
i-PMMA	isotactic poly(methyl methacrylate)
K <sub>a</sub>	association constant
MAS	magic angle spinning
NMR	nuclear magnetic resonance
PI	poly(isoprene)
ppm	parts per million

PS	poly(styrene)
$R_g$	radius of gyration
$R_h$	hydrodynamic radius
RT	room temperature
SEM	scanning electron microscopy
s-PMMA	syndiotactic poly(methyl methacrylate)
TEM	transmission electron microscopy
$T_g$	glass transition temperature
THF	tetrahydrofuran
WAXS	wide angle x-ray scattering

## SUMMARY

Fullerene research has advanced to elevated levels in a short period of time due to the unique chemical and physical properties of the caged molecule that have been utilized in numerous applications. Due to the spherical shape of the fullerene molecule which allows for a hollow cavity, encapsulation of atoms or small molecules can occur within the ball structure. This encapsulation creates an endohedral component that is limited from interacting with other molecules which creates potential of control over electronic information of the isolated molecule. Endohedral fullerenes have the potential as serving as the base unit in a quantum computer if control over global alignment is attained. Thus, by using the inherent self-assembling capabilities of some organic materials, ordered endohedral fullerenes can be achieved. This dissertation investigates the ability to use self-assembling strategies to obtain alignment which include ordering within a morphologically controlled copolymer matrix, forming a supramolecular polymer complex with cyclodextrin, and encapsulation within the helical wrap of polymer chains. The ultimate goal is to understand the dynamics that control association and orientation of varying fullerene-based molecules in each strategy in order to maximize control over the final alignment of endohedral elements.

# CHAPTER 1

## INTRODUCTION

Studies in nanotechnology can be simply described as understanding and controlling behavior of a material down to the nano-scale. Improvements in research and technology have allowed for many obstacles and limitations to be overcome when tailoring performance of materials at the molecular level. These advancements and future possibilities have led nanotechnology to being a major driving force in research. Computing is one area of research where design and optimization of a material at the nano-level is needed in order to induce quantum behavior. Fullerenes are one molecule that has been proposed as being an ideal molecule to serve as the base unit in a quantum computing. The work in this dissertation can be grouped into three main strategies for developing fullerene based molecules:

- Using helical forming s-PMMA to encapsulate fullerenes and use electrospinning to direct the orientation.
- Investigation into the supramolecular polymer formation of fullerenes with ditopic cyclodextrin.
- Determination of the increased solubility and alignment of fullerenes into a co-polymer matrix by grafting addition of polymer arms onto the cage.

In Chapter 2, a background on fullerenes is given including discussion on previous methods of templating buckyballs and potential uses for these unique molecules. Also introduced, are endohedral fullerenes and the opportunity these molecules possess in

advancing the quantum computer research efforts. A brief introduction is given to quantum computing in order to obtain restrictions and guidelines for design of the endohedral fullerene.

In Chapter 3, the first aligning approach of using s-PMMA as the host matrix is described. This method offers similar results as the alignment of fullerenes within carbon nanotubes. However, the destructive methods used to load the fullerenes within the carbon nanotubes are not needed when using the helical forming s-PMMA. Once the complex between the fullerene and the polymer is formed, electrospinning is performed in order to drive orientation of the polymer chains. The spectroscopic results are then discussed, detailing the achieved alignment of the fullerenes within the fibers.

Chapter 4 discusses the results of investigating the supramolecular complex formed between a cyclodextrin dimer and C<sub>60</sub>. This method involves using the known interaction between the cavity of the cyclodextrin molecule and the C<sub>60</sub> host and forming a polymer chain through use of a ditopic host. The dimeric cyclodextrin host must be synthesized so the reaction details and spectroscopic results are highlighted. Studies of the complex including light scattering, NMR, and TEM are discussed for determination of the resulting structure of the complex.

The third and final strategy to align fullerenes, which involves the grafting of polymer chains onto the cage, is discussed in Chapter 5. This method increases the solubility of the fullerene molecule both in common organic solvents and within a polymer matrix. By increasing the solubility, higher concentrations of fullerenes can be loaded within a co-polymer matrix without inducing aggregation. By tailoring the correct

polymer weight percentages within the matrix, tube morphologies can be produced allowing for control over alignment of the fullerene molecules.

In Chapter 6, the results of studying the ESR signal of the endohedral fullerenes after using one of the aligning strategies is discussed. The first method attempted was using the grafting of PS chains onto the cage as discussed in Chapter 5. ESR results are discussed showing that the chemistry used during this method negatively affected the stability of the nitrogen atom encapsulated within the endohedral fullerenes. The other method discussed in using endohedral fullerenes is the electrospinning of the helical s-PMMA. Effective retention of the ESR signal is maintained concluding that the technique has potential in obtaining a material containing aligned endohedral fullerenes.

The conclusion in Chapter 7 summarizes the results from the different alignment strategies and presents a plan for future work. Appendix A includes the calculations used to determine the filling content of fullerene encapsulated within the helical polymer. Appendix B shows the NMR spectra of the starting materials and intermediate products while synthesizing the  $\beta$ -cyclodextrin dimer. Appendix C shows the mass spectra of the  $\beta$ -cyclodextrin intermediate products that are discussed in Chapter 4. Appendix D shows the calculations of the  $R_g$  values of the  $C_{60}$ -PS<sub>6</sub> stars discussed in Chapter 5.

## CHAPTER 2

### BACKGROUND

#### 2.1 Introduction to Fullerenes

Fullerenes are a family of molecules composed entirely of carbon atoms that form a 3-dimensional shape including spheres, ellipsoids, and tubes. Although the term fullerene is most often associated with buckyballs, carbon nanotubes and nano-onions are also fundamentally included in the fullerene family. In the work associated within this dissertation, the term fullerene will be used to describe the spherical carbon molecules known as buckyballs. The [60]fullerene and [70]fullerene molecules, more commonly abbreviated as  $C_{60}$  and  $C_{70}$ , are the two most stable buckyballs and the structure of these fullerenes are shown in Figure 2.1. The number in the subscript refers to the number of carbon atoms contained in the spherical molecule.

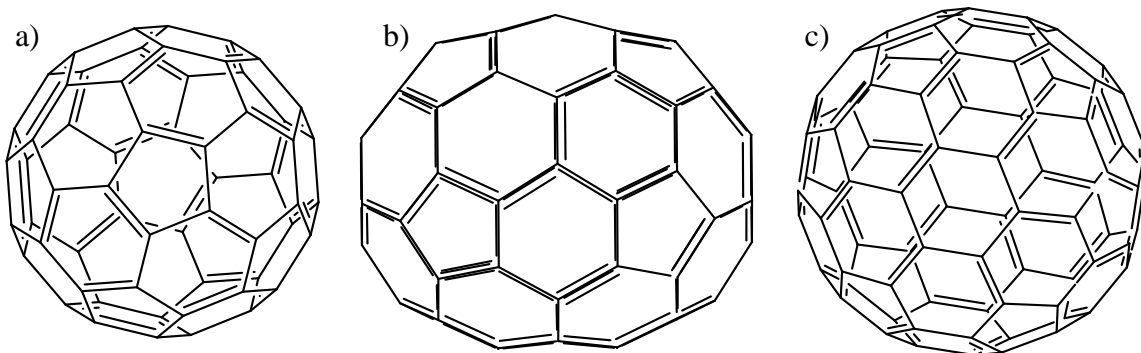


**Figure 2.1:** Illustration of the various fullerene molecules structure including the spherical  $C_{60}$  (a), ellipsoidal  $C_{70}$  (b), and  $C_{84}$  (c).

#### 2.1.2 Formation and Isolation of Buckyballs

The discovery of the spherical, crystalline structure that carbon forms earned Kroto *et al.* [1] the Nobel Prize in Chemistry in 1996. This discovery has produced new

research opportunities involving fullerenes. Since the initial discovery in 1985, there have been significant improvements in the production of fullerene molecules, including the commonly used Huffman-Kratschmer method, which has led to increases in synthetic yield allowing for large scale production [2]. Fullerenes are formed from carbon rods that are stacked closely together in a high pressure helium gas atmosphere [3]. When the rods are heated above 2000°C and a voltage is applied, the electric current produces carbon soot in the arc discharge that contains unpurified fullerene molecules. Numerous variations in reactor design have resulted in the ability to form hundreds of grams of fullerenes from one arc-discharge apparatus during one day of operation [4].

Fullerene molecules are solvent extracted from the produced carbon soot in low yields of ~15%; however, since graphite is the only byproduct in the soot, recycling of the waste product helps minimize production costs [5]. The C<sub>60</sub> and C<sub>70</sub> are the two most highly yielded cages that are produced by the arc-discharge method as the recovered product is composed of 75% and 24%, respectively, of the fullerene molecules. The increased availability of fullerenes has led to enhanced research studies involving the spherical molecules, which has resulted in the use of fullerene molecules in numerous applications and innovations that are further discussed in section 2.3 of this chapter [6-8].

Once the carbon soot is produced, the fullerenes are commonly isolated by column chromatography using Elorit carbon as the stationary phase, which shows retention of the varying sizes of the caged molecule [9]. By elution of the fullerenes in various solvents, the C<sub>60</sub> and C<sub>70</sub> molecules can be separated from each other and the remainder of the fullerene soot. However, since fullerenes still require a detailed purification method in order to isolate the different sizes of molecules, this has kept costs

of production high and wide-scale commercial use rather low except in applications where the fullerene provides enhanced properties. The details of the extraction and isolation process for recovering fullerenes from the carbon soot are detailed in Figure 2.2.

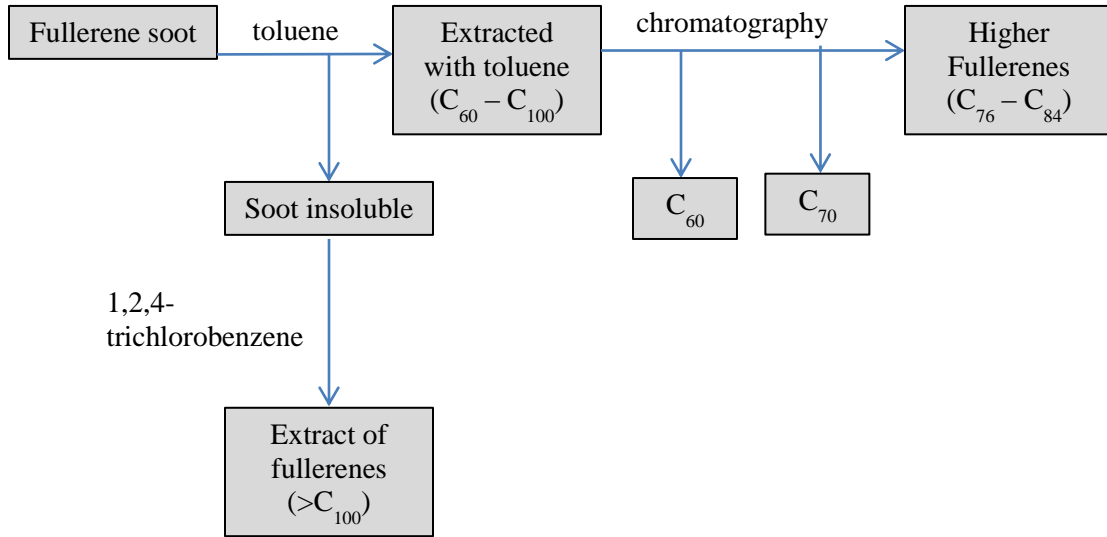


**Figure 2.2:** Schematic diagram of the conventionally used extraction process of fullerenes from the carbon soot produced from the arc discharge.

### 2.1.2 Structure of Fullerenes

The buckyballs are composed of  $2 \times (10 + M)$  carbon atoms that organize into exactly 12 pentagons with  $M$  hexagons [10]. According to Euler's theorem the 12 pentagons are required in order to form the closure of the carbon network, because the pentagons help stabilize the necessary bending in order to form the spherical shapes. As seen in Figure 2.1,  $C_{60}$  has 20 hexagons and  $C_{70}$  has 25 hexagons and both are constructed in a manner which prevents any two edges of the pentagons from touching. Since all the carbon molecules in the buckyballs are connected to three other carbon atoms, the fullerenes are entirely comprised of  $sp^2$  hybridized carbon atoms,

The shape of the  $C_{60}$  is classified as a truncated icosahedron which is more commonly known to resemble the shape of a soccer ball. The van der Waals diameter of a  $C_{60}$  molecule is about 1.1 nm [11] while the nucleus to nucleus diameter of a  $C_{60}$  molecule is about 0.71 nm. The  $C_{60}$  molecule contains two bond lengths: the 6:6 ring bonds (between two hexagons) can be considered "double bonds" and are shorter than the 6:5 bonds (between a hexagon and a pentagon). Therefore, the average bond lengths in a  $C_{60}$  molecule are 1.38 and 1.45 angstroms [12-14]. However, the larger fullerenes contain lower symmetry, which leads to more variations in the lengths of the bonds between atoms. Research has shown that  $C_{70}$  contains 8 different bond types due to the higher elongated structure [15]. Due to the spherical shape of the buckyballs, these molecules contain a high degree of symmetry. The  $C_{60}$  has an icosahedron shape leading to 120 symmetry point groups making it the most symmetric stable molecule known to exist [16].

### **2.1.3 Chemical Properties**

Since fullerenes were discovered as the "third form of carbon" in 1985, the spherical  $\pi$ -electron containing molecule has been shown to react in with numerous compounds. The extra stability of  $C_{60}$  is attributed to the truncated icosahedron structure that it forms with  $I_h$  symmetry [1]. However, despite the high stability of the molecule to remain unreactive in inert conditions, the fullerenes, in particular  $C_{60}$ , show high reactivity in numerous organic reactions. The  $sp^2$ -hybridized carbon atoms have a high degree of angle strain due to the bending needed to form the closed sphere. The characteristic reaction of buckyballs is electrophilic addition at the carbons in the 6,6-double bonds, which reduces angle strain by changing  $sp^2$ -hybridized carbons into a  $sp^3$ -

hybridization [17]. The change in the hybridized orbitals causes the bond angles to decrease from about  $120^\circ$  in the  $sp^2$  orbitals to about  $109.5^\circ$  in the  $sp^3$  orbitals. This decrease in bond angles allows for the bonds to become more flexible when closing the sphere and, thus, the molecule becomes more stable.

One of the issues when working with fullerenes is that the unreacted buckyballs are sparingly soluble in many solvents. However, fullerenes are the only known allotrope of carbon that can be dissolved in common solvents at room temperature. Some of the most commonly used solvents in fullerene chemistry include aromatic-containing solvents, such as toluene, 1,2-dichlorobenzene, and 1-chloronaphthalene due to their higher degree of interaction with the cage which leads to greater solubility [18, 19]. Table 2.1 lists the solubility of  $C_{60}$  and  $C_{70}$  in commonly used solvents. Fullerenes in the solid state have a dark color much like graphite; however, solutions of pure  $C_{60}$  have a deep purple color while solutions of  $C_{70}$  are a reddish brown. The higher fullerenes  $C_{76}$  to  $C_{84}$  have a variety of colors ranging from blue to yellow [20]. Many of the larger fullerenes like  $C_{76}$  has two optical forms from different structural isomers, which can be separated leading to different color solutions [21]. The diverse colors of fullerenes and their derivatives have led to research of these molecules as light emitting diodes which is discussed later in this chapter. Some fullerene structures such as,  $C_{28}$ ,  $C_{36}$ , and  $C_{50}$ , are not soluble because they have a small band gap between the ground and excited states [22]. Interestingly, the  $C_{72}$  structure is also insoluble, but the endohedral version with a trapped lanthanide-group atom within the cage is soluble due to the interaction of the metal atom and the electronic states of the fullerene [23].

**Table 2.1:** Solubility of C<sub>60</sub> and C<sub>70</sub> in various solvents. The shaded boxes indicate solvents used in experiments in this dissertation [24-27].

Solvent	C <sub>60</sub> Solubility (mg/mL)	C <sub>70</sub> Solubility (mg/mL)	Boiling Point
1-chloronaphthalene	51	-	259 °C
1-methylnaphthalene	33	-	240 °C
1,2-dichlorobenzene	24	36.2	181 °C
carbon disulfide	8	9.875	46 °C
xylene	5	3.985	138 °C
toluene	3	1.406	111 °C
benzene	1.5	1.3	80 °C
cyclohexene	1.2	-	83 °C
carbon tetrachloride	0.4	0.121	77 °C
chloroform	0.25	-	61 °C
n-hexane	0.046	0.013	69 °C
cyclohexane	0.035	0.08	81 °C
tetrahydrofuran	0.006	-	66 °C
acetonitrile	0.004	-	82 °C
methanol	0.00004	-	65 °C
water	1.3x10 <sup>-11</sup>	-	100 °C

### 2.1.4 Physical Properties

The interesting physical properties of fullerenes have garnered numerous research efforts to exploit these properties in materials for applications in nanotechnology. Since each sp<sup>2</sup> carbon atom in the C<sub>60</sub> is bonded covalently to 3 other carbon atoms, these bonds use 7 electrons in the outer shell. This leaves one non-bonded electron that can freely move around the carbon atoms on the cage. However, buckminsterfullerenes do not exhibit superaromaticity where the electrons in the hexagonal rings delocalize over the entire molecule [28]. Superaromaticity of fullerenes can be defined using the three-dimensional analogue of Hückel's rule, which is  $2(N + 1)^2$  with N being any integer [29]. Therefore, fullerenes react as an electron deficient molecule readily reacting with

molecules that have electron rich characteristic. Since electrons can effectively carry charge across the fullerene cage, the conductivity of these molecules is pronounced and is the reason fullerene derivatives have potential as materials for organic photovoltaic cells.

Much like is seen in carbon nanotubes [30], fullerenes exhibit a high degree of mechanical strength [31]. However, unlike the carbon nanotubes that can increase the mechanical strength in materials due to length scales of the nanotubes reaching hundreds of nanometers long, the fullerene does not greatly improve a materials mechanical strength due to its limited size and relatively low self-binding behavior. Fullerenes also possess a high temperature stability as they begin to break down into amorphous carbon particles around 1260°C [32].

In 1999, researchers demonstrated that wave-particle duality applied to large molecules such as  $C_{60}$  [33]. By using the dual slit experiment, the spherical molecule was found to diffract despite having a de Broglie wavelength 400 times smaller than the molecule size. Many aspects of this duality behavior is still not understood. Still today,  $C_{60}$  is considered to be the largest molecule that exhibits this duality of behavior [34].

### **2.1.5 Endohedral Fullerenes**

Due to the spherical shape of the buckyballs, the molecules have a hollow core which has been shown to encapsulate atoms and molecules [35-37]. The diameter of this hollow space ranges from 0.4 to 1.0 nm for fullerenes between the sizes of  $C_{60}$  to  $C_{240}$ . This unique ability to encapsulate other atoms has provided much interest in endohedral fullerenes, especially in the biochemical world. The endohedral fullerenes are described with the notation  $X@C_n$  where X is the trapped atom or molecule inside the cage and n is

the size of the fullerene. For possible biochemical applications, one can imagine the ability to capture a drug in this very stable carbon cage in order to control the delivery time of the drug to the body [38]. Other possibilities proposed have been to place a radioactive tracer in the fullerene in order to safely inject it into the blood stream or use as MRI contrast agents [39, 40]. As discussed later in the applications part of this chapter, endohedral fullerenes are also believed to be a potential molecule that can be used for information storage molecule in a quantum computer [41].

Unfortunately, one of the issues with endohedral fullerenes is the difficulty in the synthesis and purification of these molecules. The endohedral atoms or molecules do not alter the properties of the cage very much making it difficult to differentiate between fullerenes with or without encapsulated atoms. Another issue in the production of endohedral fullerenes is that they have very low yields due to their complex formation. Thus, the isolation and production of large amounts of endohedral fullerenes is quite difficult. The first endohedral fullerenes to be discovered were metallofullerenes like  $\text{La@C}_{82}$  [42]. The formation of these first endohedral fullerenes was achieved by a high-temperature contact arc method. New methods for achieving encapsulation at lower temperatures needed to be developed in order to make nonmetal endohedral fullerenes [43].

The possibility of what fullerenes can hold inside their cage is always growing and Table 2.2 shows the known atoms that have been encapsulated within fullerene molecules. Nonmetals and noble gases are primarily found to exist only in  $\text{C}_{60}$  and  $\text{C}_{70}$  while the larger metallic molecules favor the larger fullerenes. The endohedral fullerene that was used in the research contained within this dissertation was the  $^{14}\text{N@C}_{60}$ . The

main characteristic of N@C<sub>60</sub> is that the encapsulated atom keeps its atomic structure and is inert toward the outside despite being a highly reactive molecule. Nitrogen containing endohedral fullerenes have very long T<sub>1</sub> relaxation times in the solid state [44]. This characteristic has prompted this molecule to be proposed as the base molecule in a quantum computer which is further discussed later in this chapter.

**Table 2.2:** Periodic table with shading around elements that have been experimentally shown to be included within a fullerene cage. As noted with the green shading, the work in this dissertation involves endohedral fullerenes containing a nitrogen atom [45].

I	II	IIIb	IVb	Vb	VIb	VIIb	VIIIb	Ib	IIb	III	IV	V	VI	VII	0		
1	2	3	4	5	6	7	8	9	10	11	12	13	14	15	16	17	18
H																	He
Li	Be										B	C	N	O	F		Ne
Na	Mg										Al	Si	P	S	Cl		Ar
K	Ca	Sc	Ti	V	Cr	Mn	Fe	Co	Ni	Cu	Zn	Ga	Ge	As	Se	Br	Kr
Rb	Sr	Y	Zr	Nb	Mo	Tc	Ru	Rh	Pd	Ag	Cd	In	Sn	Sb	Te	I	Xe
Cs	Ba	La*	Hf	Ta	W	Re	Os	Ir	Pt	Au	Hg	Tl	Pb	Bi	Po	At	Rn
Fr	Ra	Ac**	Rf	Db	Sg	Bh	Hs	Mt	Uun	Uuu	Uub		Uuq		Uuh		
Lanthanides *			Ce	Pr	Nd	Pm	Sm	Eu	Gd	Tb	Dy	Ho	Er	Tm	Yb	Lu	
Actinides **			Th	Pa	U	Np	Pu	Am	Cm	Bk	Cf	Es	Fm	Md	No	Lr	

The temperature dependent stability of the N@C<sub>60</sub> molecule studied using electron spin resonance has been studied in previous research [46]. After ten hours of heating at 140°C, the entire signal from the endohedral fullerene has disappeared confirming the loss of encapsulated nitrogen molecule. At the lower temperature of 80°C, the loss of signal is much slower as half the signal still remains after 50 hours. From these results it can be concluded that materials containing nitrogen endohedral fullerenes must be maintained at low temperatures in order to ensure stability. Also, any methods used to assemble the molecules must be done at low temperatures in order to maintain same concentration of spins.

## **2.2 Potential Applications for Aligned Fullerenes**

Fullerene molecules have been shown to have authentic properties that have been applied in numerous applications [47]. Some of these materials are currently used in society; however, the industrial use of these molecules is much lower than initially proposed soon after their discovery. Many of the fullerene properties are complex to study but allow for potential in areas of science that are still being developed. In this section, a brief discussion is given that includes a few fields of research that offer specific potential in aligned or templated arrays of fullerene molecules. The use of fullerenes can potentially be enhanced in these fields by utilizing the methods developed later in this dissertation.

### **2.2.1 Quantum Computing**

Quantum computing is one such application in which endohedral fullerene molecules are desired in linear arrays that would allow for use as information carriers [48]. Due to the hollow, spherical shape of the fullerene molecules, encapsulation of atoms can occur within the cage, creating an isolated molecule that is fixed to a limited volume. This method of isolation has become of interest in quantum computing research, as control over nanoparticles creates potentially new ways that information can be processed. By isolating a particle inside the fullerene cage, spin quantum effects can be used to dominate control over how the information is stored [41]. Quantum information processing is believed to become a significant area of research since current limitations with classical information processing can be resolved. The size of the information

carriers can be reduced down to the atomic level, which can possibly overcome size limitations currently restricting classical information processing.

The qubit serves as the basic component of a quantum computer and can be comprised of electronic or nucleic spins of the atoms encapsulated within the fullerene cage [41]. Practical solid-state quantum computers have been proposed using nitrogen isotopes as the atom isolated as the endohedral element. It has been shown that  $^{14}\text{N}$  and  $^{15}\text{N}$  encapsulation can be achieved and their electronic spin easily manipulated and controlled [41]. Controlled interaction between the electronic spins of a two qubit system is required to create entanglement. Quantum entanglement involves when the state of a molecule depends upon the properties of other molecules even if there is spatial separation [49]. The entanglements of the quantum information that occur between isolated molecules are due to non-classical correlations. As shown in Figure 2.3, the proposed method of alignment involving a two qubit system involves a fullerene dimer containing atoms with two different controllable spin energies [50]. Quantum computing is one such application in which endohedral fullerene molecules are desired in linear arrays that would allow for use as information carriers [48]. Due to the hollow, spherical shape of the fullerene molecules, encapsulation of atoms can occur within the cage creating an isolated molecule that is fixed to a limited volume. This method of isolation has become of interest in quantum computing research, as control over nanoparticles creates potentially new ways that information can be processed. By isolating a particle inside the fullerene cage, spin quantum effects can be used to dominate control over how the information is stored [41]. Quantum information processing is believed to become a significant area of research since it can resolve issues associated with current limitations

of classical information processing. The size of the information carriers can be reduced down to the atomic level, which can possibly overcome size limitations restricting classical information processing defined by Moore's law [51]. However, for maximum interaction to allow for effective transfer and entanglement of spin information between atoms, alignment of the dimeric endohedral fullerenes must be achieved.

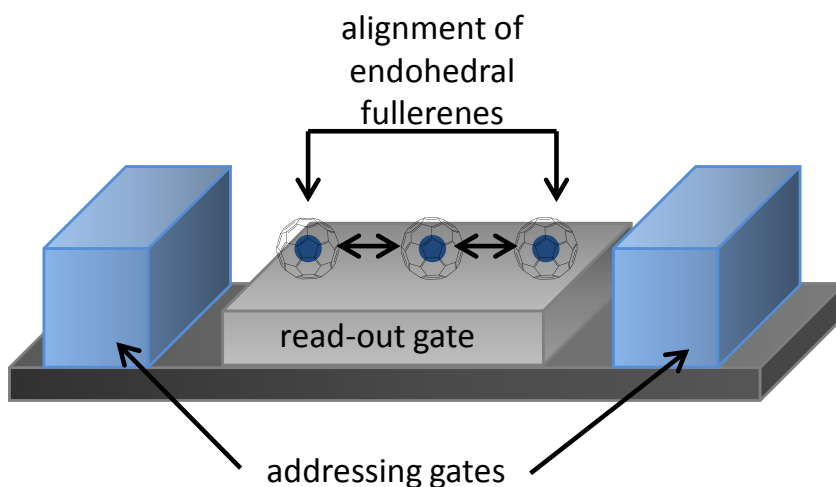


**Figure 2.3:** Proposed structure for a solid-state spin quantum computer based on linear chains of endohedral fullerenes.

### 2.2.2 Photovoltaic Devices

Fullerenes possess interesting electrical properties [52] which has prompted extensive research of these molecules in polymeric solar cells [53-55]. Organic solar cells are a relatively novel technology that is still currently being optimized. The potential in organic solar cells is that they would offer a substantial price reduction and a faster return on investment over currently used thin-film silicon solar cells. Currently, polymer solar cells are built from thin films (typically hundreds of nm) that consist of organic semiconductors including polymers, such as polyphenylene vinylene and small-

molecule compounds like copper phthalocyanine and fullerenes or fullerene derivatives such as phenyl-C61-butyric acid methyl ester, or more commonly known as PCBM [55]. The active region of these fullerene containing polymeric devices consists of two materials, one which acts as an electron donor and the other as an acceptor [56]. Nanostructured layers in the devices can improve performance. Thus by studying methods of organizing fullerenes this area of research can be enhanced.

### **2.3 Previous Methods of Templating Fullerenes**

One important component in many functional materials is global alignment for obtaining maximum control over properties. Fullerene molecules do not have natural self-assembling characteristics that would allow for controlled alignment. However, by incorporating other molecules or by modifying the fullerene cage, potential control over arrangement can be attained. So, by studying the self-assembling alignment of fullerene molecules, many applications can benefit from an understanding of the factors that allow for defined arrangements.

#### **2.3.1 Fullerene Polymers**

Many methods have been developed in order to create aligned polymeric materials. As seen in Figure 2.4, fullerenes have been covalently attached to polymers in many different ways allowing for diverse architecture in resulting structures [57]. By combining these two fields of research, the study aligned polymeric fullerenes can be analyzed [58]. However, the fullerene polymers require covalent linkages which mean

potential use with endohedral elements is very limited due to the high reactivity of the encapsulated atom during most chemical reactions.

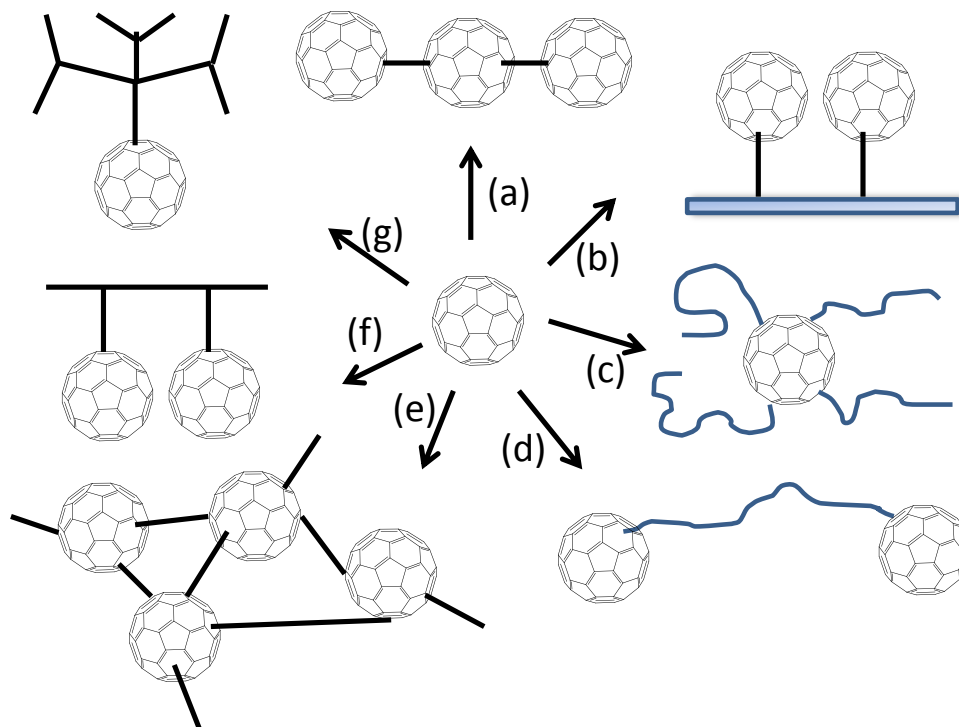


**Figure 2.4:** Different types of polymeric  $C_{60}$  derivatives: (a) main-chain fullerene polymer; (b) immobilization of fullerenes on solid surface; (c) star-shaped fullerene polymers; (d) fullerene-end-capped polymers; (e) crosslinked polymeric fullerene derivatives; (f) side-chain fullerene polymers; (g) fullerodendrimer.

### 2.3.2 Carbon Nanotubes

Previous studies on approaches for templating and aligning of fullerenes include insertion into single-walled carbon nanotubes (SWCNTs). As shown in Figure 2.5, the carbon nanotubes provided a natural one-dimension alignment in which the fullerenes formed a peapod like structure [59, 60].

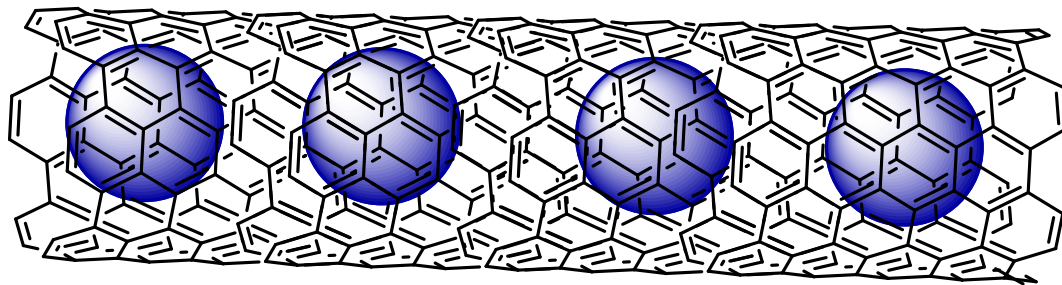


**Figure 2.5:** Carbon nanotubes provide excellent host for encapsulation of fullerene molecules creating a 1-D tube of aligned molecules.

However, despite being a well-defined structure, the SWCNTs are very difficult to process and the fullerenes must be loaded within the tubes using processing conditions that would be detrimental to the stability of endohedral fullerenes [61]. This loading process involves applying heat to sublime the fullerene cage or by use of supercritical fluids [60]. Applying heat is known to negatively affect the stability of endohedral atoms allowing for more atoms to escape the cage [62]. Other problems arise with use of fullerene dimers as they contain chemical bonds that break upon vaporization in the sublimation process. The fullerene dimers also show much lower solubility in supercritical fluids. So other methods of alignment need to be investigated to maintain stability of the endohedral fullerene for quantum computing applications. Also, the very good alignment in CNTs was accompanied by short relaxation times, probably due to strong interaction with the CNT. In order to maintain the extremely long  $T_1$  relaxation times of the  $N@C_{60}$  molecules, the interaction with the aligning matrix needs to be minimized.

### 2.3.3 Liquid Crystalline Systems

Previous research has looked to orient endohedral fullerenes by dissolving them in different liquid crystals (LC) [63, 64]. One of the liquid crystals that showed greatest alignment of fullerenes was 4-methoxybenzylidene-4'-n-butylaniline (MBBA). The achieved orientation was not very good when compared to the carbon nanotube method for alignment. The electron spin resonance spectra of the samples show that the signal from the  $N@C_{60}$  is split into three components suggesting that the symmetry of the fullerene carbon cage is lowered. Studies on the dimer  $N@C_{60}-C_{60}$  does not increase the zero field splitting of the endohedral atom suggesting this molecule does not align like the monomer. In all the samples there was no change or anisotropy of the hyperfine constant. Unlike in the carbon nanotube method, the relaxation of the endohedral atom was not significantly affected probably due to the weak interaction with the LC molecules. However, due to the weak interaction only partial alignment was found which is insufficient for quantum computation.

Currently, there is not a sufficient method developed for aligning endohedral fullerenes to a high degree that ensures the stability of encapsulated atom. The aligning methods discussed in the following chapters try to address this issue. The research involving quantum computers would be greatly enhanced if a method was developed that ordered fullerenes maintaining the integrity of the endohedral element. The key restraints learned from previous methods to align endohedral fullerenes are to limit high temperature exposure and use methods that minimize chemical reactions to the cage of the fullerenes.

## **CHAPTER 3**

### **ELECTROSPINNING OF FULLERENE ENCAPSULATED FIBERS**

#### **3.1 Introduction**

Helical forming materials have been an interesting research area primarily due to important biological entities, such as proteins and nucleic acids. Although much less common in synthetic polymers, the helical molecule provides unique research opportunities due to the stabilized and well-defined structure. Optical activity of the fullerene based materials is an intriguing aspect as addition of the carbon cages to the helical forming polymer induces chiral activity while maintaining the unique electronic properties of the fullerenes [65]. This inclusion of fullerenes onto or within these helical forming materials can potentially offer unique opportunities in organic nanodevices or as optoelectronic materials [24]. This chapter involves encapsulating fullerenes into the s-PMMA helix and aligning the helices using electrospinning. Several characterization techniques were used to identify resulting behavior.

##### **3.1.1 Pendant Fullerenes Attached to Helix**

Recently, research efforts have looked at incorporating fullerene molecules as pendants onto side chains of helical forming polymers by covalent and non-covalent interactions [66-69]. These fullerenes incorporated onto the helical polymers contain excellent mechanical strength and can be easily processed due to the polymer matrix. In the helical conforming polymers, a characteristic induced circular dichroism is expressed when a preferred handedness is formed, which creates interesting optically active polymers. Both covalently and non-covalently linked fullerenes have been attached to

the side groups forming a unique 3-dimensional array of molecules that has been studied for interesting optical and biological applications [70, 71]. However, due to the rotation of the helix, alignment of the fullerenes attached to side groups would not provide uniaxially aligned structures as discussed as the objective in Chapter 2. Another issue with attaching fullerenes as pendants onto the helix is reactivity of the endohedral fullerenes which would limit potential methods of forming covalent bonds to the polymer. The only fullerene molecules that have been attached though non-covalent interactions with the helix have been cationic, which also poses an issue with reactivity with the endohedral element within the cage.

### **3.1.2 Encapsulation of Fullerenes in Helix**

One recent development in the area of incorporating fullerenes with helical forming polymers is the inclusion of the caged molecules within the inner helical space [72]. This alignment approach first developed by Yashima *et al.* involves using syndiotactic poly(methyl methacrylate) (s-PMMA), which forms a thermoreversible, hollow helix in aromatic solvents that acts as a vehicle to deliver a path of alignment. This helix contains 74 repeat units per 4 turns which allows for an internal helix diameter of ~1 nm to be formed [73]. Since  $C_{60}$  has an outer cage diameter of 1.02 nm, the helix cavity contains enough space to encapsulate fullerene molecules which has been shown by Yashima *et al.* As shown in Figure 3.1,  $C_{60}$  complexes with s-PMMA to form 1-dimensional linear arrays or peapods. These supramolecular molecules form an interconnecting network through physical entanglements which is a gel at room temperature. Yashima *et al.* showed that s-PMMA containing 94% syndiotacticity

induces a maximum filling volume of  $C_{60}$  within the helix of 86%. They also showed through X-ray diffraction that the d-spacing increased when larger fullerenes of  $C_{70}$  and  $C_{84}$  were used [72].

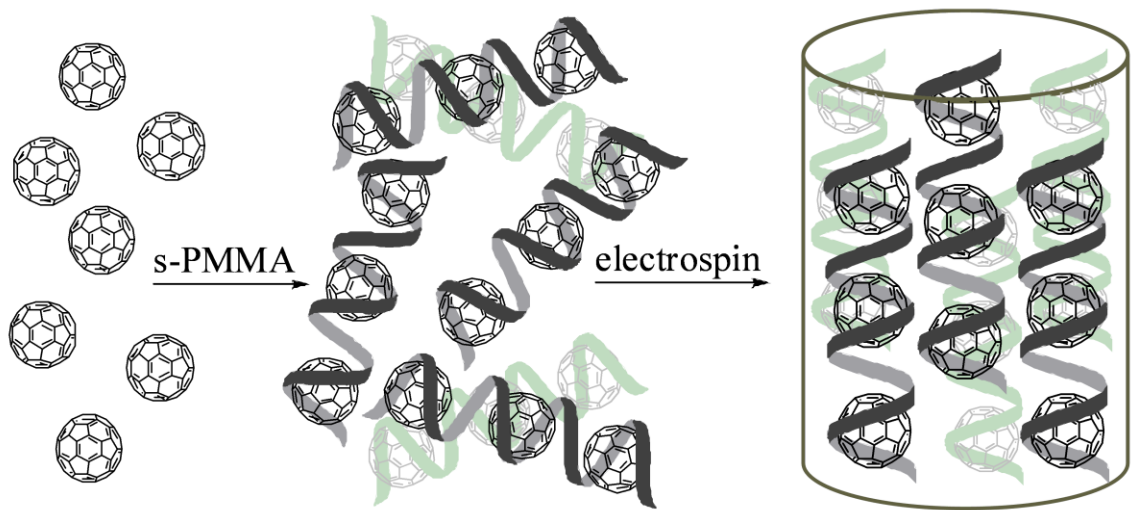


**Figure 3.1:** Illustration of the encapsulation of free  $C_{60}$  within helix of s-PMMA forming unaligned gel. The gel can then be processed by electrospinning the solution resulting in aligned fibers.

The AFM images captured by Yashima *et al.* [72] show stripe like individual bundles of the helices which showed a lateral spacing of 1.9 nm and pitch of 0.9 nm. These values correlated with the proposed model calculations of the energy minimized structure of the complex which resulted with distances of 2.3 nm for the diameter of the helix, 0.947 nm per helical turn, and 1.002 nm between the centers of neighboring fullerene molecules [74]. Another interesting property of the fullerene encapsulated complex is its ability to retain the preferred-handed helical structure when induced by an optically active alcohol [72]. Once the alcohol was completely removed from the complex the induced helical structure was retained due to the inclusion of the fullerene molecules. Even though the fullerene is an achiral molecule, induced circular dichroism

activity was detected in the encapsulated C<sub>60</sub> chromophore regions due to the surrounding chiral PMMA helix.

Helical encapsulation within s-PMMA mimics the use of carbon nanotubes to align fullerene molecules, which was described in Chapter 2, since both have hollow cylinders that allow for linear arrays of fullerene molecules to align within the structure. Carbon nanotubes are very difficult to process at high concentrations due to their lack of solubility and highly aggregating nature in other matrices. However, PMMA is used in numerous commercial applications due to its ability to be processed in a variety of methods. Therefore, the encapsulation using s-PMMA offers an interesting alternative with potentially more advantageous processing opportunities.

To induce alignment of the s-PMMA polymers containing fullerenes for this work, the use of electrospinning is proposed to produce aligned fibers with diameters in the micron range. Electrospinning, which is a variant of electrospray [75, 76], is a fiber spinning technique described in the simplest degree as extruding polymer in melt or solution from a syringe using an applied voltage. This applied voltage causes rapid motion of the solution from the needle to the grounded collector. Bending instabilities due to the electrostatic interactions between the surface charges on the solution and the external electric field occur in the polymer flow which causes continually whipping and elongation that results in formation of fibers with very narrow diameters [77-79]. To electrospin the s-PMMA:fullerene complex, the solution in the syringe must be maintained at 110°C because the gel viscosity prevents electrospinning at temperatures below this. Commercial uses of the electrospray technique have become widespread in

printing and painting industries while electrospinning has more recently begun to be used in industry for filtration and even tissue engineering applications [80-82].

Due to the rapid motion of the thin polymer fibers, the solvent evaporates quickly and the polymer chain rapidly cools and solidifies before collection. This rapid heat loss allows for the potential to electrospin s-PMMA complexes which has been shown by Crne *et al.* [83]. S-PMMA also forms a thermoreversible complex gel with isotactic PMMA, i-PMMA [84, 85]. In this stereocomplex, the s-PMMA forms an outer helix that wraps around an inner double helix composed of i-PMMA chains. To electrospin this PMMA stereocomplex the solution in the syringe must be maintained at elevated temperatures because physical gels have very high viscosity preventing them from being electrospun [60].

This work looks at encapsulating both  $C_{60}$  and  $C_{70}$  in the s-PMMA helix and further aligning the helices into nanofibers using electrospinning. Both  $C_{60}$  and  $C_{70}$  were used to compare the effect of size on the encapsulation and resulting rigidity with  $C_{60}$  being smaller than  $C_{70}$ . However,  $C_{60}$  is more common and more readily available, therefore more likely to be used in commercial applications. In some analyses performed in this work, only  $C_{60}$  complexes were studied due to limited materials or equipment availability.

### 3.2 Materials

All reagents were used without further purification unless otherwise specified. The  $C_{60}$  was purchased from Alfa Aesar at 99.5+% purity. The  $C_{70}$  was prepared by collaborators at Oxford University in 99% purity and was used without further

purification. S-PMMA was purchased from Scientific Polymer Products, Inc. containing 85% syndiotactic content. The approximate  $M_w$  of the polymer was 50,000 g/mol. VWR reagent grade 1,2-DCB, DMF, and toluene were used without further purification as solvents as described in the experimental section. Scotch double-sided tape was used to collect the fibers in order to maintain the induced orientation by the parameters of the electrospinning setup.

### 3.3 Experimental

#### 3.3.1 Synthetic Procedures

The s-PMMA (10 mg) and  $C_{60}$  or  $C_{70}$  (11 mg) were dissolved in 1 mL of a (1:1) toluene:DCB co-solvent mixture at 110°C in a glass vial. At this elevated temperature the dissolved polymer chains and the fullerene molecules were interacting [72]. After complete solvation and mixing for 10 minutes at the elevated temperature, the vial was then removed from the heating source and allowed to cool to room temperature. The fullerene encapsulation occurs as a gel is formed when the s-PMMA chains stiffen as they become less soluble in the solvent at lower temperatures. The gel was then transferred to a centrifuge tube and spun at 2500 rpm for 30 minutes at room temperature. This caused the gel to condense to the bottom of the tube by separating from the solvent mixture. The supernatant liquid was decanted out of the centrifuge tube. Two washes to remove the fullerene molecules not encapsulated within the polymer helix were performed in the centrifuge tube by further additions and centrifuging with 1 mL co-solvent at 2500 rpm for 30 minutes. After each wash, the supernatant was poured off and

collected in order to determine gravimetric recovery of fullerene not encapsulated within polymer.

Heated electrospinning experiments were performed using a heated syringe which is discussed later in section 3.2.2. After collection of the condensed gel, the complex was dried under vacuum at 60°C for 12 hours to remove solvent. Then the complex was added back into a (1:1:1) toluene:DCB:DMF solvent mixture at a complex concentration of 20 wt. % at 110°C for 10 minutes. The use of DMF helps maintain uniform fiber diameters as it has a higher dielectric constant than the other solvents, which aids in preventing charge buildup, which is further discussed in section 3.3.2.1. Once in solution, addition to the already heated syringe at 110°C was achieved by pouring into the syringe barrel instead of sucking up through the needle. After the solution was sucked through the needle, rapid heat loss occurred within the solution which resulted in an increase of gelation and thus, caused the needle to become clogged. By removing the plunger and pouring directly into the syringe barrel, the clogging effect was negated. Once the solution was within the syringe, the barrel was placed back into the heated syringe and the trapped air was expelled by pushing in the plunger while holding the syringe upside down with heat resistant gloves. Once the air was removed, the syringe was placed back in the heated oil jacket to maintain the elevated temperature of the mixture. The syringe pump was then started at the 1 mL/hr flow rate and the electrical clamps needed for applying voltage to needle were attached in order to apply charge. The additional processing conditions used during the electrospinning process are discussed in the following section.

### 3.3.2 Processing Conditions

There are three major parts included in the electrospinning setup, which are shown in Figure 3.2: the high voltage power supply, the pump and syringe with metal needle, and the grounded collection plate. The electrospinning setup is relatively simple; however, the real challenge in obtaining the desired fibers lies in using the correct processing conditions. The morphology and diameter of the fibers are highly dependent upon numerous factors which can be broken down into two categories, polymer solution and process parameters. Since so many variables contribute to the type of fibers formed, finding the correct balance in order to spin uniform fibers was difficult and is further discussed in the following two parameters sections.

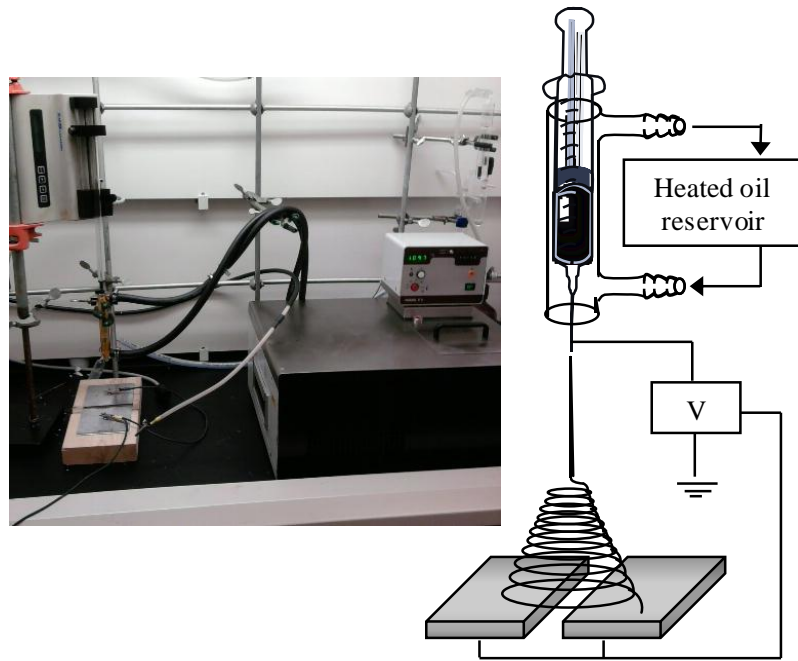


**Figure 3.2:** Electrospinning setup containing heated jacket for syringe and needle which is needed in order to keep solution above gelling point during electrospinning process. Split electrode collection plates provide uniaxially aligned fibers across gap allowing for method to align fibers.

### 3.3.2.1 Polymer Solution Parameters

Included variables that deal with the polymer solution parameters are the polymer molecular weight, solution concentration, type of solvent used, and conductivity of the sample. These variables have the most direct influence on the resulting fiber morphology. To electrospin fibers, the solution must contain polymer molecules of sufficient molecular weight and appropriate concentration. Short chains do not entangle enough to ensure that breakup does not occur during the stretching of the fiber [86, 87]. Viscosity of the solution is not only related to the molecular weight of the polymer but also the concentration. Using a sample with a high viscosity also will not work as clogging of the needle can occur preventing electrospinning to be initiated [88]. Higher viscous solutions are also more resistant to the alignment obtained during the stretching of the fibers resulting in larger fibers with less aligned polymer chains [89]. To determine the optimal concentration that balanced out molecular weight and solution viscosity for uniform fibers, concentrations of s-PMMA and fullerenes were systematically altered and electrospun until uniform fiber diameters were consistently collected. These experiments found that this was achieved using a polymer concentration of greater than 25% of 50 kg/mol s-PMMA with 19 wt.% C<sub>60</sub> encapsulated within the helical chains.

One of the common effects seen in electrospinning is formation of beaded fibers, which are caused by fluctuations of fiber diameter. Surface tension usually plays a role in the formation of beads as the solvent molecules have a greater tendency to congregate which can be minimized at higher concentrations [90]. Solvents that have low surface tensions can be used as they encourage formation of smooth fibers [91]. Since

electrospinning involves the stretching of the polymer fibers due to the repulsion of charges at the surface, the conductivity of the solution is another important variable. Greater stretching and thus alignment of the fibers is achieved when solutions of higher conductivity are used [89]. However, most of the organic solvents that fullerenes are soluble in have very low conductivity so improving conductance is difficult in our case. The final solution parameter that affects fiber formation is the dielectric effect of the solvent. Generally, using solvents with high polarizability reduces the bead formation and helps reduce the diameter of the resulting fibers [92, 93]. Table 3.1 shows the conductivity of various solvents including the three solvents used in the electrospinning of the s-PMMA encapsulated complex. The DMF was used in order to smooth the resulting fibers that were spun due to the higher dielectric constant and conductivity compared to the toluene and DCB. Since fullerenes are insoluble in DMF, the solvent mixture was kept to less than a third of DMF to prevent negative interactions resulting in breakdown of the complex.

**Table 3.1:** Constants for various solvents with the solvents used in the experimental procedure shaded [94, 95].

Solvent	Conductivity (mS/m)	Dielectric Constant
Acetone	0.0202	20.7
Acetonitrile	$6.0 \times 10^{-9}$	35.92
Chloroform	$<1 \times 10^{-9}$	4.8
1,2-Dichlorobenzene	$<1 \times 10^{-9}$	9.93
Dimethylformamide	1.090	36.71
Methanol	0.1207	32.6
Toluene	$8.0 \times 10^{-15}$	2.44
Water	0.447	80.2

### 3.3.2.2 Process Parameters

The external factors that affect the electrospinning process are the applied voltage, feedrate, temperature of solution, needle diameter, distance between needle tip, and humidity. The type of collector can also be associated in this group; however, that is discussed in more detail in the next section. These external factors can influence the fiber morphology but do so at a much lower degree than the solution properties. The voltage is what induces the jet formation so applying a significant charge is crucial in forming fibers. Generally, the voltage is in the range of 1-30 kV with greater stretching and acceleration of the jet occurring at the higher voltages [76, 90, 93]. However, in certain cases the higher voltages can cause greater tendency to form beads due to instabilities in the Taylor Cone at the needle tip [96]. For the chosen voltage applied, a corresponding feedrate should be used in order to maintain a stable Taylor Cone [97]. Since the effective voltage serves as pulling the solution for the needle tip, the syringe pump must then feed the solution into the needle at a comparable rate. Using a higher feedrate causes the ejection of more solvent which may take a longer time to evaporate than flight time. Solvent that is not completely evaporated can cause fibers with porous surfaces or fuse together the fiber causing an increase in the diameter.

To electrospin the PMMA stereocomplex fibers we modified the approach used by Crne *et al.* [83] so that a shaped glass condenser easily fits around the syringe and a large portion of the metal needle instead of immersing the syringe in an oil bath as shown in Figure 3.2. At the electrospinning temperature, heating of the needle was essential to avoid heat loss between the syringe and end of the needle which would have resulted in the solution gelling and clogging the needle. Heat loss in the needle was found to occur

rapidly due to the large increase in surface area to volume ratio, which resulted in increases to the viscosity that prevented fluid withdrawal from the needle. The glass condenser was connected to a temperature bath allowing for exact control of the solution temperature and hence viscosity within the syringe and needle. The process parameters used in this study included applied voltage of 15 kV and feedrate of 1 ml/hr. The solution temperature was maintained at 100°C. An 18 gage needle with an inner diameter of 0.838 mm was used at a distance of 15 cm from the collector plates.

#### 3.3.2.3 Aligned Fibers

The previously described parameters affect the morphology of the nanofibers but do not deal with the various types of patterning of the fibers. Classic collection on a metal plate only results in randomly aligned fibers due to the constant whipping motion of the fibers. However, for this project the fullerenes need to be aligned both at the nanometer scale inside the polymer matrix and at the micron level with the fibers having defined orientation. In order to align the spun fibers, collection of the fibers must be performed in a manner to obtain one-dimensional alignment. One method of obtaining aligned fibers is collecting on a rotating cylindrical drum [98, 99]. Since the fiber jet is traveling at a fast rate, the spinning collector must also be rotating at a high speed in order to obtain aligned fibers. This creates another parameter that must be determined in order to obtain aligned fibers. Advances have been made to the initial system over the previous years to increase the degree of alignment; however, the rotating collector is still not easy to set up due to the high speeds at which the collector must be spun [98, 100, 101].

A much more novel and simpler method for obtaining aligned electrospun fibers can be achieved by utilizing a split electrode collection plate as shown in Figure 3.3 [102]. The parallel split electrodes produce a void gap in which the fibers experience electrical forces that align the fibers perpendicularly to the electrode plates due to the applied charges in the polymer fibers. Not only does the electrospun jet align across the gap, the fibers are also stretched across the void due to the electrostatic field profile which increases the degree of orientation. Since this method does not use any mechanical rotation of the collector plates, it is much easier to set up. Also, because the void is simply air, the removal and collection of the aligned fibers was easily achieved by transfer to a sticky substrate. However, the quantity of aligned fibers is much less using the split electrodes due to the decreased collection area as less than 2% of the collected electrospun fibers were experimentally obtained within the void. Calculations of the predicted amount of fibers based on area are shown in Appendix A. The void between the two electrodes was maintained at a distance of 7 mm during the experiments, which was found to be an ideal size in order to be able to effectively collect the fibers with a flat spatula.



**Figure 3.3:** Split electrode collector plates which induce the fibers to align within the void.

In order to maximize the amount of obtained aligned fibers, a multi-void comb collector plate was designed as shown in Figure 3.4. This collector plate allowed for multiple locations for the fibers to form aligned material increasing the amount of aligned fibers to nearly 30%. This increase is significant when trying to electrospin endohedral fullerenes that are difficult to produce and decompose upon continual heating. Since only approximately 1.3% of the material is aligned using a single void collector method, the remaining unaligned fibers can be re-dissolved in solution and electrospun again. However, this method involves re-heating of the solution which negatively affects the endohedral element. By using the comb collector plate then, more of the endohedral fullerene could be electrospun without continually heating. The gaps between the arms was designed to be 7 mm as this was the distance used in the two-plate split electrode method.

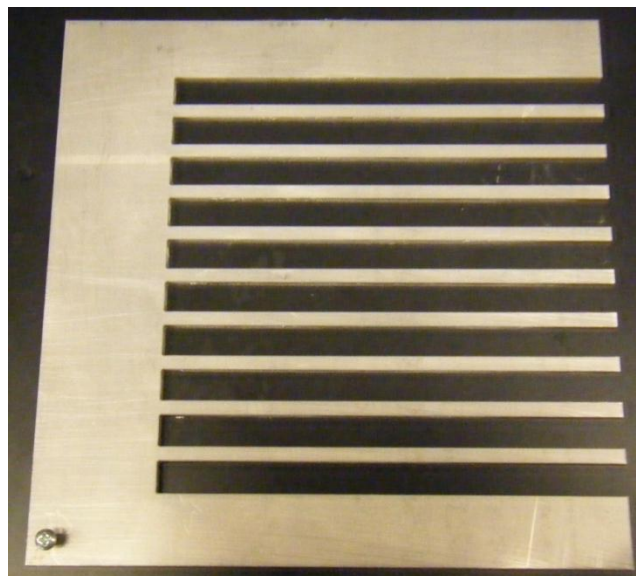


**Figure 3.4:** Comb designed collector plate increases the amount of obtained aligned fibers.

In order to maintain the alignment achieved during the electrospinning process, a method of collection had to be used in order to transfer the fibers for characterization techniques. The details of the collection method used for each instrument is described later in the next section.

### 3.3.3 Instrumentation

Small angle neutron scattering (SANS) measurements from a dilute solution of s-PMMA and C<sub>60</sub> in deuterated toluene were taken as a function of temperature on the LOQ beamline at the ISIS Facility at the Rutherford Appleton Laboratory in Oxford, UK. A 1 mL solution in a quartz cuvette was measured in-situ from 105°C to room temperature (RT).

Images of the alignment of the fibers were taken on a LEO 1530 scanning electron microscope (SEM). The nanofibers were sputter coated with gold to facilitate

imaging. The fiber mats were lightly placed onto the carbon dot tab. To ensure that the alignment of the fibers was maintained, the carbon dot paper was used to collect the fibers across the void. Due to the sticky nature of the carbon dots, the alignment of the fibers was maintained until images were taken. The voltage of the electron beam had to be maintained at a lower energy level to ensure damage to the s-PMMA fibers was not induced.

Differential scanning calorimetry (DSC) was performed on a TA Instruments Q200 using a 10°C/minute heating rate under a nitrogen atmosphere. Approximately 5-10 mg of the sample enclosed within an aluminum pan was initially cooled to 0°C then heated to 300°C to determine any glass transition temperatures or melting transitions. Processing and encapsulation information was determined by comparing thermal data during a second heating to 300°C after the samples were cooled back to 0°C.

Wide angle X-ray scattering measurements of the nanofibers were performed on a Rigaku Micro Max 002 X-ray generator operated at 45 kV and 0.66 mA and equipped with R-axis VI++ detector. To ensure alignment of the fibers was maintained, the edges of the fibers were taped to Kapton film which acted as a support during the scattering measurements. AreaMax software from Rigaku Americas Corporation was used for background subtraction of the Kapton film and integration of the electrospun fiber scattering data.

Solid-state Nuclear Magnetic Resonance (NMR) measurements were performed on a Bruker AV3-400 spectrometer operating at 400 MHz. The cross-polarization (CP) and proton decoupling techniques were combined with magic-angle spinning (MAS) in order to obtain high resolution  $^{13}\text{C}$  spectra. A double bearing CP/MAS probe was used

with 4-mm rotor where the samples were packed tightly into a rotor. All spectra were recorded at a spinning speed of 6 kHz because spinning at that frequency minimizes overlapping of resonances at isotropic positions with spinning sidebands resulting in a clearer spectrum. For obtaining the signal from fullerenes, 7.5 ms contact time was used. Adamantane was used to optimize the Hartmann-Hahn condition for cross polarization and as an external secondary chemical shift reference.

### 3.4 Results and Discussion

Before electrospinning, the s-PMMA:C<sub>60</sub> solution was studied for gelation behavior to confirm encapsulation of the fullerenes in the s-PMMA. The small angle neutron scattering (SANS) behavior of the s-PMMA:C<sub>60</sub> solution in deuterated solvent was measured as a function of decreasing temperature and is shown in Figure 3.5. The SANS data show a distinct increase in the scattering intensity between 63 and 71°C, which is indicative of the gelation point. This gelation point is consistent with the results of Yashima *et al.* [72] who reported a gelation temperature of 60°C determined via <sup>1</sup>H NMR analysis of the solutions as a function of decreasing temperature. The gelation point of pure s-PMMA is reportedly 29°C, which is lower than that of the s-PMMA:C<sub>60</sub> solution [72]. This shows that the fullerenes accelerate the gelation process since the s-PMMA helices are more rigid with the fullerene inclusions.

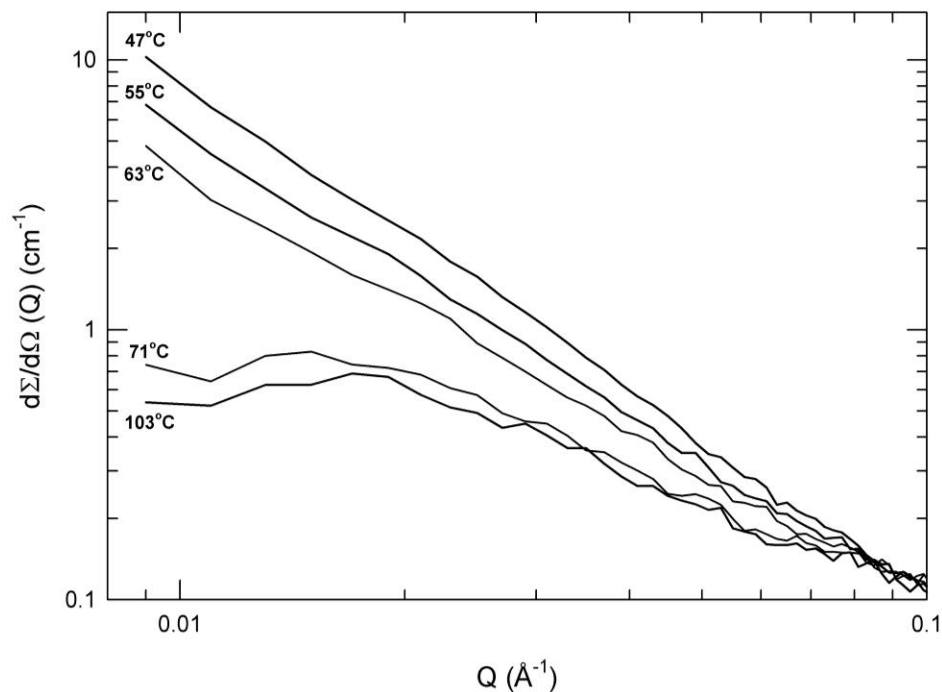


**Figure 3.5:** SANS of s-PMMA:C<sub>60</sub> gel at various temperatures. A solution of s-PMMA:C<sub>60</sub> was mixed together at elevated temperatures and the scattering behavior was analyzed as the solution cooled. The transition between 71 and 63°C can be attributed to the gelation of the solution.

Nanofibers were electrospun as discussed in the experimental section. SEM images in Figure 3.6 identify random and aligned fibers with uniform diameters as well as examples of porous and beaded fibers. The electrospun fibers show a high degree of macroscopic alignment in the split electrode gap. These fibers have a diameter of around 1.5  $\mu\text{m}$ , which can be controlled by varying the needle diameter and temperature, applied voltage, and the applied syringe pump rate. The fibers also show good uniformity in diameter along the length of the fibers aligned in the gap between the electrodes. This effect has been observed with gap separation of up to 5 mm. As the distance between the electrodes is increased, the amount of the fibers collected begins to decrease because the strength of the fiber can no longer hold up the increasing weight. Unfortunately, the fiber

alignment is affected by the amount of fiber that is collected across the void. As more fibers are collected, the empty space between the gaps begins to decrease causing more interaction between the fibers. Since the fibers obtain a positive charge during the electrospinning process, the fibers repel each other when in close proximity. Consequently as more fibers are collected, the forces controlling alignment across the gap are affected by the fiber interactions resulting in a reduction of macroscopic alignment of the fibers due to charge repulsion.

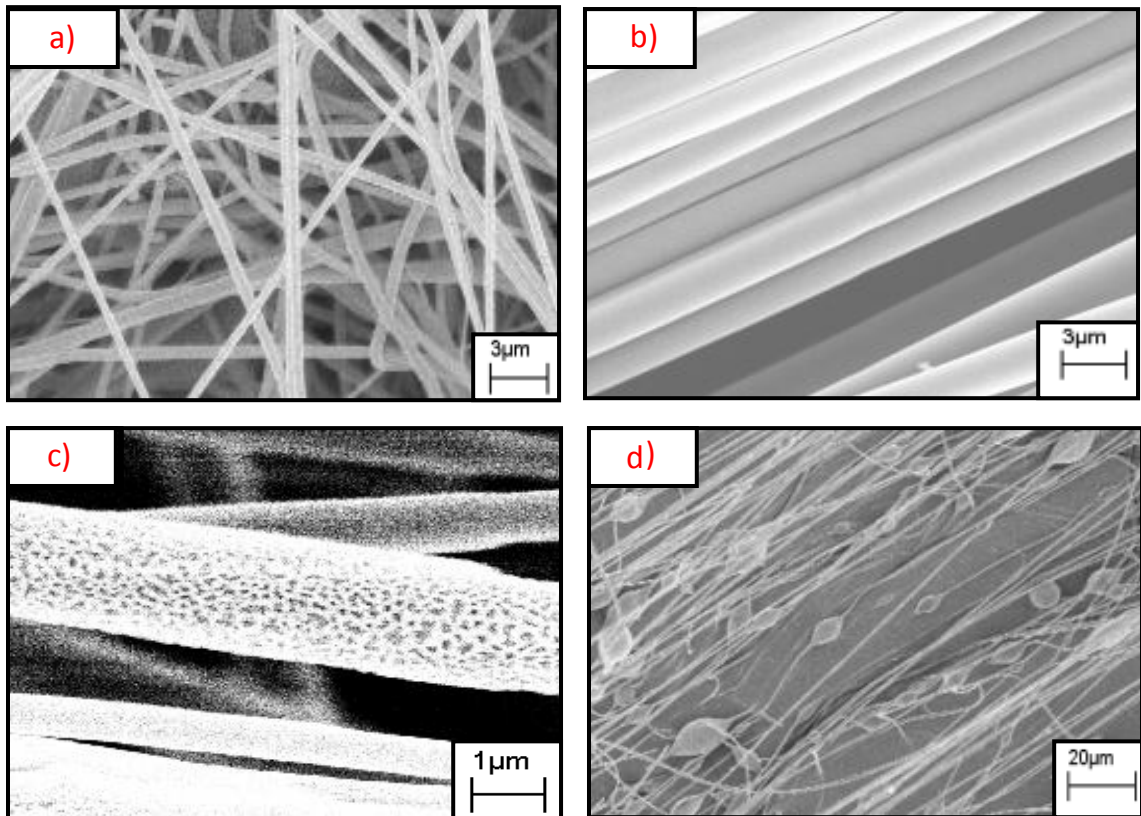


**Figure 3.6:** SEM images of fullerene encapsulated s-PMMA electrospun fibers including a) randomly aligned fibers, b) uniaxially aligned fibers, c) fibers collected with porous surface, and d) fibers with varying diameters due to bead formation.

The degree of fullerene inclusion in the s-PMMA helices was determined from the concentration of fullerene in the supernatant liquid [72]. By washing the gel and

fibers with toluene, any fullerene that was not encapsulated within the helix could be dissolved and extracted. After the wash, the supernatant was dried resulting in 87.6 mg of recovered C<sub>60</sub> from formation of the gel. This amount of recovered fullerene correlates into 22.4 mg of encapsulated C<sub>60</sub>. Due to our use of commercially available s-PMMA which only had an 85% syndiotactic repeat unit content, we were only able to obtain fibers that contained up to 19.6% wt. of C<sub>60</sub> and 14.7% of C<sub>70</sub>. Yashima *et al.* [72] used PMMA that contained 94% syndiotactic repeat units which allowed them to obtain a gel with higher weight percent of fullerene. This concentration was determined by gravimetric measurements of the fullerene contained in the supernatant of the gel. Calculations of the filled helical space with the s-PMMA, which are shown in Appendix A, resulted in 82 and 55% filled for C<sub>60</sub> and C<sub>70</sub>, respectively. These results are expected because the smaller size of C<sub>60</sub> results in a tighter fit of more particles as compared to the larger C<sub>70</sub>. The washing of the electrospun fibers with toluene showed no evidence of dissolving any free fullerene which suggests that the s-PMMA:C<sub>60</sub> complex stayed intact during the electrospinning process.

Thermal analysis by DSC showed only a glass transition temperature (T<sub>g</sub>) in pure s-PMMA. However, s-PMMA:C<sub>60</sub> fibers exhibited a melting peak in addition to the T<sub>g</sub>; this melting peak can be attributed to the helical inclusion of the fullerene. This melting peak was not observed on the second heating due to the breakdown of the complex at high temperatures. The fullerene containing fibers show a melting transition that begins at 180°C that is not evident in fibers only containing s-PMMA as seen in Figure 3.7. This melting peak disappears during the second heating cycle in the DSC as the inclusion of the fullerene within the s-PMMA is broken down at elevated temperatures. Also seen

in the electrospun fibers is the appearance of a broad melting transition due to the induced orientation of the fibers during the spinning process. These transitions also are not seen after heating due to the breakdown of the induced orientation. These DSC results are consistent with those of Yashima *et al.* [72].

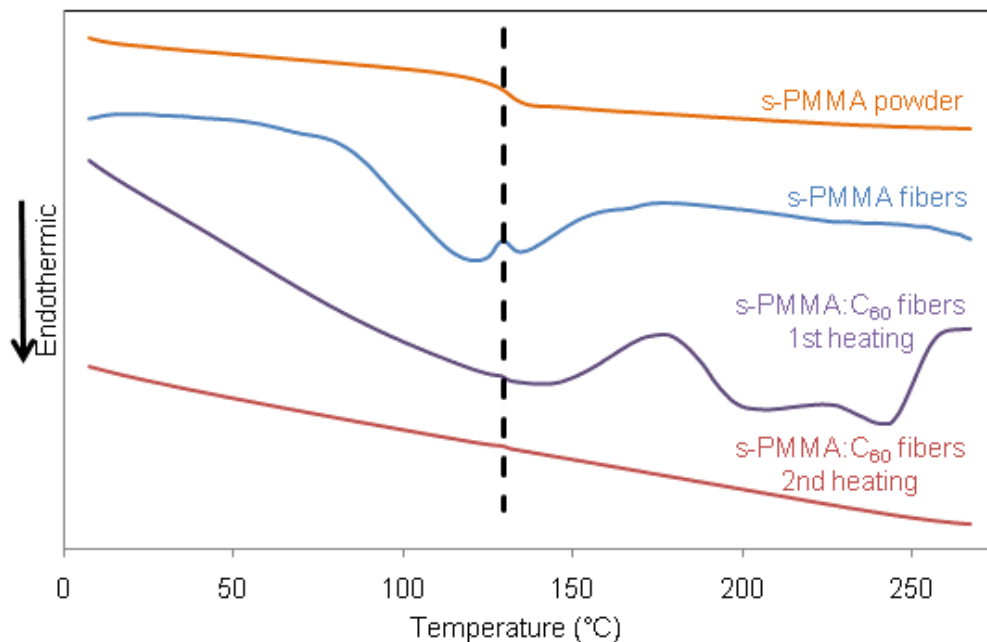


**Figure 3.7:** DSC curves of s-PMMA powder and electrospun fibers which shows  $T_g$  and melting transitions. The arrow indicates the endothermic direction. The s-PMMA powder shows a characteristic  $T_g$  at 130°C and no melting transition. When the s-PMMA is electrospun a new melting transition around 120°C is seen due to the induced chain orientation achieved during the process. An additional melting transition around that begins at 180°C is seen when  $C_{60}$  is added to the s-PMMA and electrospinning is used to orient the fibers. As expected, the fiber orientation and inclusion complex is broken down once the sample is heated above 250°C as shown in the second heating of the fibers.

Wide-angle x-ray scattering (WAXS) measurements of the electrospun fibers were made to determine the molecular alignment of the helical complexes within the fibers. Due to the applied charge in the electrospinning method, the spun fibers experience large drawing forces when exiting the needle tip. These shear forces cause

the polymer complexes to orient into the shear field, that is parallel to the fiber long axis. The 2-D WAXS patterns of the electrospun fibers collected between the split electrodes, as seen in Figure 3.8, clearly show anisotropy and therefore orientation of the helical complexes. The degree of anisotropy of oriented electrospun fibers of pure s-PMMA or s-PMMA:C<sub>70</sub> are much less than that observed for s-PMMA:C<sub>60</sub> complexes. Quantification of the degree of orientation can be evaluated by using an azimuthal scan of the reflection at  $2\theta = \sim 25^\circ$ , which typically shows a Gaussian shaped peak as shown in Figure 3.9. The full width at half maximum (FWHM) of this peak is largest for the pure s-PMMA oriented fibers and much narrower for the s-PMMA gelled in the presence of C<sub>60</sub> and C<sub>70</sub>.

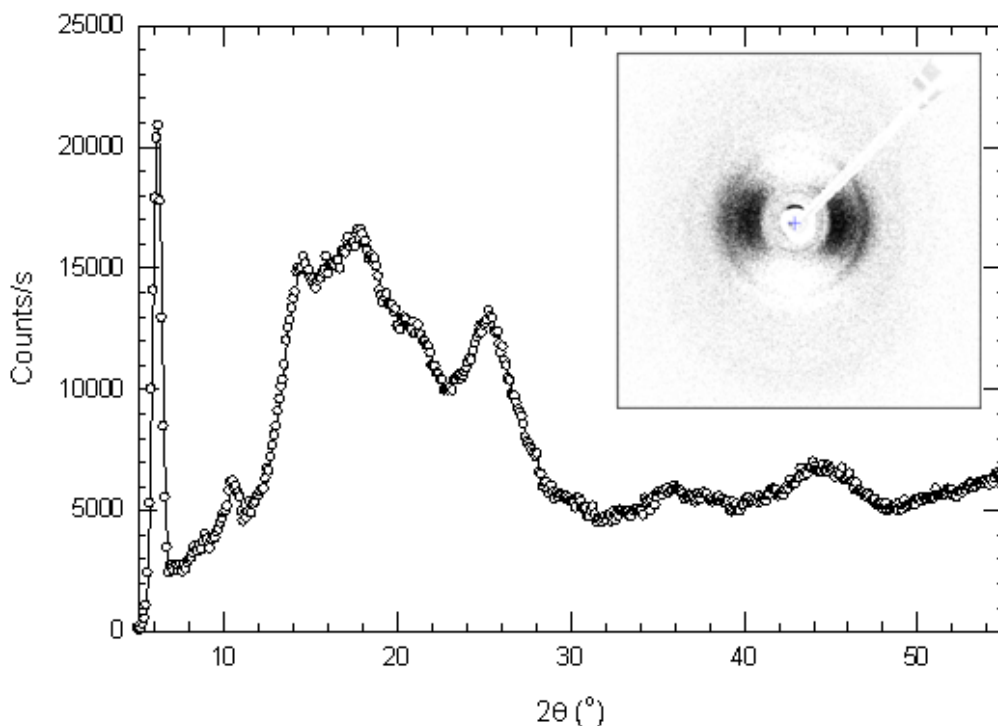


**Figure 3.8:** 1D averaged WAXS diffraction pattern from sPMMA+C<sub>60</sub> radially averaged over all azimuthal angles. Inset shows the raw 2D scattering data, clearly showing the high degree of anisotropy and therefore alignment of the fibers.

A quantitative determination of the degree of orientation, i.e. the Hermann's orientation factor ( $F$ ), can be obtained from the azimuthal scans by evaluating Equation 3.1:

$$F = \frac{3\langle \cos^2 \phi \rangle - 1}{2} \quad \text{Eq. 3.1}$$

Where,

$$\langle \cos^2 \phi \rangle = \frac{\int_0^\pi I(\phi) \cos^2 \phi \sin \phi \, d\phi}{\int_0^\pi I(\phi) \sin \phi \, d\phi} \quad \text{Eq. 3.2}$$

and  $\phi$  is the azimuthal angle. From this analysis we obtain values of  $F = 0.27, 0.51$  and  $0.70$  for the s-PMMA, s-PMMA+C<sub>70</sub> and s-PMMA+C<sub>60</sub>, respectively. This increase is thought to be due to the increased stiffness of the s-PMMA helices by the fullerene. While an orientation of  $F = 0.7$  is not perfect, it is possible that with further parameter modification this can be improved. Despite this, recent theoretical studies have shown that this degree of orientation may be sufficient for demonstration of quantum information processing in such materials.

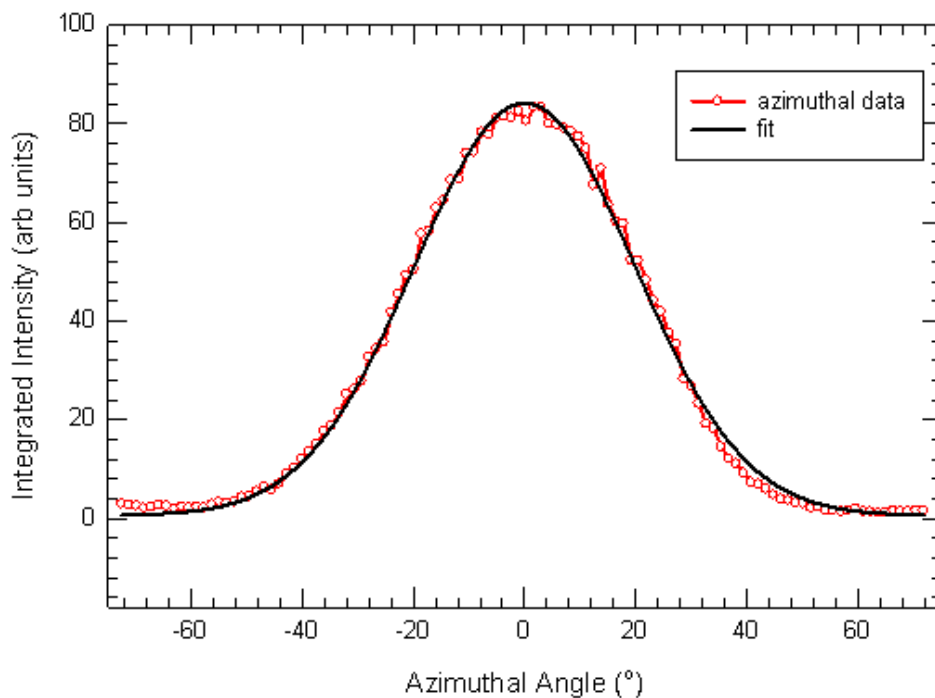


**Figure 3.9:** Plot of the azimuthal angle data obtained from the  $2\theta = 25^\circ$  peak (open circles) with fit using the Hermann's orientation equations.

To compare the chemical shift of fullerenes in the PMMA fiber, two other samples were also measured. These two samples were the unwashed gel and physical mixture of PMMA and  $C_{60}$ . The CP/MAS spectra of these three samples are shown in Figure 3.10.

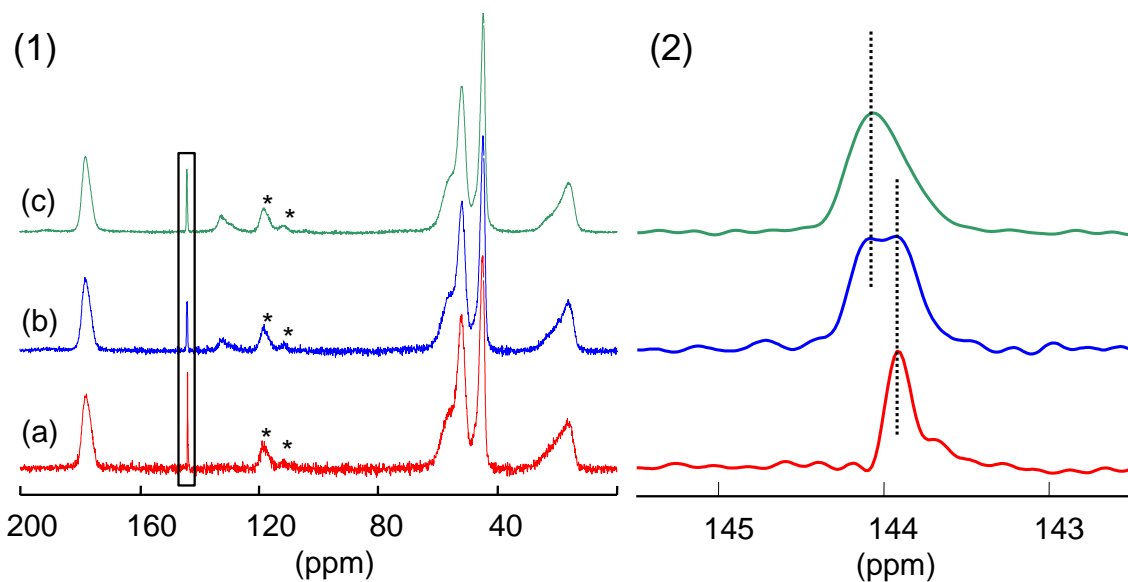


**Figure 3.10:** (1) The full CP/MAS spectra of (a) the physical mixture of s-PMMA and  $C_{60}$  (b) unwashed gel of s-PMMA- $C_{60}$  and (c) s-PMMA- $C_{60}$  fiber. (2) The enlarge region (142.5 – 145.5 ppm) of the respective spectrum, where the resonance responsible for fullerenes is observed. The spinning side bands are marked with \*.

As observed in Figure 3.10, in all spectra the resonances arising from s-PMMA and  $C_{60}$  are observed. In unwashed gel and fiber another extra resonance is observed around 130 ppm due to the toluene. This resonance is due to the solvent molecules which are trapped within the helical structure of s-PMMA. In the enlarged region where the resonance responsible for fullerenes is observed, we observed a peak at 143.9 ppm for the physical mixture of s-PMMA and  $C_{60}$ , two peaks at 143.9 ppm and 144.1 ppm for the gel of s-PMMA: $C_{60}$  and a peak at 144.1 ppm for the fiber of s-PMMA- $C_{60}$ . From this study it can be concluded that when  $C_{60}$  is in the free state it gives resonance at 143.9 ppm, which is observed in the physical mixture and gel samples; however, when it is encapsulated in the helical structure of s-PMMA then a resonance at 144.1 ppm is observed as seen in the gel and fiber samples. From this study the presence of  $C_{60}$  in the

helical structure of s-PMMA can be confirmed. According to our knowledge this is the first spectroscopic proof of the C<sub>60</sub> in the helical structure of s-PMMA.

By identifying shifts in different fundamental properties, fullerene encapsulation in s-PMMA can be confirmed with very different experimental methods. This study used scattering techniques to identify that the fullerenes aid in accelerating gelation by rendering s-PMMA helices more rigid (SANS) and also that C<sub>60</sub> undergoes a peak shift when encapsulated as opposed to its free state (CP/MAS). Further, thermal characterization was used to identify shifts in thermal fluctuations, specifically melting properties, that occur only when encapsulated fullerenes are present. A simple analysis was also performed by identifying that free fullerenes could be removed by washing with toluene (?) while encapsulate fullerenes remain. All of these methods measured shifts in various properties to identify the presence of encapsulated fullerenes. It is also important to note that the supernatant analysis identified C<sub>60</sub> as a better fit for filling the s-PMMA helix, therefore making it more rigid than its C<sub>70</sub> counterpart. The higher rigidity results in a system that is easier to align using shear forces.

The analyses have shown the presence of encapsulated fullerenes and that electrospinning is an effective method for achieving multi-scale fibers. SEM confirmed that proper processing conditions can result in uniform fibers while WAXS showed that higher orientation factors are reached when the s-PMMA has increased rigidity. Although the optimal orientation factor (F=1) was not achieved, the fibers have shown some of the high degree of orientation for this type of system which has not been studied before and the outlook for further optimization is promising.

### **3.5 Conclusions**

In this work we have reported the ability to align fullerene containing fibers that are formed under self-assembling interactions with helical forming s-PMMA. By using a split electrode collection method with the electrospinning we were able to achieve macroscopic fiber alignment and molecular orientation of the fullerene molecules. These new studies may prove to be effective methods of processing functional fullerene based materials that can be used in numerous applications.

## CHAPTER 4

### SUPRAMOLECULAR FULLERENE: CYCLODEXTRIN COMPLEX

#### 4.1 Introduction

Fullerenes [1] and cyclodextrins [103] have both become important molecules due to their unique properties which have been applied to numerous materials and biochemical applications. Cyclodextrins have been shown to act as excellent molecular receptors effectively binding to a variety of different molecules forming complexes, which has been utilized most notably in the pharmaceutical industry [104-106]. Supramolecular chemistry has garnered great consideration among researchers lately due to the important role of taking the properties of single molecules and assembling them in order to make functional materials [105, 107]. By utilizing supramolecular chemistry, we can create materials without having to covalently link molecules together that potentially causes a change in the molecular properties.

Previous research has shown that the fullerene molecule forms an inclusion complex with a variety of host molecules [102, 108, 109]. An inclusion complex consists of non-covalent binding between host molecules that have cavities which associate with components of the guest compound. Most of these host molecules have a concave structure, which can act to enhance the interaction between the two surfaces since the fullerene molecule has a spherical, convex shape. The external  $\pi$ -electron surface of the fullerene molecule allows for  $\pi$ - $\pi$  interactions with molecules that contain interior  $\pi$ -electron surfaces or that have hydrophobic cores [110]. Two notable molecules that have strong interactions with the fullerene molecule are the cyclic oligomers of cyclodextrin

[111] and calixarene [112]. Since these are cyclic molecules, the shape allows for a bowl-like structure that allows interaction between interior walls of the host and the exterior surface of the fullerene molecule. Both cyclic oligomers can complex with fullerene strong enough to make a water-soluble complex even though the fullerene molecule is extremely hydrophobic [113, 114].

**Table 4.1:** Association constants of host molecules interacting with C<sub>60</sub>. The shaded β-CD is the molecule chosen for studies.

Host Molecule	Type of interaction (H:G)	K <sub>a</sub>	Solvent
cyclic porphyrin trimer [115]	1:1	2.1 x 10 <sup>7</sup> M <sup>-1</sup>	cyclohexene
γ-CD [116]	2:1	2.6 x 10 <sup>7</sup> M <sup>-2</sup>	water
β-CD [117]	2:1	1.7 x 10 <sup>5</sup> M <sup>-2</sup>	water
bis-calix[5]arene [118]	1:1	7.6 x 10 <sup>4</sup> M <sup>-1</sup>	toluene
calix[5]arene [119]	1:1	2.1 x 10 <sup>3</sup> M <sup>-1</sup>	toluene

Both β- and γ-cyclodextrin molecules have been shown to form inclusion complexes with C<sub>60</sub> [111, 117]. Due to the symmetric ball shape of the C<sub>60</sub>, two cyclodextrin molecules can surround the fullerene molecule allowing for some degree of encapsulation. Modeling studies have shown that the diameter at the upper rim of β- and γ-cyclodextrin is 15.3 and 16.9 Å while the diameter of the cavity at the lower rim is 7.8 and 9.5 Å, respectively [117]. Since the outer diameter of the C<sub>60</sub> is only 10.2 Å, this allows the fullerene cage to sit within the cup of the cyclodextrin molecules allowing for some but not complete penetration due to the narrower diameter at the lower rim. Due to the increased cavity diameter size, the γ-cyclodextrin molecule can interact more with the C<sub>60</sub> allowing for greater binding. However, the α-cyclodextrin has not been shown to form an inclusion complex with C<sub>60</sub>.

One of the numerous molecules that cyclodextrins can form an inclusion complex with is fullerene, more specifically C<sub>60</sub> and C<sub>70</sub> [111, 114, 117]. Unfortunately, one of the limiting factors when performing research on fullerenes is the limited solubility of the molecule in common organic solvents [18, 120]. However, the cyclodextrin inclusion complex with fullerene is actually more soluble in numerous solvents including water. Therefore, studying the interesting complexation behavior between these two molecules can serve as important investigation into the world of nanomaterials for designing materials with desired supramolecular assemblies. Herein, we report on a simple method for preparation of a supramolecular fullerene assembly that shows interesting behavior in solution and fibrous formation in the solid state through studies involving <sup>1</sup>H NMR spectroscopy, mass spectroscopy, dilute solution viscometry (DSV), dynamic light scattering, and transmission electron microscopy (TEM).

The strong binding ability of CDs with many molecules, including self-assembly, is evident in past research results making it an ideal molecule and is designed in order to make unique supramolecular assemblies. β-CD molecules are known to self-assemble in water, forming multiple structures due to aggregation depending on concentration and sample preparation including sheets, globular particulates, and even fibers [121-124]. The ability of the cyclodextrin to form complex nanostructures makes it an ideal candidate to design materials for fullerene science.

The inclusion complex between the C<sub>60</sub> and β-CD molecules forms due to the enthalpic contributions from the hydrophobic interactions between interior cavity of the cyclodextrin and the outer cage of the fullerene molecule [111, 114, 117]. Since the interaction is non-covalent the association is reversible and the complex will break down

over time if put in strained environments. Due to the truncated cone shape of the cyclodextrin molecule and the spherical shape of the fullerene molecule a 2:1 complex is formed with the CD molecules encapsulating the C<sub>60</sub> limiting the interaction with the solvent. The association constant of the fullerene with the host molecule β-CD in water has been reported to be 1.7 x 10<sup>5</sup> M<sup>-2</sup> [117].

The association constant, K<sub>A</sub>, reflects the strength of interaction between the host and guest molecules. This value can be determined using UV-vis spectrometry and applying the Benesi-Hildebrand equation for a 2:1 complex as shown in Eq. 4.1 [125].

$$\frac{[C_{60}]}{A} = \frac{1}{K\varepsilon} \cdot \frac{1}{[CD]^2} + \frac{1}{\varepsilon} \quad \text{Eq. 4.1}$$

In this equation, [C<sub>60</sub>] is the guest concentration, [CD] is the host concentration, K is the association constant, A is the absorbance, and ε is the extinction coefficient for the absorbing molecule. The association constant between the complex of γ- and β-cyclodextrin and C<sub>60</sub> is 2.6 x 10<sup>7</sup> and 1.7 x 10<sup>5</sup> M<sup>-2</sup>, respectively [116, 117]. The UV-vis measurements are taken at a wavelength of 342 nm in water so that the only absorbing molecule in the solution at this wavelength is the C<sub>60</sub> that is forming a complex with the cyclodextrin molecules. C<sub>60</sub> molecules that are not interacting with the cyclodextrin molecules will not dissolve in water thereby excluding them from being able to absorb light. As shown in Figure 4.1, absorbance measurements obtained in our lab of the 2:1 β-cyclodextrin and C<sub>60</sub> complex confirmed a similar result as Murthy *et al.* [117] as the association constant calculated was 8.0 x 10<sup>4</sup> M<sup>-2</sup>. The slope and y-intercept of the trendline was used to solve for the association constant and the extinction coefficient for the complex. Host-guest ratio is important to determine in order to apply the correct

Benesi-Hildebrand equation and can be determined by nuclear magnetic resonance, (NMR) and thermogravimetric methods.

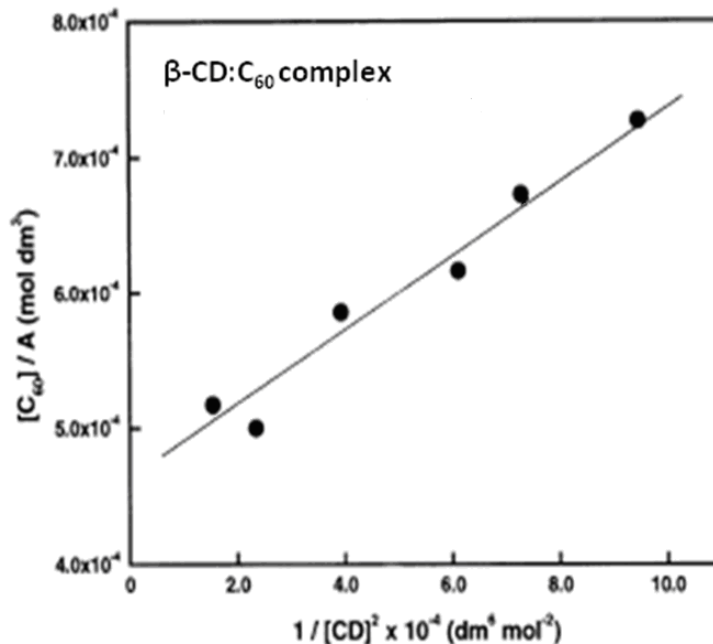


**Figure 4.1:** Absorbance data plotted with use of Benesi-Hildebrand equation.

Another method of determining the strength of the association between molecules is by using NMR chemical shift information [126]. Interaction between the fullerene cage and the  $\gamma$ -cyclodextrin molecules has shown to cause shifts in the  $^1\text{H}$  and  $^{13}\text{C}$  chemical spectra upon complexation. This chemical shift can be measured at varying concentrations and used in a double reciprocal plot as shown in Eq. 4.2 to calculate the association constant.

$$\frac{1}{\Delta\delta} = \frac{1}{K\Delta\delta_{\max}} \cdot \frac{1}{[CD]^2} + \frac{1}{\Delta\delta_{\max}} \quad \text{Eq. 4.2}$$

Where,

$$\Delta\delta = (\delta_{CD} - \delta_{obs}) \text{ and } \Delta\delta_{\max} = (\Delta\delta_{CD} - \Delta\delta_{2CD:C_{60}}) \quad \text{Eq. 4.3}$$

In this equation, [CD] is the host concentration, K is the association constant, and  $\delta$  is the chemical shift observed for the pure cyclodextrin or the solution containing the complex. One key feature of applying the Benesi-Hildebrand equation to spectroscopic data is being able to work with solutions that contain a large excess of host molecule in order to ensure that the uncomplexed host concentration can be set as the initial concentration of host molecules.

One method for obtaining the alignment of fullerene molecules is by using the host-guest complex to induce formation of a supramolecular polymer [127]. The general strategy is to use a ditopic guest molecule to create extended molecular chains with fullerene molecules. Without a ditopic host molecule, the fullerene molecule can only bind to two CD molecules which prevents chain formation. By controlling the concentrations of the two molecules, the length of the supramolecular complex can be directed to give ideal properties. Meijer *et al.* [128] show a theoretical relationship between the strength of the association constant between host-guest molecules and the length of the corresponding supramolecular structure. According to Meijer's use of the multistage open association model, the association constants of  $\beta$ -CD/ $C_{60}$  inclusion complexes would allow for the degree of polymerization of the supramolecular polymer to reach above 100 repeat units even at low concentrations.

The estimation of the degree of polymerization can be made from Eq. 4.4, which shows the theoretical relationship at various concentrations of self-associating molecules [129]. This model is derived from Carothers equation using the fraction of monomer conversion in a polymeric reaction. Using this equation with the known association constant between  $C_{60}$  and  $\beta$ -CD of  $1.7 \times 10^{-5} \text{ M}^{-2}$  and an overall concentration of 0.004 M,

an estimation of the degree of polymerization of 37 repeat units is calculated if a ditopic host cyclodextrin molecules is used.

$$DP = \frac{1}{1-p} = \frac{1}{\alpha} = \frac{4K_{dim}C_t}{\sqrt{8K_{dim}C_t + 1} - 1} \quad \text{Eq. 4.4}$$

In this equation,  $p$  is the extent of reaction,  $K_{dim}$  is the dimerization constant,  $\alpha$  is the mole fraction of unassociated groups, and  $C_t$  is the total molar concentration.

Bis-cyclodextrins will provide the ditopic host needed for supramolecular polymer formation. These molecules have been synthesized with many linking groups offering various uses [130]. However, due to numerous hydroxyl groups located around the ring of the cyclodextrin molecule leading to multiple reaction sites, the yields of cyclodextrin substitution reactions are relatively low. Thus, the synthetic procedure and purification of bis-cyclodextrins is not trivial. However,  $\beta$ -cyclodextrin mono-substituted by tosylation has been historically used as the initial precursor for other substitution reactions. This is because the desired product falls out of solution once mono-tosylation occurs at one of the primary hydroxyl groups on the  $\beta$ -cyclodextrin [131, 132]. This precipitation allows for easy separation between the desired product and any side reactions that occur on the cyclodextrin molecule. Currently, the bis-cyclodextrin molecule that has been synthesized for use in analyzing the complex formation with fullerene molecules is linked using click chemistry [133]. The synthetic procedure to make this molecule is shown in Figure 4.2. The “click” chemistry route was chosen over other synthetic routes due to advantages of providing higher yields and relatively simple reaction conditions. Linking of two mono-azide substituted  $\beta$ -cyclodextrins is achieved

by Cu(I)-mediation using a dialkyne linker resulting in a Huisgen 1,3-dipolar cycloaddition reaction [134].

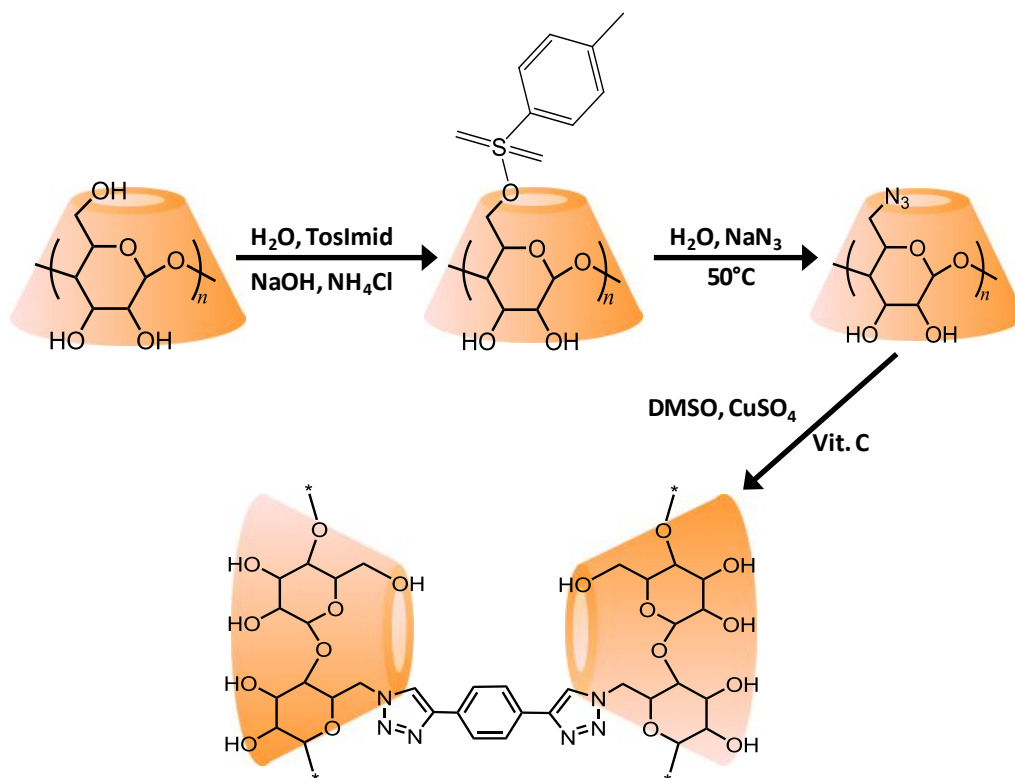


**Figure 4.2:** Synthetic procedure used to make bis-β-cyclodextrin used in supramolecular studies.

The use of bis-CD molecules to bind with fullerenes has been demonstrated as researchers have formed a supramolecular fullerene chain using a metallo-bridged β-CD dimer as the host molecule [135]. Other β-CD molecules have also been shown to form interesting supramolecular structures with fullerenes [136]. These results effectively show formation of linear supramolecular structures on length scales of 150-200 nm that correspond to 60-80 repeat units. We desired to use this concept but to apply the use of a cyclodextrin dimer that was much simpler to synthesize and did not involve use of toxic chemicals.

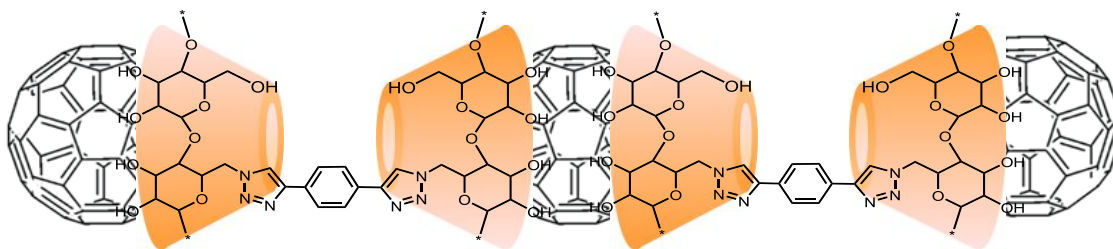


**Figure 4.3:** Synthetic procedure used to make bis- $\beta$ -cyclodextrin used in supramolecular studies.

## 4.2 Materials

The C<sub>60</sub> was purchased from Alfa Aesar at 99.5+% purity and was used without further purification. The tosyl chloride, imidazole, Na<sub>2</sub>SO<sub>4</sub>,  $\beta$ -CD, and Sephadex G-25 were purchased from Sigma-Aldrich while NH<sub>4</sub>Cl, NaN<sub>3</sub>, NaOH, CuSO<sub>4</sub>, ammonia solution (8%), and sodium ascorbate were purchased from VWR, but all were used without further purification. Reagent grade acetone, dichloromethane, DMSO, and DMF was purchased from VWR and were used without further purification. Distilled water was used from the general water still in the MS&E building on the Georgia Tech campus.

## 4.3 Experimental

### 4.3.1 Synthetic Procedures

**Synthesis of 1-(p-toluenesulfonyl)imidazole [132].** To a solution of tosyl chloride (5 g, 26.3 mmol) in dichloromethane (50 ml), imidazole (7.12 g, 104.5 mmol) was added. The mixture was left 2 h under magnetic stirring at room temperature, and then it was diluted with more dichloromethane (50 ml) and extracted with water (3 x 80 ml). The organic layer was dried over anhydrous Na<sub>2</sub>SO<sub>4</sub> and evaporated to give the

final product as a white powder. Yield: 90%.  $^1\text{H}$  NMR (500 MHz,  $\text{CDCl}_3$ ):  $\delta$  = 8.02 (s, 1H), 7.84 (d, 2H), 7.37 (d, 2H), 7.31 (s, 1H), 7.10 (s, 1H), 2.46 (s, 3H) ppm.

**Synthesis of 6<sup>I</sup>-O-mono(p-toluenesulfonyl)- $\beta$ -cyclodextrin [137].**  $\beta$ -CD (1.3 g, 1.14 mmol) was dissolved in water (30 ml). 1-(p-toluenesulfonyl)imidazole (1.01 g, 4.58 mmol) was then added and the mixture was sonicated for 10 min for formulation of the inclusion complex. 2 ml of aqueous NaOH (560 mg, 14 mmol) were then added dropwise over 10 min and after another 30 min the milky suspension was transferred to a flask and  $\text{NH}_4\text{Cl}$  (1.67 g, 31.5 mmol) was added. The mixture was filtered and the collected solid washed with ice-cold water (5 ml) and acetone (5 ml), and finally dried under vacuum to yield the final expected compound as a white solid. Yield: 55%.  $^1\text{H}$  NMR (500 MHz,  $[\text{D}_6]\text{DMSO}$ ):  $\delta$  = 7.75 (d, 2 H, Har), 7.45 (d, 2 H, Har), 6.7 (m, OH-2 and OH-3), 4.85 (d, 7 H, H-1), 4.1-4.5 (m, 14 H, H-6-OTs, H-6'-OTs, and OH-6), 3.13.8 (m, 28 H, H-3, H-4, H-5, and H-2), 2.45 (s, 3 H, Me) ppm.

**Synthesis of 6<sup>I</sup>-monoazido-6<sup>I</sup>-monodeoxy- $\beta$ -cyclodextrin [53].** Sodium azide (0.160 g, 2.4679 mmol) was suspended in 10 mL water and 6<sup>I</sup>-O-mono(p-toluenesulfonyl)- $\beta$ -cyclodextrin (0.3 g, 0.23 mmol) was added. The mixture was stirred for 5 hours at 80°C. Then acetone (50 ml) was added and the precipitate filtered off. Yield: 74%.  $^1\text{H}$  NMR (500 MHz,  $[\text{D}_6]\text{DMSO}$ ):  $\delta$  = 5.7 (b, 14 H, OH-2 and OH-3), 4.8 (m, 7 H, H-1), 4.5 (m, OH-6), 3.8-3.5 (m, 28 H, H-3, H-5, H-6, H-6'), 3.3 (m, 14 H, H-4, H-2) ppm.

**Synthesis of 1,4-Bis[1-(6A-deoxy- $\beta$ -D-cyclodextrin)-1,2,3-triazol-4-yl]benzene [131].** Mono-6-azido- $\beta$ -CD (1.3 mmol) and hydrated copper sulfate (1.1 mmol) were added to a solution of the alkynyl derivative (0.5 mmol alkynyl function) in DMSO (25

mL). After the subsequent dropwise addition of a freshly prepared solution of sodium ascorbate (2.2 mmol) dissolved in water, the solution was stirred for 18 h at room temperature. Addition of acetone (100 mL) induced the precipitation of a yellowish-white powder that was recrystallized from a water/acetone mixture. The solid was recovered, dissolved in an ammonia solution (8%) and stirred overnight before being purified by column chromatography using silica gel with water as eluent. The dimer product was isolated from unreacted starting material after column chromatography using Sephadex G-25 as the matrix. Yield: 62%.  $^1\text{H}$  NMR (500 MHz,  $[\text{D}_6]$ DMSO):  $\delta$  = 7.92 (s, 2 H), 7.48 (d, 2 H), 7.12 (d, 2 H), 5.7 (b, 28 H, OH-2 and OH-3), 4.8 (m, 14 H, H-1), 4.5 (m, 12 H, OH-6), 3.8-3.5 (m, 52 H, H-3, H-5, H-6).

**Formation of supramolecular polymer.** A mixture of cyclodextrin derivative and fullerene were stirred for three weeks in a mixture of toluene and DMSO (v/v=1:1), during which the purple solution turned brown. The solvents were removed under vacuum and the solid residue collected.

#### 4.3.2 Instrumentation

$^1\text{H}$  and  $^{13}\text{C}$  NMR spectra were obtained on a Bruker AMX-400 spectrometer using 5 mm outer diameter tubes. Sample concentrations were about 25% (w/v) in DMSO containing 1% TMS as an internal reference. Mass spectra were recorded on an Applied Biosystems 4700 Proteomics Analyzer tandem time-of-flight/time-of-flight (TOF/TOF) mass spectrometer. The ions were generated by MALDI using 200Hz Nd:YAG laser and 2,5-DHB as the matrix with detection in positive reflection mode.

UV-vis measurements were taken on a Thermo Spectronic Genesys 20 spectrometer at a wavelength of 342 nm. Capillary viscometry was performed using a Ubbelohde type viscometer with a size 0 capillary at 25°C. Automatic detection of the flow times were recorded on Schott Viscopump II.

Light scattering measurements were carried out in a 3D dynamic light scattering instrument designed and commercialized by LS Instruments (Switzerland). The apparatus is equipped with a He-Ne laser operating at a wavelength of 632.8 nm and with 25 mW of power. This beam is split into two parallel beams that are focused onto the sample. The scattered light is collected and guided using optical fibers towards two avalanche photodiodes mounted into a motorized goniometer, which is used to change the scattering angle from  $\theta=20^\circ$  to  $155^\circ$ . The arrangement of the beams allows the performance of two simultaneous experiments with the same scattering vector. Images of the  $\beta$ -cyclodextrin dimer and the complex were captured on a JEOL JEM-1400 TEM operating at 120 kV.

#### **4.4 Results and Discussion**

The mass spectroscopy and  $^1\text{H}$  NMR results, as shown in Figures 4.4 and 4.5 respectively, provide insight into the determination of the structure of the synthesized bis- $\beta$ -CD. The mass spectrum of the dimer revealed a peak at the  $m/z$  of 2467.4 which is expected for the  $[\text{M}+\text{Na}]^+$  peak. From the  $^1\text{H}$  NMR spectrum, the four phenyl protons from the linker show up as one peak at 7.48 ppm indicating the symmetric nature of the linking bridge. Also seen were the two triazole protons formed during the 1,3-

cycloaddition reaction that appear at 7.92 ppm. Another important aspect of the  $^1\text{H}$  NMR is the integration ratios between the protons associated with the hydroxyl groups on the  $\beta$ -CD and the phenyl protons located on the linking molecule. The ratio of these peaks corresponds to the expected value in molecule as there are 4 phenyl protons and 28 primary substituted As expected for a substituted cyclodextrin product, the protons associated with the glucopyranose repeat units were difficult to investigate due to overlapping and broadening of peaks caused by the asymmetrical substitution on the secondary side of the  $\beta$ -CD.

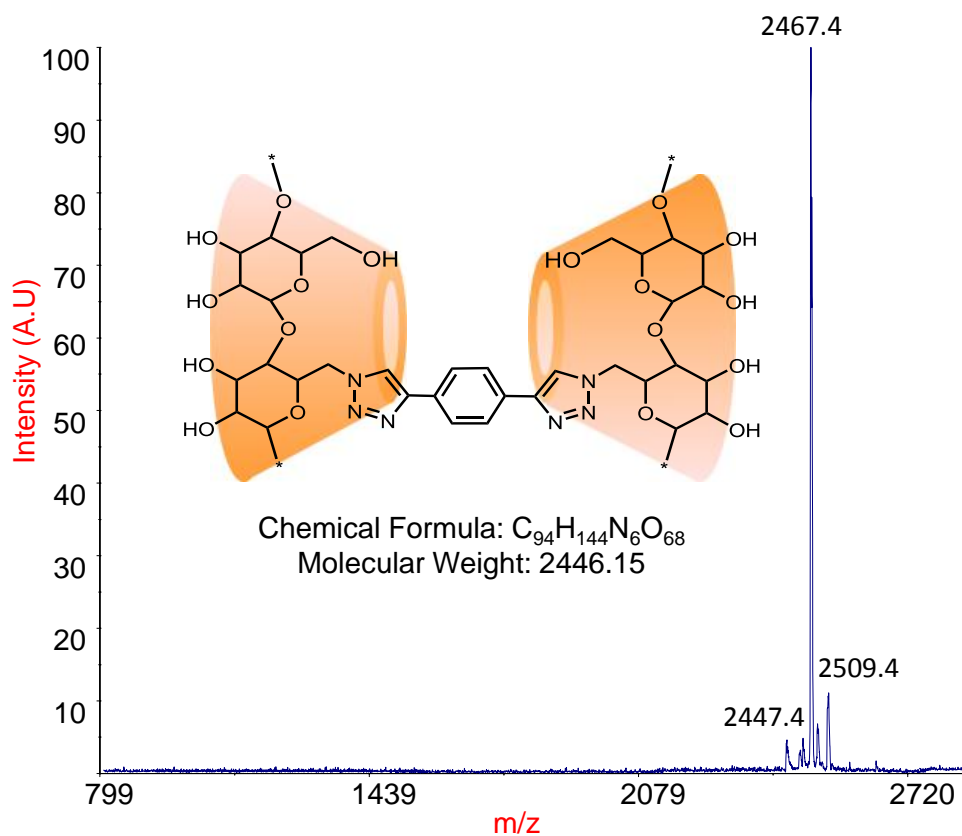


**Figure 4.4:** Mass spectrum of the  $\beta$ -CD dimer.

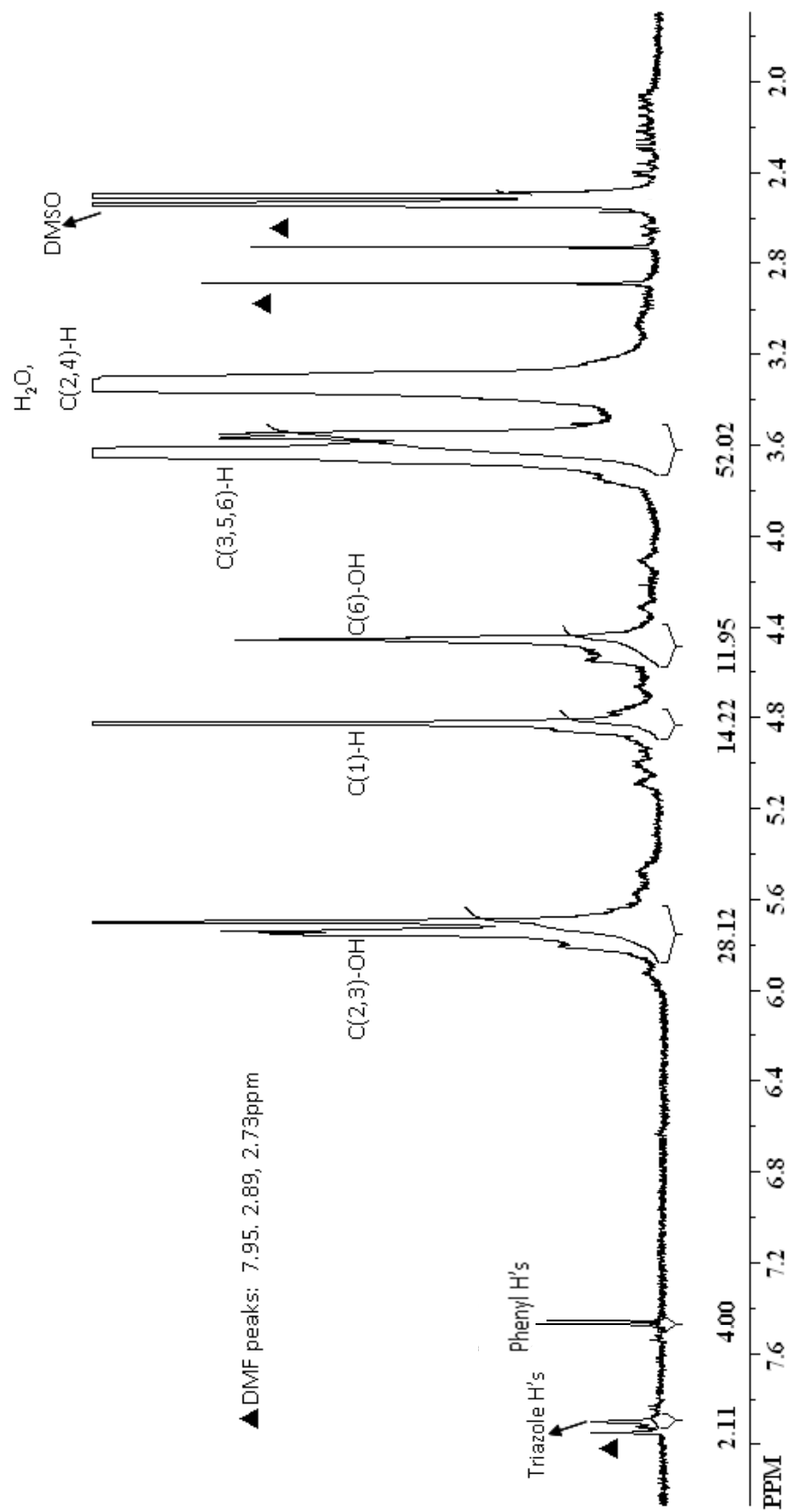


**Figure 4.5:**  $^1\text{H}$  NMR spectrum of the  $\beta$ -CD dimer.

Once the ditopic  $\beta$ -cyclodextrin was synthesized, the formation of inclusion complex with  $C_{60}$  was studied by analyzing the UV-vis data of resulting solutions. After addition of the molecules in a toluene:DMSO (1:1) solvent mixture, the solution is a purple color which is typical of  $C_{60}$ . However, as seen in Figure 4.6, the color of the solution changes to a brown color suggesting changes in the electronic properties of the fullerene molecule due to inclusion complex formation with the bis- $\beta$ -cyclodextrin host. The resulting product after mixing for 24 hours also showed  $C_{60}$  absorption bands in the UV-vis spectrum at 342 nm in water which is consistent with formation of an inclusion complex.

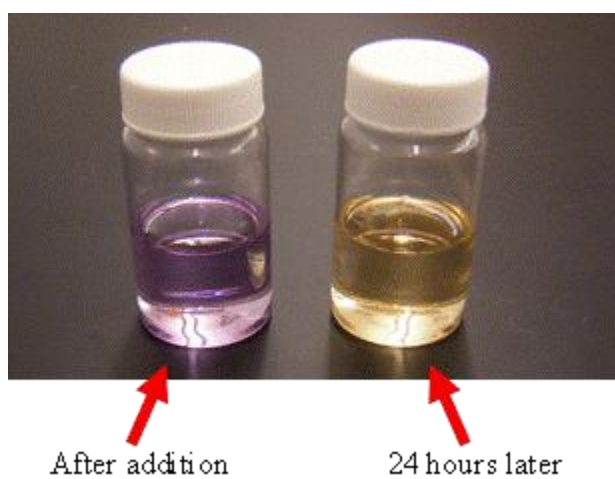


**Figure 4.6:** Evident color changes in  $C_{60}$ /bis- $\beta$ -cyclodextrin solution over time.

However, to induce supramolecular chain formation the concentration of host to guest must be equimolar. If the host molecule is kept and maintained at a large excess then only short oligomeric species can be formed [128]. Dilute solution viscometry measurements allowed for a method for determining the effect of the supramolecular structure on the flow behavior of the solution. As seen in Table 4.2, the viscosity of the

solutions were measured using a size 0 capillary in a Ubbelohde type viscometer and maintained the temperature of the solutions constant at 25°C using a water bath. Automatic detection of the efflux times were recorded by a Schott Viscopump II limiting error involved in human time recording. Since  $\beta$ -CD does not self-assemble in DMSO, it was chosen as the solvent in order to directly see the effect of supramolecular assembly due solely to addition of fullerene. The dilute concentration of 1mg/mL was chosen due to the poor solubility of the  $\beta$ -CD dimer:C<sub>60</sub> complex. As expected, the efflux time upon addition of the  $\beta$ -CD and  $\beta$ -CD dimer did not change much, which indicates no interaction between the molecules in DMSO. However, upon addition of the fullerene to the  $\beta$ -CD dimer there is a noticeable difference in the efflux time indicating increased molecular size of the particles in the solution.

**Table 4.2:** Dilute solution viscometry data showing drastic increase in the flow of the complex solution through a capillary.

Solution	Efflux Time (secs)	% Increase
DMSO	87.0 ± 0.3	-
1mg/ml $\beta$ -CD	89.6 ± 0.2	3.0
1mg/ml $\beta$ -CD dimer	89.7 ± 0.1	3.1
1mg/ml [1:1] $\beta$ -CD dimer:C <sub>60</sub>	112.9 ± 0.5	29.7

Dynamic light scattering allowed analysis of the supramolecular structure in solution. These measurements were also performed in DMSO to limit the interaction between the CD molecules. As seen in Figure 4.7, by plotting the linear fit of relaxation frequency,  $\gamma$ , to the wave vector,  $q^2$ , the mean diffusion coefficient can be calculated from the slope. From this diffusion coefficient, hydrodynamic radius can be calculated for the

structures in solution via the Stokes-Einstein equation. From these calculations it was determined that the  $R_h$  for the supramolecular assemblies of  $\beta$ -CD dimer: $C_{60}$  is 220 nm.

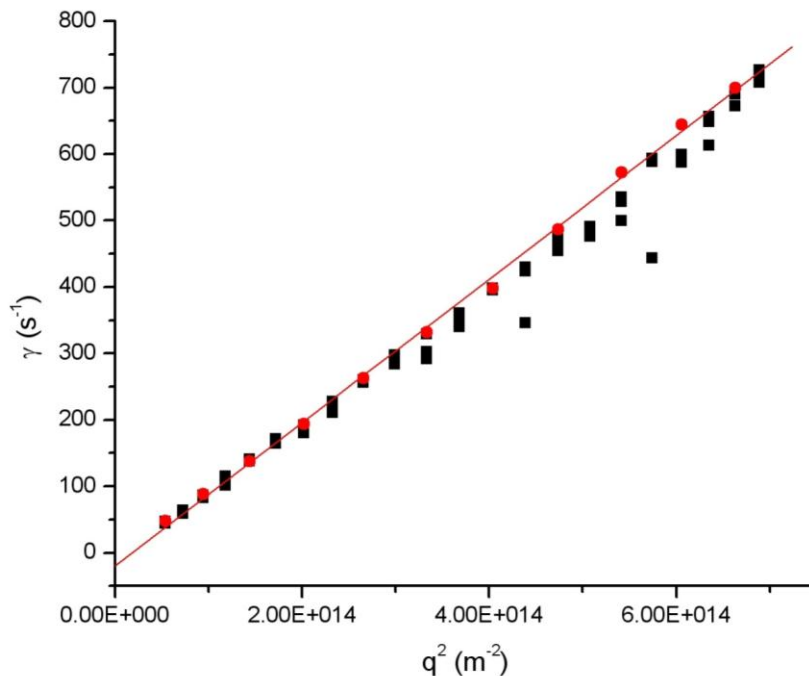


**Figure 4.7:** Dynamic light scattering of the  $\beta$ -CD dimer: $C_{60}$  complex.

The  $\beta$ -CD dimer was transferred to the TEM carbon coated grid from solution in DMSO. The DMSO was removed under vacuum at a temperature of  $60^\circ\text{C}$ . From the TEM images of the  $\beta$ -CD dimer it can be seen that the dimer particles aggregate into clusters with average sizes of  $57 \pm 13$  nm calculated by using image software analysis tool. Also analyzed were the individual particle sizes that are clearly visible as seen in Figure 4.8, which make up the aggregates. The average size of the randomly chosen particles was  $5.1 \pm 0.9$  nm. This width is slightly larger than the calculated outer rim diameter of a  $\beta$ -cyclodextrin ring of 1.5 nm, which may suggest that the dimer particles are self-assembling in some fashion. Since the linking molecule contains a benzene ring, there could potential be ring stacking due to  $\pi$ -electron interactions. If two neighboring

$\beta$ -cyclodextrin dimer molecules can undergo this induced assembling this would attribute to the increase particle size seen in the TEM images. These particles were roughly spherical shaped which suggests that the aggregation is symmetric. This aggregation seen in the  $\beta$ -cyclodextrin dimer molecules can occur upon solvent evaporation during conventional TEM sample prep, leading to the structures seen.

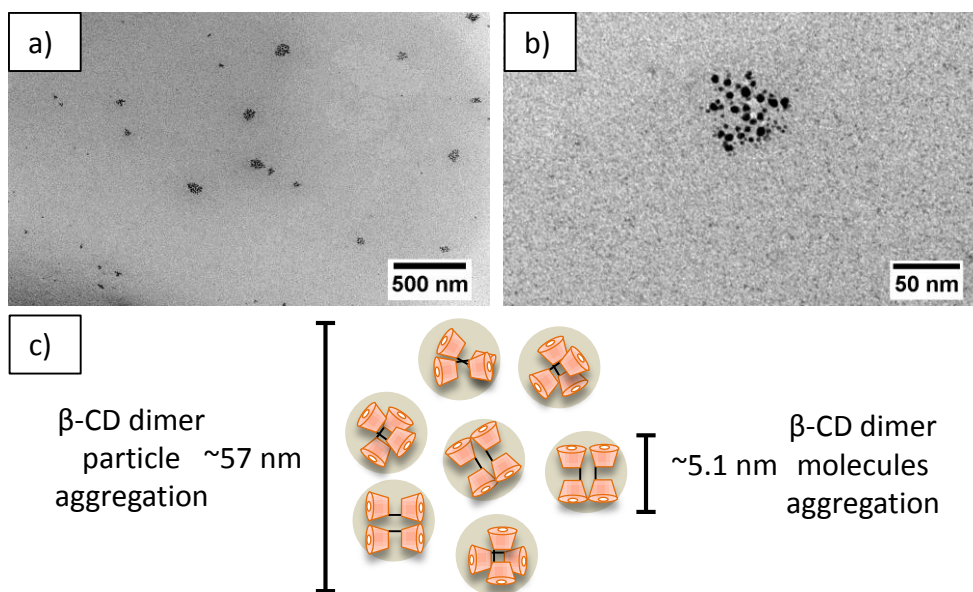


**Figure 4.8:** TEM images of the  $\beta$ -CD dimer. Image a) shows the clustering occurring between the particles while image b) taken at higher magnification shows the relative uniformity of the size of the particles forming the clusters. Image c) shows a cartoon of the proposed association occurring between the  $\beta$ -CD dimer molecules resulting in the formation of the aggregates.

Images of the supramolecular complex were also obtained using TEM as shown in Figure 4.9. A noticeable difference in resulting solid-state structure was clearly seen to the  $\beta$ -CD dimer once the fullerene molecules were included. Formation of fibers were directly seen in the sample suggesting formation of polymeric chains through the induced non-covalent bonding with fullerene since fibers are not seen in the sample containing only the  $\beta$ -CD dimer. These fibers were greatly varied in length with an average length

of  $1.9 \pm 1.5 \mu\text{m}$ . This average length is much longer than the 150-200 nm previously reported for a bis-CD:C<sub>60</sub> supramolecular polymer [135]. This could suggest that the chains are aggregating together thereby forming larger structures. Although the length of the chains widely varied, the fibers maintained a much narrower distribution for the average width calculated at  $45 \pm 11 \text{ nm}$ . However, this width is still larger than expected for a single chain, which further suggests that bundling of the complex may be occurring. Figure 4.9 contains a schematic of the proposed aggregation occurring between the supramolecular chains that causes the extended length and increased widths of the structures. It is unclear whether this bundling is occurring to the same degree in solution since the average size measured in light scattering suggest smaller average sizes. This bundling may occur upon solvent evaporation under vacuum.

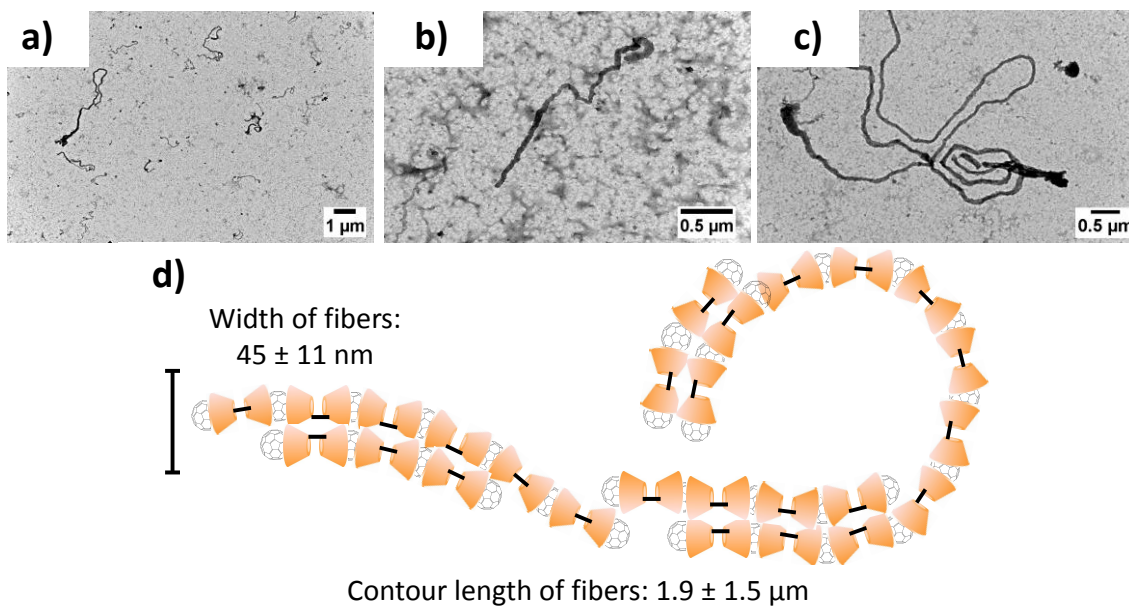


**Figure 4.9:** TEM images of the  $\beta$ -CD dimer:C<sub>60</sub> complex. Image a) shows the high degree of variation in the length of the fibers formed while images b) and c) shows the relative uniformity of the width maintained throughout the length of a fiber. Image d) shows cartoon of the potential inclusion complex formation and potential bundling of chains.

## 4.5 Conclusions

In conclusion we have reported the interesting formation of fibers containing fullerene molecules resulting from the supramolecular complex association with  $\beta$ -CD dimer molecules. The reversible inclusion complex that facilitates the supramolecular assembly is formed at room temperature through non-covalent interactions. Formation under these inert conditions makes this method of self-assembly an ideal candidate for use with less stable endohedral fullerenes. The solution behavior suggest large aggregate formation of the  $\beta$ -CD dimer before and after addition of fullerene as seen in the light scattering data; however, a dramatic increase in solution viscosity is only seen in the complex solution which suggest that the self-assembling nature of the  $\beta$ -CD dimer breaks apart upon strain in the capillary. Solid-state aggregates were also seen in the TEM images; however, the size and shape of these aggregates greatly differed in the samples containing  $C_{60}$  molecules. This work provides motivation for further analyze of the ability to control orientation of the supramolecular aggregates.

## CHAPTER 5

# SYNTHESIS AND INCLUSION OF FULLERENE STARS INTO A POLYMER MATRIX

### 5.1 Introduction

The final approach to impart global alignment of fullerene based molecules is by incorporation into diblock copolymers with controlled geometry. Diblock copolymers can self-assemble over nanometer length scales into ordered arrays based on the volume fractions of polymer components [138, 139]. By effectively incorporating nanoparticles into the copolymer system, then, ordering can be achieved by selective segregation into one of the phases [140-142]. The most direct route for linear orientation would be to incorporate the fullerene molecules within cylindrical or lamellae forming arrays [143]. However, fullerene molecules have low association with polymeric chains thereby limiting the inherent ability to self-assemble selectively with high degrees of precision [144]. The concentrations at which fullerenes can be added to copolymers matrices is therefore too low for effective use in applications involving quantum computing. In order to increase the solubility of the fullerene molecule, chemical modifications must be done to the cage to increase loading concentrations within the matrix.

One polymer that fullerene molecules have shown slight association with is polystyrene, PS [145]. However, this association is much lower than that compared with cyclic oligomers as discussed in Chapter 4. One method of improving the fullerene incorporation into the polystyrene phase is to covalently attach polystyrene chains on the cage of the  $C_{60}$ , which are called fullerene stars as shown in Figure 5.1 [146]. Since  $C_{60}$  can accept six electrons as it strengthens aromatic character, the number of polystyrene

chains added onto the cage can vary from one to six based on stoichiometric additions of “living” polystyrene [147].  $C_{60}$  cannot accept more than six electrons, so when the “living” polystyrene is added in excess the resulting fullerene molecules can have a maximum of six grafted chains attached to the cage resulting in a star type molecule. The “living” PS is made by anionic polymerization of styrene initiated by sec-butyl lithium in toluene at room temperature.

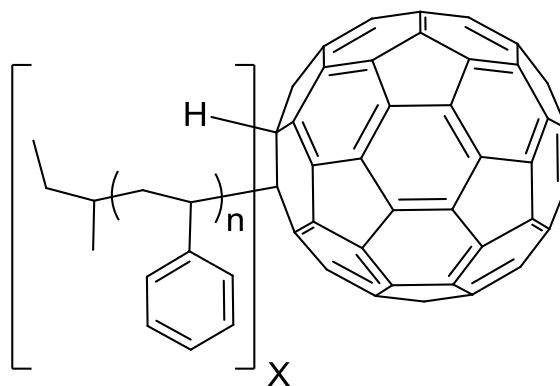


**Figure 5.1:** Fullerene stars with number of polystyrene chains grafted X, from 1-6.

The addition of the PS arms to the  $C_{60}$  cage has been well studied [148, 149]. The addition of the six carbanions to  $C_{60}$  occurs through addition at one of the 30 6,6-bonds. The anionic charge can be delocalized through neighboring carbons that construct a pyracyclene unit. Due to the delocalization between these carbon atoms and the strong, repulsive Coulombic interactions observed between negative charges, another carbanion cannot attach within this pyracyclene unit of the cage. Therefore, the addition of the six polystyrene chains is evenly distributed allowing for uniform coverage of the cage.

By attaching PS chains onto the cage of the fullerene molecule, the dissolution of these star molecules is greatly increased in common organic solvents [148]. The grafting of PS chains to the fullerene cage has also been shown to increase dispersion of

fullerenes in PS and PS-PI symmetric block copolymers [141, 150]. In this approach the variables that can be manipulated to optimize the conditions for achieving ordered cylindrical or lamellae arrays include the grafting polymer chain length, number of arms grafted on the cage, type of copolymer matrix, and size of the chains in the of block copolymer matrix. Incorporation within the cylindrical phase would impose segregation upon the fullerene molecules as seen in Figure 5.2. However, the characteristic radius of the cylinder phase in most copolymer systems is 20-30 nm [138]. This size is an order of magnitude larger than the diameter of the cage of the fullerene, so controlled segregation within the cylinder must be addressed in order to achieve maximum alignment. One method of restricting the diameter of the cylinder phase is to use low molecular weight copolymers. However, below a critical molecular weight diblock copolymers do not micro-phase separate to give well-defined morphologies. Therefore, in this work we use low MW block copolymers to form lamella arrays of the fullerene stars. In this chapter, we analyze the behavior of fullerene stars with grafted PS arms of low molecular weight in solution and in thin films.

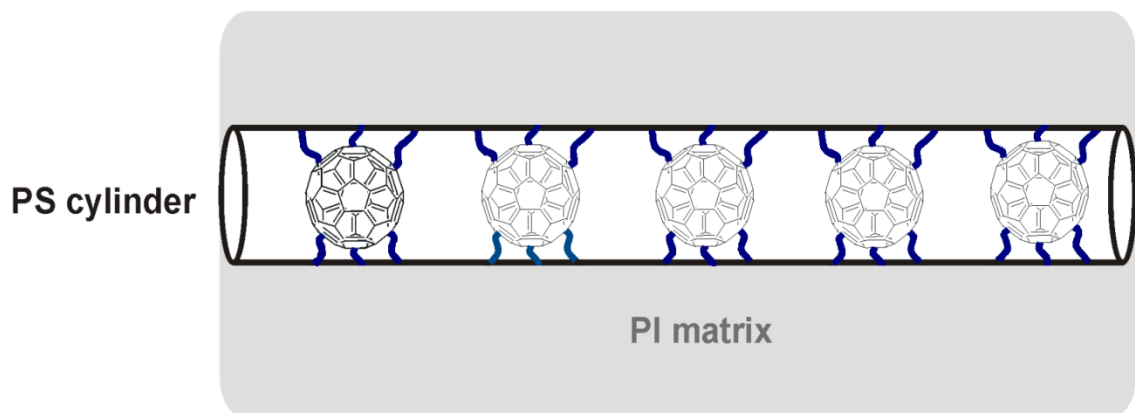


**Figure 5.2:** Increased incorporation of fullerene molecules within the cylindrical phase due to polymeric grafts.

## 5.2 Materials

HPLC grade toluene was purchased from Sigma-Aldrich and used as received as a solvent for both the block copolymer and fullerenes. Symmetric poly(deuterated styrene-*b*-methylmethacrylate) (dPS-PMMA) was purchased from Polymer Source, Inc with an  $M_n$  of 15-*b*-15 kg/mol by block and PDI of 1.09. For end-grafting of polystyrene onto silicon oxide surfaces,  $\omega$ -hydroxy terminated polystyrene was also purchased from Polymer Source, Inc with an  $M_n$  of 50 kg/mol and a PDI of 1.06. All polymer materials were used as received. C<sub>60</sub> was purchased from Sigma-Aldrich at 99% purity and was used without further purification. Sec-butyl lithium (sec-BuLi) and styrene were purchased from Sigma-Aldrich and used in anionic polymerization of PS. The 1.4 M sec-BuLi was used as received; however, the styrene was further purified using a two-step method. Water was first removed from the styrene by addition of calcium hydride (CaH<sub>2</sub>) at approximately 20 mg of CaH<sub>2</sub> per 1 mL of styrene under an inert Argon atmosphere in a Schlenk flask for 12 hours. The styrene was then distilled under vacuum

into a Schlenk flask containing di-butylmagnesium and stirred for an additional 12 hours. This second purification step removes protic impurities contained in the styrene. After completion of the purification, the styrene was then distilled under vacuum into a Schlenk tube to begin polymerization.

## 5.3 Experimental

### 5.3.1 Synthetic Procedures

Fullerene stars were synthesized by addition of living PS addition using a procedure modified from Mathis *et al.* [147]. Break-seal ampules were not used as described by Mathis *et al.*; however, all steps were still performed within a pressurized Schlenk line under an inert Argon atmosphere. The anionic living polymerization of the 2.2 kg/mol PS was initiated by 3.47 mL of sec-BuLi addition to 9.72 g of styrene dissolved in freshly distilled toluene in a Schlenk tube. Upon addition of the initiator the solution turned orange which is consistent with the color of living styryl carbanions. Desired molecular weights of the PS were achieved by controlling the stoichiometric addition of initiator to monomer. For the larger 6.2 kg/mol PS, 0.63 mL of sec-BuLi was added to 5.53 g of styrene. After reacting for 10 hours, a small amount of the living PS was removed from the Schlenk tube for molecular weight analysis by GPC. Once the desired size of polymer was achieved, the living PS was added in 10-fold excess to 50 mg of C<sub>60</sub> dissolved in freshly distilled toluene and stirred for 2 hours. The color of the fullerene solution changed from purple to brown upon addition of the PS. Deactivation of the anionic charge on the cage of the fullerene was achieved by addition of methanol. Precipitation of the fullerene stars can be induced by further addition of methanol.

allowing for isolation through filtration. Purification of the fullerene stars was achieved by the fractionation method using THF as solvent and methanol as non-solvent. The yield of the fullerene stars after isolation and purification was 90%.

### 5.3.2 Instrumentation

Molecular weights of the fullerene stars were measured using gel permeation chromatography (GPC). Polystyrene standards were used to create a calibration curve used for analyzing retention times of polymers. The GPC is composed of a Waters 2410 Separations Module and is equipped with Waters Styragel HR 4, 3, and 1 toluene columns with detection performed by a Waters 410 refractive index detector. Molecular weights were determined to be 2.2 kg/mol and 6.2 kg/mol per arm,  $C_{60}PS_{6(2.2\text{kg/mol})}$  and  $C_{60}PS_{6(6.2\text{kg/mol})}$  respectively, with six PS arms grafted to the fullerene cage in both cases.  $^1\text{H}$  and  $^{13}\text{C}$  NMR spectra of the molecules were obtained on a Bruker AMX-400 spectrometer using 5 mm outer diameter tubes. Sample concentrations were approximately 25% (w/v) in  $\text{CDCl}_3$  containing 1% TMS as an internal reference.

The fullerene stars were thermally characterized using a TA Instruments Q200 Differential Scanning Calorimeter (DSC). Using PS standards of varying molecular weight as received from Polymer Standards ( $M_n$ : 2.62, 6.24, 41.4, 109 kg/mol). Measurements were conducted using a flow of nitrogen air a heating rate of  $10^\circ\text{C}/\text{min}$ .

Light scattering measurements were carried out in a 3D dynamic light scattering instrument designed and commercialized by LS Instruments (Switzerland). The apparatus is equipped with a He-Ne laser operating at a wavelength of 632.8 nm and with 25 mW of power. This beam is split into two parallel beams that are focused onto the sample. The scattered light is collected and guided using optical fibers toward two

avalanche photodiodes mounted into a motorized goniometer, which is used to change the scattering angle from  $\theta=20^\circ$  to  $155^\circ$ . The arrangement of the beams allows the performance of two simultaneous experiments with the same scattering vector. Images of the  $\beta$ -cyclodextrin dimer and the complex were captured on a JEOL JEM-1400 TEM operating at 120 kV.

Neutron reflectivity measurements were conducted on the variable wavelength Liquid Reflectometer 4B at the Spallation Neutron Source at Oak Ridge National Lab (Oak Ridge, Tennessee). The measurements were conducted by Drs. David Bucknall and Katie Campbell from Georgia Institute of Technology. All samples were measured as prepared and after annealing. Given the wavelength range of  $2.5 < \lambda < 6 \text{ \AA}$  for this reflectometer, the measurements of reflectivity were taken at multiple incident angles ( $\theta = 0.15^\circ, 0.25^\circ, 0.35^\circ, 0.449^\circ, 0.65^\circ, 0.849^\circ, 1.60^\circ, \text{ and } 2.8^\circ$ ) to provide data over an extended Q-range. The resolution ( $\delta Q/Q$ ) of the instrument was determined by fitting the reflectivity data from a D<sub>2</sub>O standard that was found to be 0.078.

The ideal coherent scattering length densities (SLDs) of dPS, PMMA, PS, silicon oxide (SiO<sub>x</sub>), and Si (substrate) used were  $6.41 \times 10^{-6}$ ,  $1.07 \times 10^{-6}$ ,  $1.41 \times 10^{-6}$ ,  $3.20 \times 10^{-6}$ , and  $2.07 \times 10^{-6}$ , respectively, in units of  $\text{\AA}^{-2}$ . All relevant values for maximum SLD are provided below in Table 5.1. The neutron reflectivity curves were fit using statistical error minimization techniques until the agreement between the calculated reflectivity and the experimental reflectivity data was suitable. The resulting scattering length density profiles, SLD versus thickness,  $z$ , were then used to determine the structure of thin films in the thickness direction to assess the formation and location of a fullerene layer within the deuterated PS block of the block copolymer.

**Table 5.1:** Neutron reflectivity ideal scattering length densities (SLD) for relevant compounds.

<i>Compound</i>	<i>SLD (<math>\text{\AA}^{-2}</math>)</i>
Polystyrene (PS)	$1.41 \times 10^{-6}$
Deuterated Polystyrene (dPS)	$6.41 \times 10^{-6}$
$C_{60}$	$5.73 \times 10^{-6}$
Poly(methylmethacrylate)	$1.07 \times 10^{-6}$
Silicon oxide	$3.76 \times 10^{-6}$
Silicon	$2.07 \times 10^{-6}$

#### 5.4 Results and Discussion

In order to create materials containing a high content of fullerenes, the grafting of PS arms onto the fullerene cage was restricted to low molecular weight arms. The synthesis of low MW arms has been analyzed by GPC but further characterization in solution and in copolymer systems has not been studied [147]. Reducing the chain length to a minimum would increase the overall concentration of fullerenes in the system as both the polymer arms and polymer matrix will dilute the amount of  $C_{60}$  in an aligned material. The grafting of a smaller amount of arms would also reduce the overall molecular weight of the resulting molecule; however, for studies discussed within this chapter all fullerene stars were polymerized with 6 arms. This was done to ensure the uniformity between the molecules as grafting with fewer arms is much harder to control [151].

Grafting of the polymers onto the cage of the fullerene molecule can be monitored by GPC. As shown in Figures 5.3-5.5, the molecular weight of the grafted fullerene molecule increases drastically with the addition of six chains. This increase in molecular weight leads to lower retention times within the GPC columns allowing for peak separation. The molecular weight,  $M_n$ , of the fullerene stars was determined from analysis of the peaks using a PS calibration curve. In all the samples, the overall molecular weight of the star that was calculated by GPC was lower than the expected  $M_n$  for addition of 6 arms. This is due to the fact that star molecules are more compact than linear chains in solution so the retention seen in GPC is less. Thus, the  $M_n$  reported of the fullerene stars in this chapter was calculated by using the  $M_n$  of the parent PS and multiplying by the number of arms and addition of molecular weight of the  $C_{60}$ .

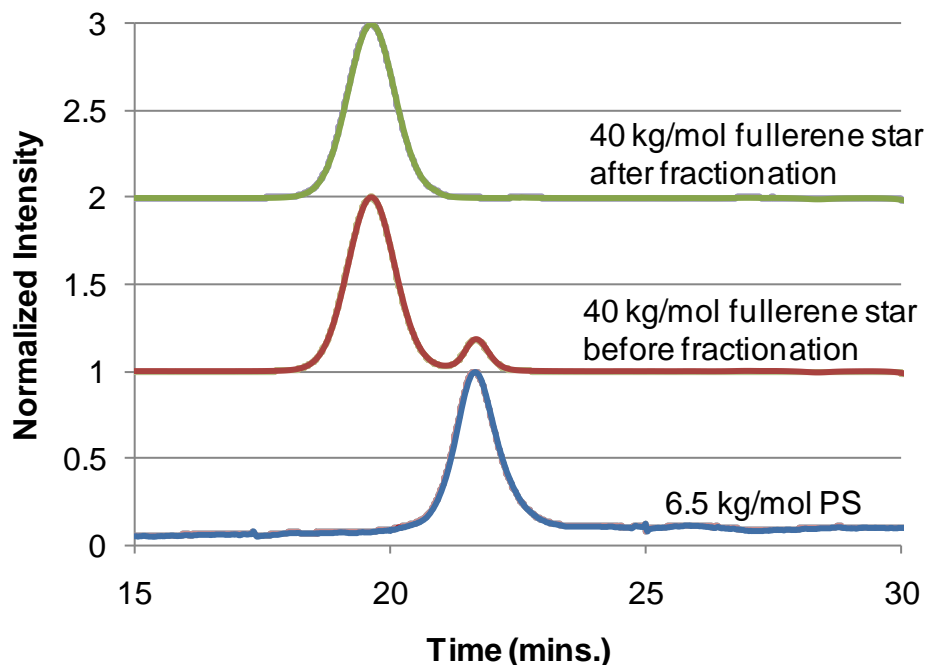


**Figure 5.3:** GPC chromatograms showing retention differences seen between the 6.5 kg/mol PS and 40 kg/mol  $C_{60}$  star.

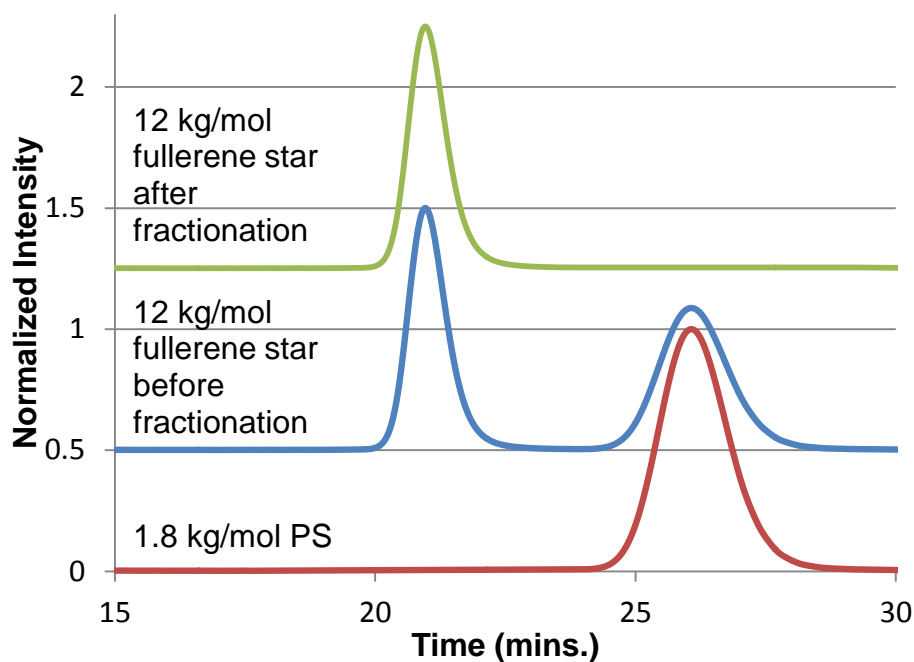


**Figure 5.4:** GPC chromatograms showing retention differences between the 1.8 kg/mol PS and 12 kg/mol C<sub>60</sub> star.

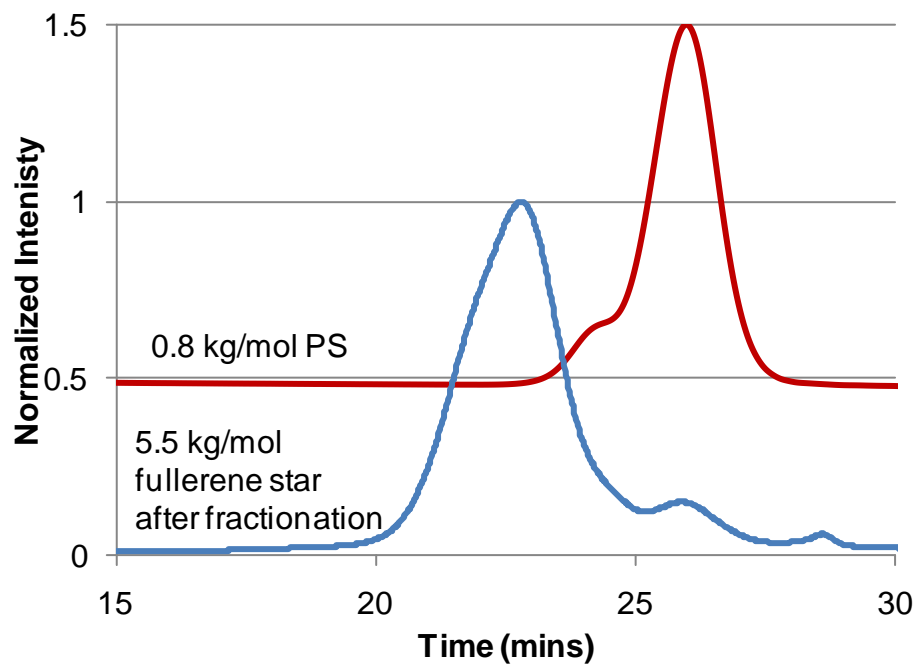


**Figure 5.5:** GPC chromatograms showing retention differences between the 0.8 kg/mol PS and 5.5 kg/mol C<sub>60</sub> star. Due to the close MW of the parent PS and the fullerene star, complete removal of the unreacted PS was not achieved.

Fractionation allowed for the separation and isolation of the stars from the excess of copolymer. However, as the molecular weight of each polymer graft is decreased, the separation of peaks between the fullerene star and the excess polymer become more overlapped due to lower separating resolution. This decrease in molecular weight separation also makes the isolation of the fullerene star through fractionation more difficult. As seen in the 5.5 kg/mol fullerene star sample, there is noticeable unreacted PS remaining in the product that was not extracted out. The  $M_n$  of all the fullerene stars is summarized in Table 5.2 which includes calculation of the weight loading of  $C_{60}$  in the molecule.

**Table 5.2:** Characterization data of the fullerene stars synthesized.

Fullerene	Type of polymer arms	# of added arms	$M_n$ of each PS arm (g/mol)	Maximum fullerene weight %
$C_{60}$	PS-PI	6	14.3K	0.8
$C_{60}$	PS	6	0.9K	11.8
$C_{60}$	PS	6	1.8K	6.3
$C_{60}$	PS	6	6.5K	1.8
$C_{60}$	PS	3	0.8K	21.1

The fullerene stars were analyzed by  $^{13}C$  NMR for structure confirmation. As shown in Figure 5.6, the  $^{13}C$  NMR for the 12 kg/mol shows the typical PS peaks associated with the repeating structure. The pure  $C_{60}$  shows up as a singlet at 143.2 ppm since all carbon molecules are equivalent. However, in the fullerene star small resonances appear around the fullerene peak at 143 ppm which suggests asymmetrical behavior now seen in the carbons on the cage of the fullerene. Assignment of the PS

peaks were determined based on the well-known chemical shifts of the carbons [152]. Due to low concentration these peaks were difficult to see. The 40 kg/mol star  $^{13}\text{C}$  NMR spectrum is similar except that the fullerene peak seen at 143 ppm is no longer apparent due to the lower concentration.

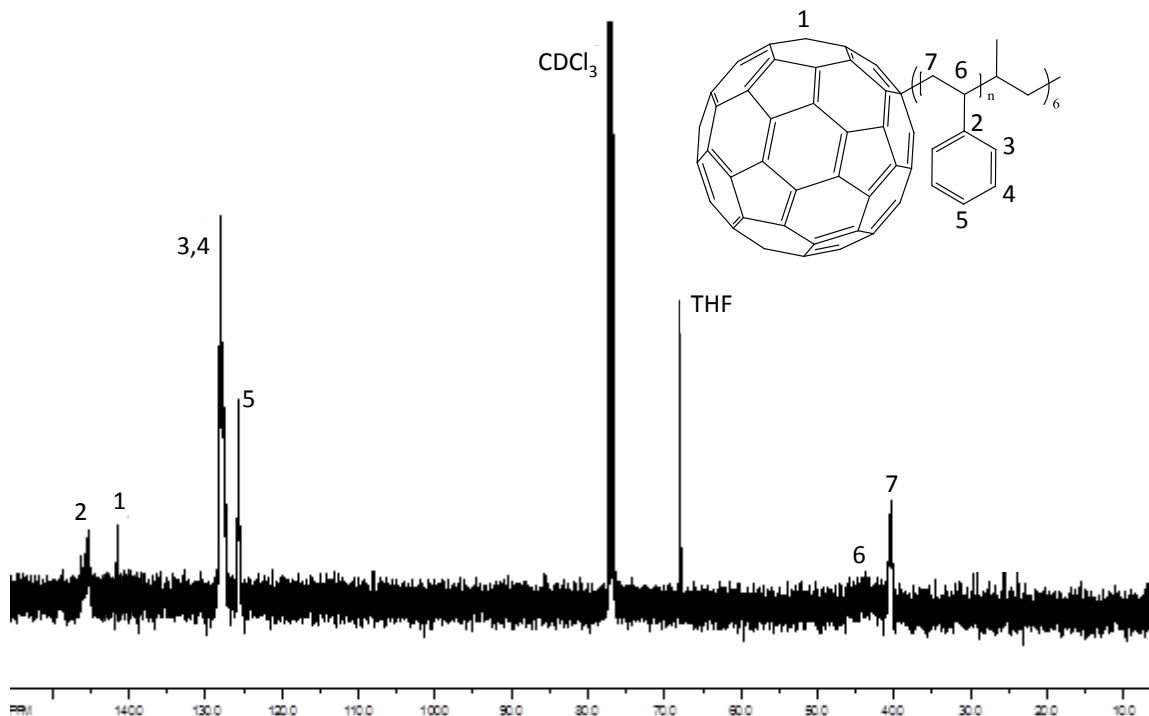


**Figure 5.6:**  $^{13}\text{C}$  NMR of the 12 kg/mol  $\text{C}_{60}\text{PS}_6$  stars.

By doing the same  $^{13}\text{C}$  NMR analysis on the 5.5 kg/mol fullerene, more peaks are seen due to the lower concentration of the repeating units of the PS which dominate in the other samples. Clearly, there are multiple resonances showing up in the fullerene region suggesting multiple resonances for the carbons on the cage. Also clearly seen are the peaks associated with the sec-butyl initiator with chemical shifts from 12-33 ppm. There should be only four peaks from the sec-butyl group; however, more peaks are seen suggesting other carbons are appearing in this region as well. Due to the overlapping

nature and broadening associated with polymers, accurate association of these peaks could not be made; therefore more in depth NMR techniques were used.

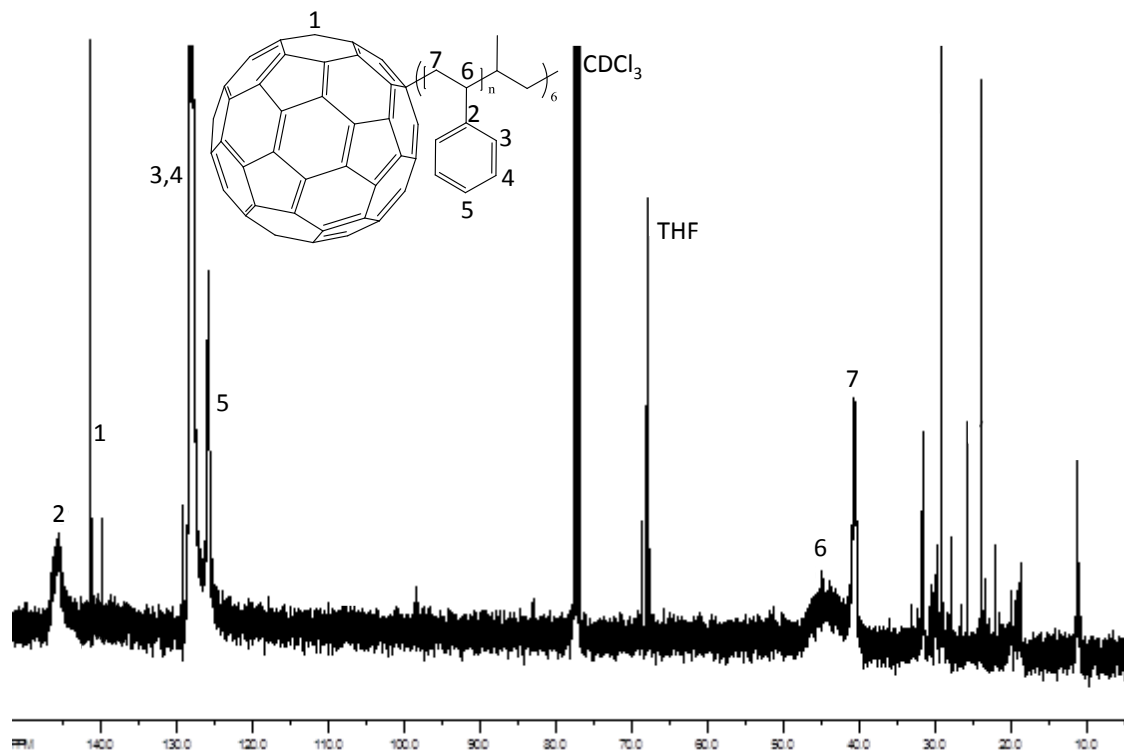


**Figure 5.7:**  $^{13}\text{C}$  NMR of the 5.5 kg/mol  $\text{C}_{60}\text{PS}_6$  star.

Further NMR analysis was done on the 5.5 kg/mol star using a technique termed heteronuclear single quantum coherence (HSQC). In HSQC experiments, the resulting two-dimensional spectrum shows the direct one-bond coupling between hydrogen and carbons atoms. As seen in Figure 5.8, the spectrum contains the carbon data along the y-axis and the proton information along the x-axis. By analyzing the cross peaks, the correlation between the carbon peaks in the 12-33 ppm can be determined. Interestingly, the carbon peaks around ~30 ppm show correlation to methyl peaks located on the backbone of the PS chains. This could suggest that the PS repeat unit that is directly

attached to the fullerene is shifted downfield due to the electron accepting behavior of the fullerene.

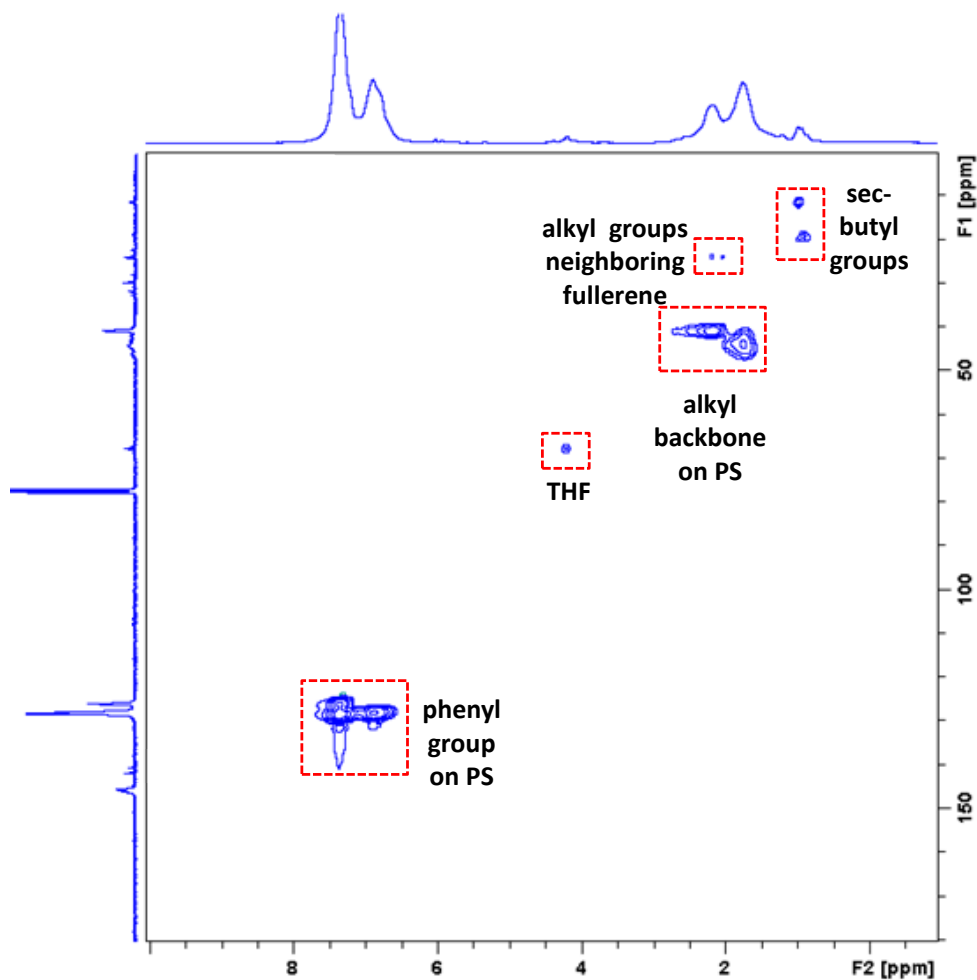


**Figure 5.8:** HSQC of the 5.5 kg/mol  $C_{60}PS_6$  star.

The thermal analysis of the fullerene stars was measured to observe the effect of adding the fullerene hard sphere to the short polymers. As shown in Figure 5.9 the glass transition temperatures,  $T_g$ , of the polymers were measured by DSC. From the results it can be concluded that the PS-modified fullerenes behave more like polystyrene chains of a molecular weight equivalent to the individual PS arms instead of like the total molecular weight of the molecule. This is probably due to the short length of the PS arms that do not

allow entanglement between the arms. This behavior has implications in terms of miscibility of the stars in a PS matrix as well as understanding the behavior of the stars in block copolymer systems.

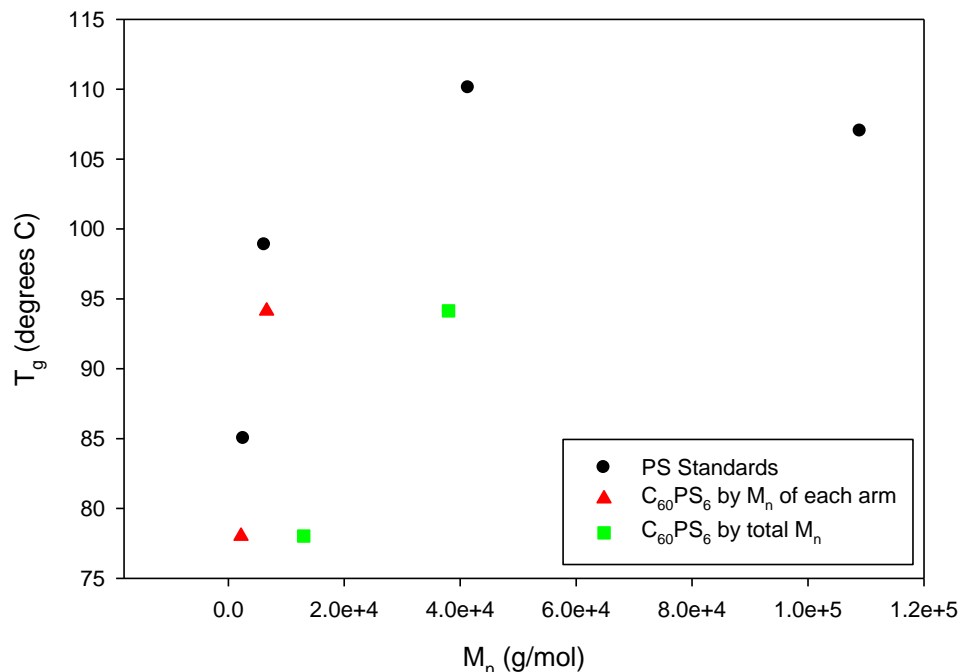


**Figure 5.9:** Glass transition temperature comparison between PS standards(●) and  $C_{60}PS_6$  stars. The  $C_{60}PS_6$  stars were plotted twice according to their single-arm  $M_n$  (▲) and total  $M_n$  (■) of the star.

Star-shaped polymers show many unique dynamic and static properties when compared to linear analogs [153-155]. Light scattering was used for analysis of how the fullerene stars behave in solution. The initial results of the fullerene stars dissolved in THF showed large particles (~200 nm) in solution even at low concentrations. This suggested that the stars were aggregating together potentially due to the inclusion of the insoluble fullerene core in THF reducing the solubility of the molecule. However, after dialyzing using a membrane that allowed for retention of molecules greater than ~100 nm, the single molecule fullerene stars could be analyzed. As shown in Figure 5.10, the

hydrodynamic radius,  $R_h$ , of the 40 kg/mol star was measured to be  $12 \pm 1$  nm. This result was compared with the theoretical calculation of the radius of gyration,  $R_g$ , of a 6-arm PS star with equal  $M_n$  as the fullerene star. There was substantial error seen in the measurements as the wave vector was increased. This could be due to the strong absorption of light by fullerenes. As shown in Appendix D, the calculated  $R_g$  of the 40 kg/mol star is 9.5 nm. This calculation however, does not take into consideration the size of the fullerene at the core of the stars. Therefore, the addition of the size of  $C_{60}$  (0.71 nm) to the theoretical value shows that the measured  $R_h$  using light scattering is likely. Further light scattering analysis was tried with the other fullerene stars in solution; however, the molecules showed a high tendency to form large aggregates even after dialysis preventing accurate data to be obtained on the size of the single molecules. The aggregation was apparent as the size of the PS arms was decreased further suggesting that lack of solubility was driving the aggregation phenomena.

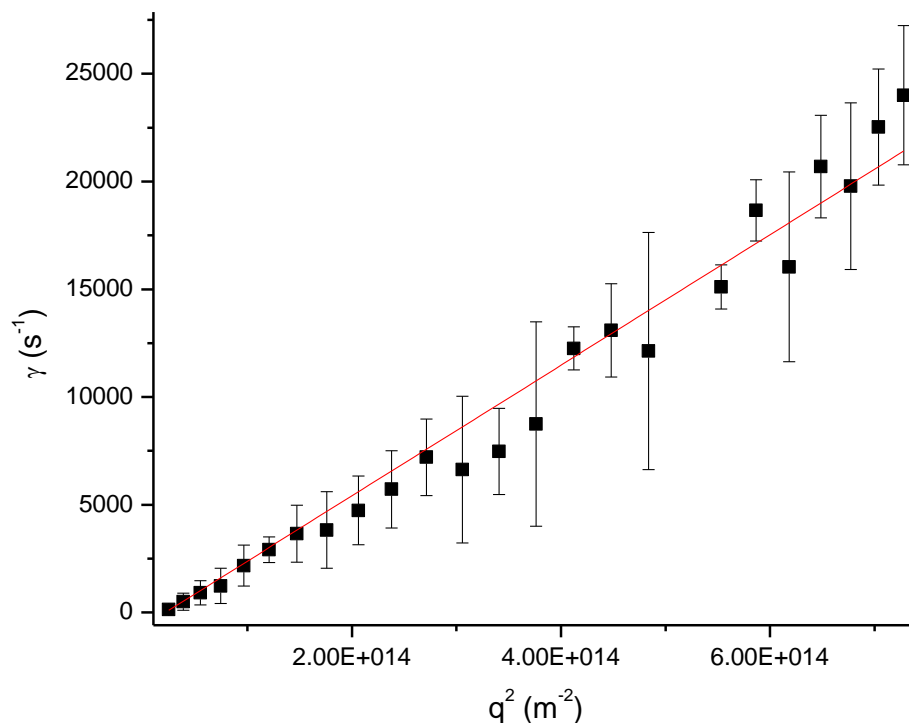


**Figure 5.10:** Dynamic light scattering results of the 40 kg/mol  $C_{60}PS_6$  stars after dialysis.

Wide angle x-ray scattering, WAXS, was used to characterize the ability to disperse the fullerene stars into a polystyrene matrix. Measurements were made on blends of 10, 20 and 50 wt% of the 12 kg/mol fullerene star. The WAXS data are shown in Figure 5.11 which indicates that full dispersion of the fullerene star in a PS matrix was achieved up to 50 wt%. This was concluded based on the lack of peaks in the blends that are known to occur from fullerene aggregation. In pure fullerene blends, these characteristic aggregation peaks begin appearing even at 1 wt% loading. Therefore, the addition of PS arms onto the cage greatly enhances the solubization of fullerenes. These results further suggest that we can incorporate large concentrations of fullerene stars into a polystyrene-based block copolymer system.

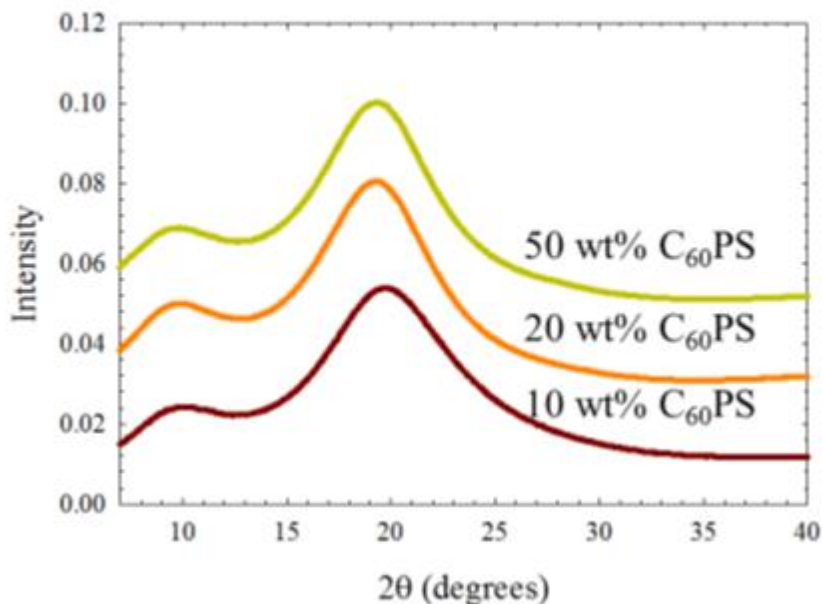


**Figure 5.11:** Wide angle x-ray scattering results for the 12 kg/mol C<sub>60</sub>PS<sub>6</sub> star blended with linear PS.

To understand the use of these fullerene stars in materials we investigated the effects of nanoparticle size on the phase behavior of a symmetric dPS-PMMA diblock

copolymer. For achieving control over desired morphology it is important to understand the dynamics that control the location and layer formation of the nanoparticle within the diblock copolymer matrix. For these measurements only the 40 and 12 kg/mol samples were analyzed. These fullerene stars were incorporated into a dPS-PMMA (15-b-15 kg/mol) diblock copolymer on both clean silicon and a PS brush layer grafted to silicon substrates. The two substrates were used to measure any differences obtained due to selectivity of the copolymer as silicon is PMMA selective while the PS brush is PS selective. The structures of the assembly in the thin films were investigated using neutron reflectivity (NR). The film thickness was also varied by controlling block copolymer concentration in solution for pure dPS-PMMA systems on both substrates.

The materials used for NR studies were selected specifically to allow for determination of the location of the fullerene stars by measured changes in the SLD at different loadings. For the fullerene star, the PS-arms were hydrogenated, where PS has a SLD of  $1.41 \times 10^{-6} \text{ \AA}^{-2}$ . Deuterated PS ( $6.41 \times 10^{-6} \text{ \AA}^{-2}$ ) has a vastly different SLD allowing for a detectable change. Although fullerene has a relatively high SLD,  $3.33 \times 10^{-6} \text{ \AA}^{-2}$ , it can be assumed that the behavior of the fullerene stars is dominated by the six grafted polymer chains. The location of the fullerene stars can be determined from data modeling because the SLD of the dPS block would be reduced due to the presence of hydrogenated  $C_{60}PS_6$ . Assuming the fullerene star remains in the PS phase, the SLD of the PMMA block should remain unchanged.

Comparing the NR profile of the 12 kg/mol ( $C_{60}PS_6$ -1) and 40 kg/mol ( $C_{60}PS_6$ -2) nanoparticle films on silicon, the development of a third Bragg peak at lower nanoparticle concentration is seen for the  $C_{60}PS_6$ -2. Figure 5.12 shows the reflectivity profiles for

both systems as a function of nanoparticle concentration. All samples were prepared from a 4 wt% polymer solution in toluene. A new structural peak for the  $C_{60}$  becomes evident at 33 wt% in the  $C_{60}PS_6-1$  while it appears at lower concentration of 17 wt% for the  $C_{60}PS_6-2$ . As seen in both materials after addition of the fullerene stars, a change in the lamellar repeat spacing is indicated by shifts in the Bragg peaks to smaller  $Q$  ( $\text{\AA}^{-1}$ ). Disruption to the lamellar structure is seen at 44 wt% in both systems as the Bragg peaks become indistinguishable at this nanoparticle concentration in the NR profile.

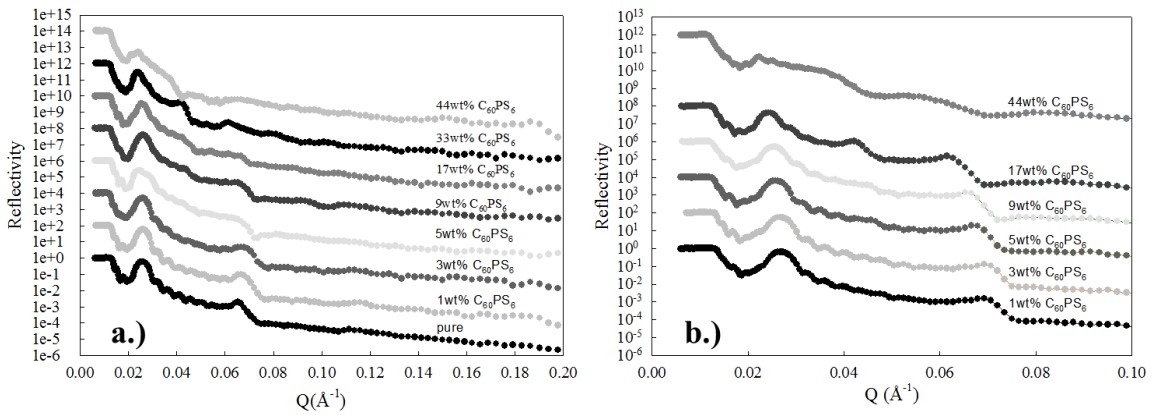


**Figure 5.12:** Reflectivity profiles for DPS-PMMA films. The concentration was varied with respect to the dPS block for a.) 12 kg/mol and b.) 40 kg/mol fullerene star.

A decrease in the SLD of the dPS block with increasing concentration of fullerene star is seen through quantitative analysis of the reflectivity profiles, which supports the model that the nanoparticles preferentially locate in the dPS block. At lower fullerene concentrations the reflectivity profiles can be fit by using a model of two layers where the dPS SLD is reduced with increasing concentration of stars. It is believed that the nanoparticles are located near the chain ends or the center of the dPS block. This assumption is based on the physical size of the layers and previous work on block

copolymer/homopolymer [156-163] and block copolymer/nanoparticle [164-175] systems. However, formation of a separate  $C_{60}PS_6$  layer is not evident at concentrations lower than 33 wt% for  $C_{60}PS_6$  1 or 17 wt% for  $C_{60}PS_6$  2 films. This is most likely due to the low concentration of fullerene stars which limits interactions with other particles. Therefore, the threshold for layer formation shows a dependence on both the size and concentration of the fullerene stars.

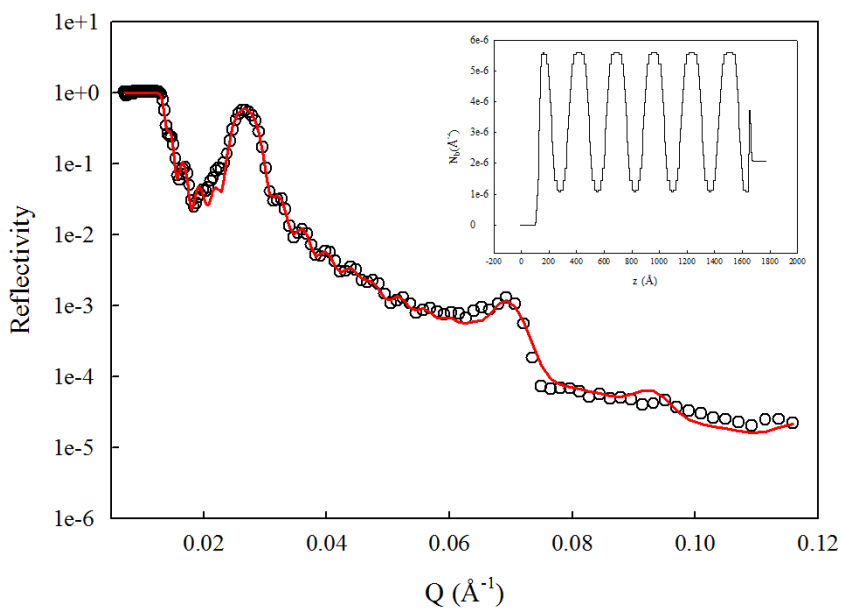


**Figure 5.13:** NR Profile of the 3 wt%  $C_{60}PS_6$  2 film including a modeled fit that determined the SLD profile as shown in the inset.

A data fitting procedure was used to determine the SLD profiles of the films. As seen in Figure 5.13 for the 3 wt%  $C_{60}PS_6$  2, the SLD determined from the experimental fits is shown in the insert. As evidenced by the SLD profiles, the fullerene stars appear to be evenly distributed among the layers showing no preferential diffusion toward the surface. This was concluded from the fact that the SLD of each dPS layer over the entire sample shows the same consistent reduction due to fullerene star inclusion into the layer. However, there is an increase in the surface roughness which is likely due to the

distortion of dPS chains from accommodating the fullerene stars into the domain. The surface distortion seen at the interfaces between the dPS and PMMA blocks is shown in Figure 5.14. At higher fullerene star concentrations there is an increase in the periodicity seen in this surface roughness. As the concentration of  $C_{60}PS_6$  stars increases in the dPS block, there is also some swelling of the dPS block similar to that seen with homopolymer/block copolymer systems [156-163].

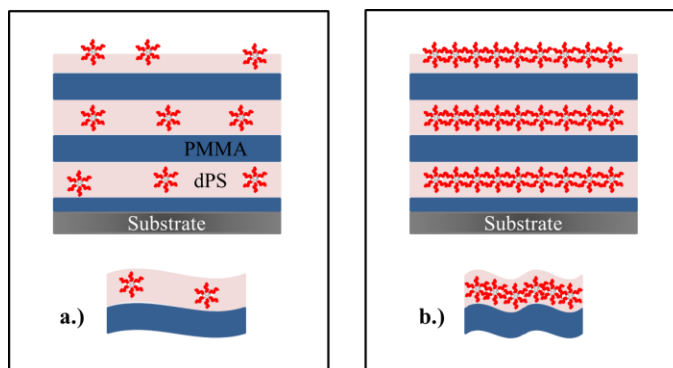


**Figure 5.14:** Illustration of the structure of the thin films at a.) lower star concentration and b.) high concentrations.

Modeling the new structural peak that developed at 17 wt% and 33 wt% for  $C_{60}PS_6$  1 proved to be more challenging. The layered dPS/PMMA model that was used for lower loadings of fullerene star did not fit the data in these high concentrated samples. In these cases there was a high enough concentration in which the fullerene stars could interact, so the data was fit using a model that assumes formation of dPS and PMMA layers with the fullerene stars forming a layer in the center of the dPS domain. The data fit at 17 wt% of  $C_{60}PS_6$  2 in Figure 5.15 shows the change in SLD of the dPS within the phase that is assumed to occur through formation of a fullerene star layer.

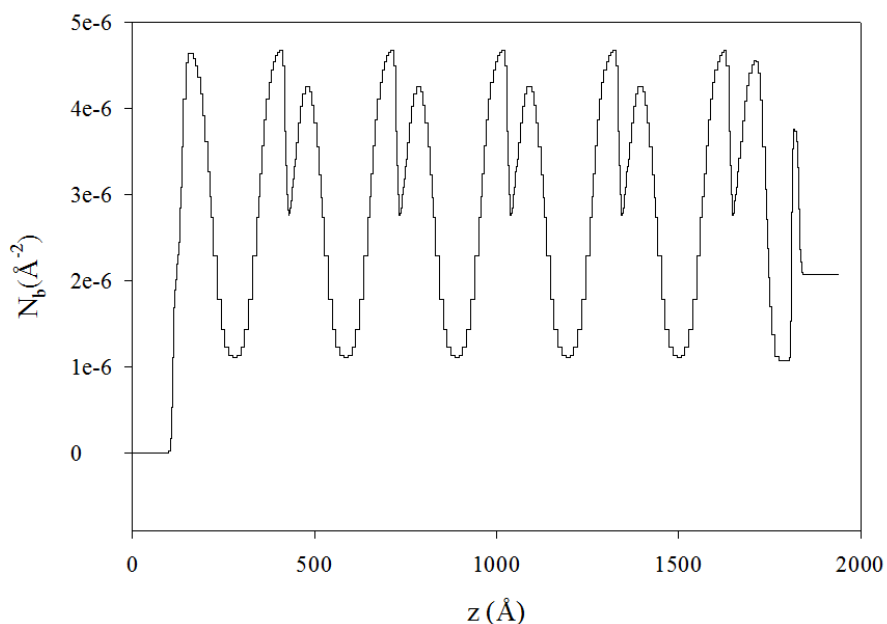


**Figure 5.15:** SLD profile using model fit for 17 wt% C<sub>60</sub>PS<sub>6</sub> in dPS-PMMA. The dips in SLD are due to the formation of layers of fullerene stars within the dPS layer.

## 5.5 Conclusions

The addition of six PS arms to the fullerene cage was successfully synthesized at varying arm molecular weights and these materials were characterized using GPC, NMR, and LS techniques. These fullerene stars showed improved solubility in common organic solvents and PS films. Pure fullerenes began to aggregate at weight concentrations exceeding 1% in PS. However, the WAXS studies on the fullerene stars did not show aggregation in the PS matrix up to 50 wt%.

Light scattering results provided characterization of the hydrodynamic radius in solution of the 40 kg/mol fullerene star. The results found in that experiment match well with the calculated values for a PS star polymer. Due to aggregation of the molecules, however, the use of LS to probe the size in solution of the smaller fullerene stars was not

achieved for the smallest fullerene stars. The thermal analysis results indicated that the  $T_g$  properties of fullerene stars behave like the PS homopolymers of equivalent molecular weight to the PS arms.

The neutron scattering experiments on the block copolymer/fullerene thin films have shown that we can confine fullerene stars of varying molecular weight in a symmetric block copolymer system. The formation of uniform layers is dependent on both size and concentration of fullerene star. Inclusion of a greater concentration of fullerene stars was shown to increase the roughness of the surface layers. These results have shown the promising ability to incorporate fullerene stars to a high degree into block copolymer films where the fullerene selectively incorporates into one of the layers.

Fullerene stars are a promising way of incorporating PS onto fullerene cages for greatly solubility allowing for higher concentrations of fullerenes to be incorporated into materials. Unfortunately in this method, the number of fullerenes that could be incorporated was diluted by the presence of the polymer arms. Only 6 wt% of the 12 kg/mol fullerene star was attributed to the fullerene cage. Therefore, out of the 50 wt% included in the PS matrix, only 3 wt% of the material was fullerene. However, future studies can look increasing this fullerene concentration by studying the dynamics of stars with fewer arms.

## CHAPTER 6

### ESR STUDIES ON ENDOHEDRAL FULLERENES USING TEMPLATING METHODS

#### 6.1 Introduction

The alignment studies of the resulting aligned fullerene materials can be studied by inclusion of a molecule in the complex that can be analyzed by electron spin resonance, ESR [176]. ESR is a form of microwave spectroscopy that is able to detect unpaired electrons at low concentrations [177]. The basic concepts of analyzing the electron spin states in ESR are similar to those used in NMR where the spin of the nuclei is measured. An electron has two spin quantum numbers, where  $m_s$  is defined as either  $1/2$  or  $-1/2$ , therefore, the spin can be aligned parallel or anti-parallel to an applied magnetic field. However, most stable molecules have all their electrons paired resulting in no signal being detected using ESR. Therefore, the type of molecules that can be studied with ESR is limited which confines its impact in the research domain than compared with NMR. When Equation 6.1 is satisfied, resonance is achieved between the two energy levels of an electron:

$$h\nu = g_e\mu_e B_0 \quad \text{Eq. 6.1}$$

where  $h$  is Planck's constant,  $\nu$  is the frequency (usually in GHz),  $g_e$  is the electron  $g$ -factor,  $\mu_e$  is the Bohr magneton, and  $B_0$  is the magnetic field strength. Therefore, the splitting of the energy is directly proportional to the magnetic field strength. A Maxwell-Boltzmann distribution is seen in the occupied population of electrons for the two energy levels as a higher number of the unpaired electrons reside in the lower energized state.

This results in more transitions occurring from the low to high energy state that creates a net absorption of energy.

In ESR the electron spins are dependent upon the surrounding environment. The unpaired electron spin is often delocalized around the area where it is centrally located. When an electron interacts with a nucleus of an appropriate spin, the electron undergoes interactions by way of its magnetic moment which allows for additional energy states to be occupied. This results in multi-lined spectra with the spacing between peaks defined by this interaction with perturbing nuclei. This process is analogous to the proton splitting often seen in  $^1\text{H}$ -NMR spectroscopy. The resulting splitting pattern is known as hyperfine coupling which is defined in Equation 6.2:

$$\text{hyperfine coupling} = 2MI + 1 \quad \text{Eq. 6.2}$$

where an electrons signal is split by equivalent nuclei,  $M$ , and the nuclear spin quantum number for the nuclei,  $I$ .

Endohedral fullerenes containing nitrogen isotopes have unpaired electrons that allow for detection with ESR. The  $^{14}\text{N}@C_{60}$  and  $^{15}\text{N}@C_{60}$  endohedral fullerenes have been successfully characterized with ESR [43].  $^{14}\text{N}$  ions have a nuclear spin of  $I=1$  while  $^{15}\text{N}$  ions have a nuclear spin of  $I=1/2$ . Therefore, the splitting behavior of the peaks from endohedral fullerenes containing different nitrogen isotopes is evident as  $^{14}\text{N}@C_{60}$  has three peaks and the  $^{15}\text{N}@C_{60}$  has only two. Also, endohedral fullerenes filled with nitrogen isotopes exhibit a zero field splitting that is dependent upon the orientation of the molecule in respect to the applied magnetic field [178, 179]. So, by analyzing the width of the zero field splitting, the degree of the orientation between the molecules can be observed. The obtained ESR spectrum of the  $^{14}\text{N}@C_{60}$  embedded into the MBBA

liquid crystals shows further splitting of the spectral lines [64]. This splitting is due to the orientation caused by the applied magnetic field. The orientation is achieved due to the change in the symmetry of the fullerene after interaction with the nematic liquid crystal.

ESR is a powerful technique despite being limited to a small amount of molecules that can be analyzed. Due to the unpaired electrons in endohedral fullerenes that make them potential candidates for functional quantum computers, ESR can be utilized to study the orientation of these unpaired electrons thereby allowing for characterization of the alignment in the material.

## 6.2 Materials

All  $^{14}\text{N}@C_{60}$  and  $^{14}\text{N}@C_{70}$  materials were obtained from collaborators at University of Oxford and used without further purification. Materials used in the synthetic procedures to align the endohedral fullerenes were the same as previously described in the corresponding chapters.

## 6.3 Experimental

### 6.3.1 Synthetic Procedures

**$^{14}\text{N}@C_{60}:\text{PS}_6$  star:** All steps were still performed within a pressurized Schlenk line under an inert Argon atmosphere. The anionic living polymerization of the 2.2 kg/mol PS was initiated by 3.47 mL of sec-BuLi addition to 9.72 g of styrene dissolved in freshly distilled toluene in a Schlenk tube. Upon addition of the initiator the solution turned orange which is consistent with the color of living styryl carbanions. Desired

molecular weights of the PS were achieved by controlling the stoichiometric addition of initiator to monomer. For the larger 6.2 kg/mol PS, 0.63 mL of sec-BuLi was added to 5.53 g of styrene. After reacting for 10 hours, a small amount of the living PS was removed from the Schlenk tube for molecular weight analysis by GPC. Once desired size of polymer was achieved, the living PS was added in 10-fold excess to 50 mg of C<sub>60</sub> dissolved in freshly distilled toluene and stirred for 2 hours. The color of the fullerene solution changed from purple to brown upon addition of the PS. Deactivation of the anionic charge on the cage of the fullerene was achieved by addition of methanol. Precipitation of the fullerene stars can be induced by further addition of methanol allowing for isolation through filtration.

**<sup>14</sup>N@C<sub>60</sub> and <sup>14</sup>N@C<sub>70</sub>:s-PMMA helical fibers:** The s-PMMA (10 mg) and <sup>14</sup>N@C<sub>60 or 70</sub> (11 mg) were dissolved in 1 mL of a (1:1) toluene:DCB co-solvent mixture at 110°C in a glass vial. At this elevated temperature the dissolved polymer chains and the fullerene molecules were interacting [72]. After complete solvation and mixing for 10 minutes at the elevated temperature, the vial was then removed from the heating source and allowed to cool to room temperature. The fullerene encapsulation occurs as a gel is formed when the s-PMMA chains stiffen as they become less soluble in the solvent at lower temperatures. The gel was then transferred to a centrifuge tube and spun at 2500 rpm for 30 minutes at room temperature. This caused the gel to condense to the bottom of the tube by separating from the solvent mixture. The supernatant liquid was decanted out of the centrifuge tube. Two washes to remove the fullerene molecules not encapsulated within the polymer helix were performed in the centrifuge tube by further additions and centrifuging with 1 mL co-solvent at 2500 rpm for 30 minutes. After each

wash, the supernatant again was poured off and collected in order to determine gravimetric recovery of fullerene not encapsulated within polymer.

Heated electrospinning experiments were performed using a heated syringe which is discussed later in section 3.2.2. After collection of the condensed gel, the complex was dried under vacuum at 60°C for 12 hours to remove solvent. Then the complex was added back into a (1:1:1) toluene:DCB:DMF solvent mixture at a complex concentration of 20 wt. % at 110°C for 10 minutes. The use of DMF helps maintain uniform fiber diameters as it has a higher dielectric constant than the other solvents, which aids in preventing charge buildup, which is further discussed in section 3.3.2.1. Once in solution, addition to the already heated syringe at 110°C was achieved by pouring into the syringe barrel instead of sucking up through the needle. After the solution was sucked through the needle, rapid heat loss occurred within the solution which resulted in an increase of gelation and thus, caused the needle to become clogged. By removing the plunger and pouring directly into the syringe barrel, the clogging effect was negated. Once the solution was within the syringe, the barrel was placed back into the heated syringe and the trapped air was expelled by pushing in the plunger while holding the syringe upside down with heat resistant gloves. Once the air was removed, the syringe was placed back in the heated oil jacket to maintain the elevated temperature of the mixture. The syringe pump was then started at the 1 mL/hr flow rate and the electrical clamps needed for applying voltage to needle were attached in order to apply charge. The additional processing conditions used during the electrospinning process are discussed in the following section.

### 6.3.2 Instrumentation

EPR analysis was conducted at room temperature using a Bruker EMX spectrometer equipped with a Bruker HS4119 high sensitivity cavity. All samples were measured in a 5mm quartz EPR tube. The temperature of the cavity was maintained with a stream of dry nitrogen.

## 6.4 Results and Discussion

To analyze the ability to align fullerenes using the templating methods discussed in previous chapters, materials containing endohedral fullerenes were prepared and measured with ESR. Unfortunately due to the difficulties associated with the synthesis of endohedral fullerenes, a very limited amount of material was available. The limited availability meant the synthetic procedures had to be scaled accordingly. Due to the poor stability of the endohedral fullerenes in strained environments, all aligning procedures were done to minimize light and elevated temperatures. As shown in Figure 6.1, the typical three peak spectrum is seen for the unmodified  $^{14}\text{N}@C_{60}$  in toluene used in the alignment studies.

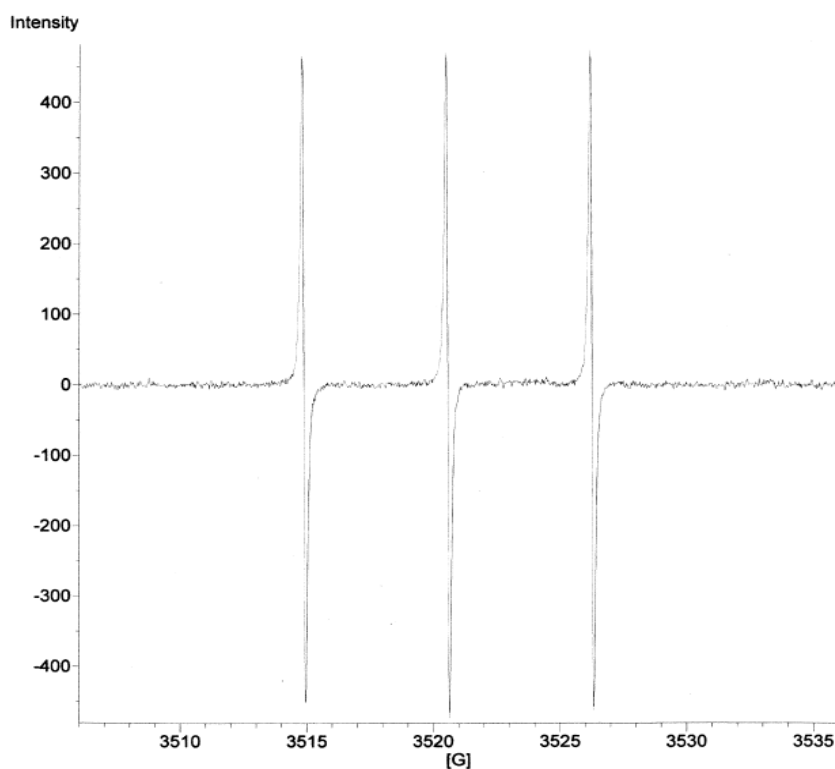


**Figure 6.1:** ESR spectrum of pure  $^{14}\text{N}@C_{60}$  dissolved in toluene.

The grafting of PS arms on the cage of the fullerene was the first method studied with  $^{14}\text{N}@C_{60}$ . Successful synthesis of the fullerenes stars with six PS arms of 1 kg/mol molecular weight grafted to the cage was achieved. As shown in Figure 6.2, the GPC chromatogram shows that the isolated fullerene star. A solution of this sample was measured in the ESR; however, there was no detectable signal from the sample. Unfortunately, this suggests that the chemical reactions that take place on the cage comprise the stability of the  $^{14}\text{N}$  ions.

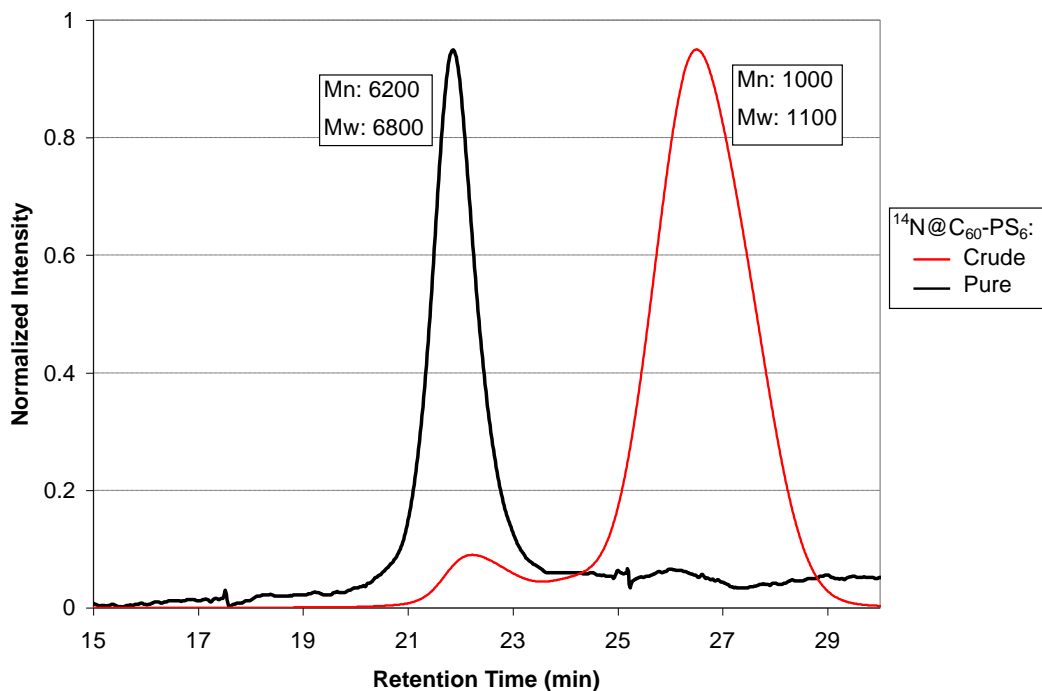


**Figure 6.2:** GPC of the N@C<sub>60</sub> product after attachment of PS arms to cage.

The other templating method analyzed with ESR was the electrospinning of the fibers containing the encapsulated fullerenes. As shown in Figure 6.3, the collection of the fibers used sticky tape to ensure the imposed orientation was maintained during the characterization with ESR. Due to the low amount of endohedral fullerene used in the experiments, multiple stripes of tape had to be stacked in order to increase the concentration in order to see the signal. The tape was then rolled into a cylinder in order to fit into the ESR tube. Analyzing the sample with respect to the applied magnetic field will potentially give important information about the asymmetrical interaction of the endohedral element. In order to control the orientation of the sample, the tape was either placed with a vertical or horizontal configuration in regards to the ESR tube length.

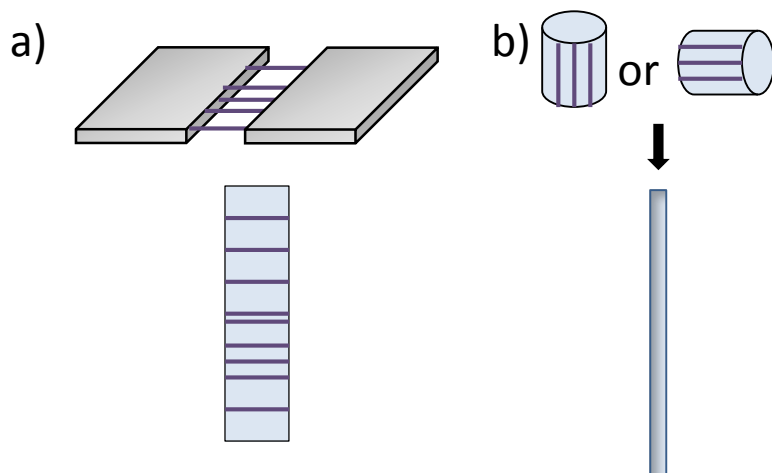


**Figure 6.3:** Method of maintaining the alignment achieved by a) collecting the electrospun fibers on a piece of tape and b) rolling up the tape and orienting the sample with respect to the magnetic field.

Figure 6.4 shows the ESR spectrum obtained from the inclusion of  $^{14}\text{N}@C_{60}$  into the electrospun fibers. The sample was orientated vertically along the sample tube length. The spectrum clearly shows the typical three peaks associated with the  $^{14}\text{N}@C_{60}$ . Therefore, this shows that endohedral nitrogen was able to survive the heating involved with making the complex and electrospinning the gel. Due to the fact that the  $^{14}\text{N}@C_{60}$  molecules are in the solid phase in the fibers, the spectral peaks are broadened. A separate sample was measured in order to see any effect on the spectrum due to the orientation in respect to the magnetic field.

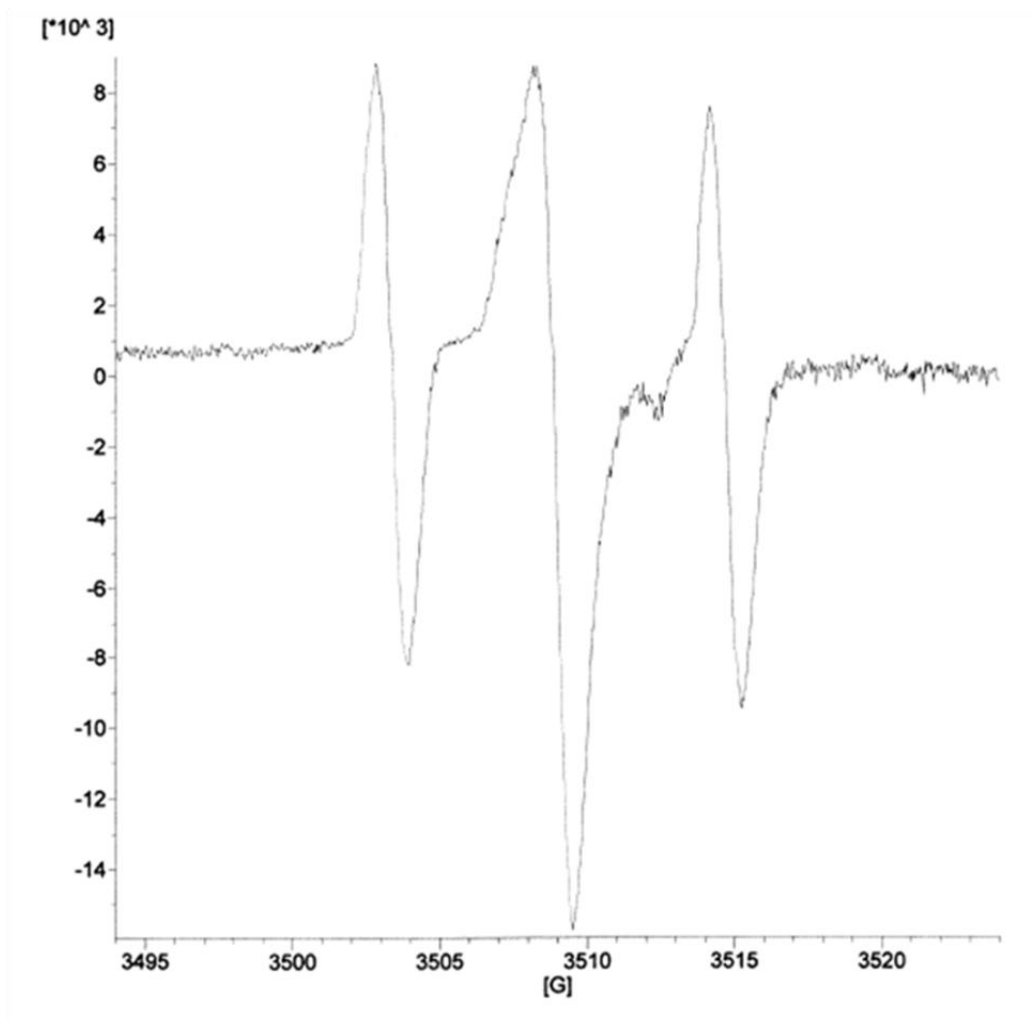


**Figure 6.4:** ESR spectrum of s-PMMA electrospun fibers containing  $^{14}\text{N}@C_{60}$  vertically aligned within quartz tube.

As shown in Figure 6.5, the spectrum of the horizontally aligned fibers also contains the typical three peaks. Due to a much lower concentration of fibers contained within the ESR tube, the intensity of the peaks is greatly reduced resulting in less spectral resolution. Therefore, it is difficult to compare the samples however, they do appear to have the same shape. This would indicate that the fullerene cage is not distorted during the encapsulation which would create asymmetrical behavior that would influence the  $^{14}\text{N}@C_{60}$ . Although the spectra have a similar shape there are some noticeable

differences in the width of the outside peaks. The vertically aligned sample has much wider peak width when compared with the middle peak than the horizontally aligned samples. Spectra simulations were done by colleagues at Oxford University to try and model this result. Unfortunately, there are no concluding results at this time that suggest why a change in the peak width is evident.

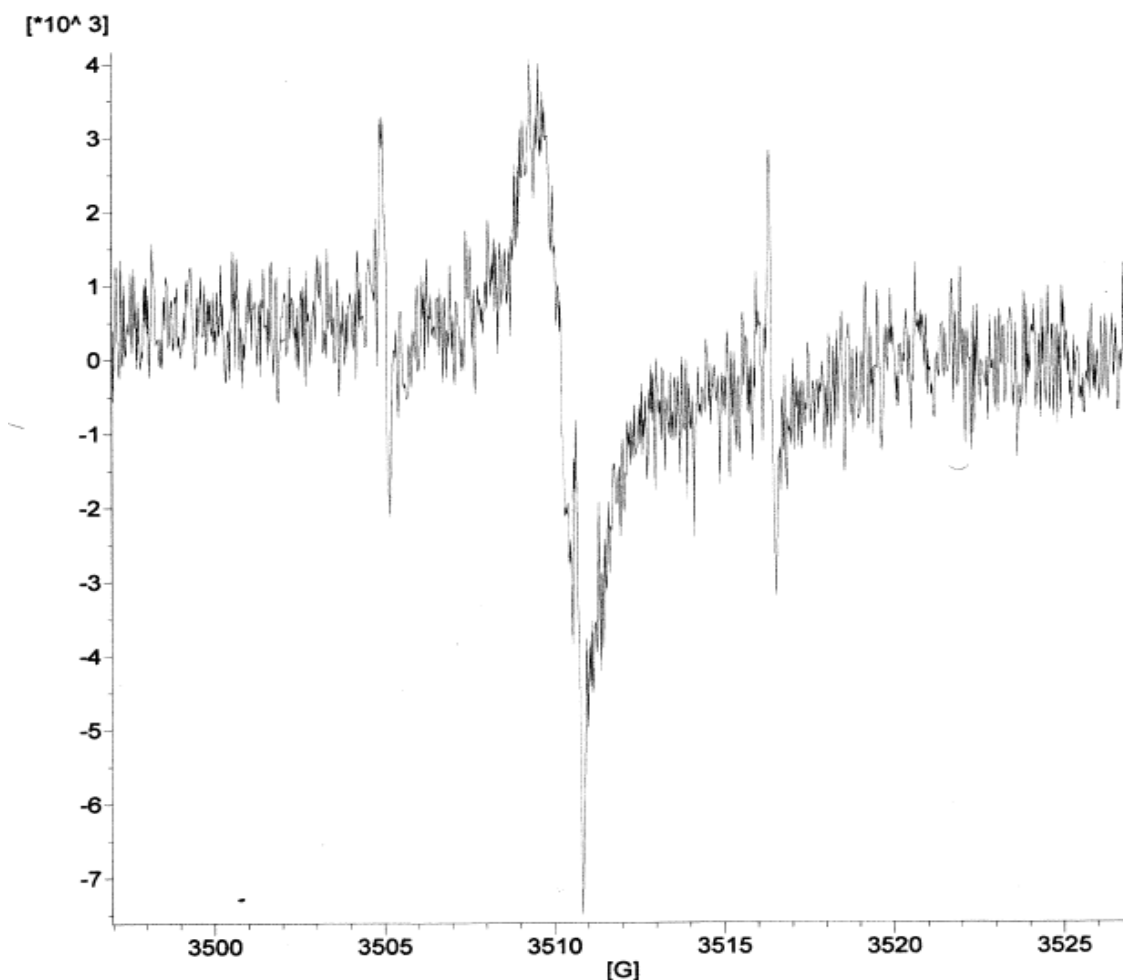


**Figure 6.5:** ESR spectrum of s-PMMA electrospun fibers containing  $^{14}\text{N}@C_{60}$  horizontally aligned within quartz tube.

The ability to electrospin fibers containing  $^{14}\text{N}@C_{70}$  was also analyzed. As seen in Figure 6.6, the ESR spectrum still contained the typical three peaks associated

with the  $^{14}\text{N}$  ions. Due to the presence of the peaks, the conclusion was made that the  $^{14}\text{N}@C_{70}$  molecule can also survive the synthetic procedure. The general shape of the spectrum is similar to the other samples measured; however, the peak width of the outside peaks is similar to the vertically aligned  $^{14}\text{N}@C_{70}$  which may further suggest this is due to the imposed orientation. Additional studies with higher concentration of endohedral fullerenes in the fibers would further help to understand any imposed orientation using electrospinning.

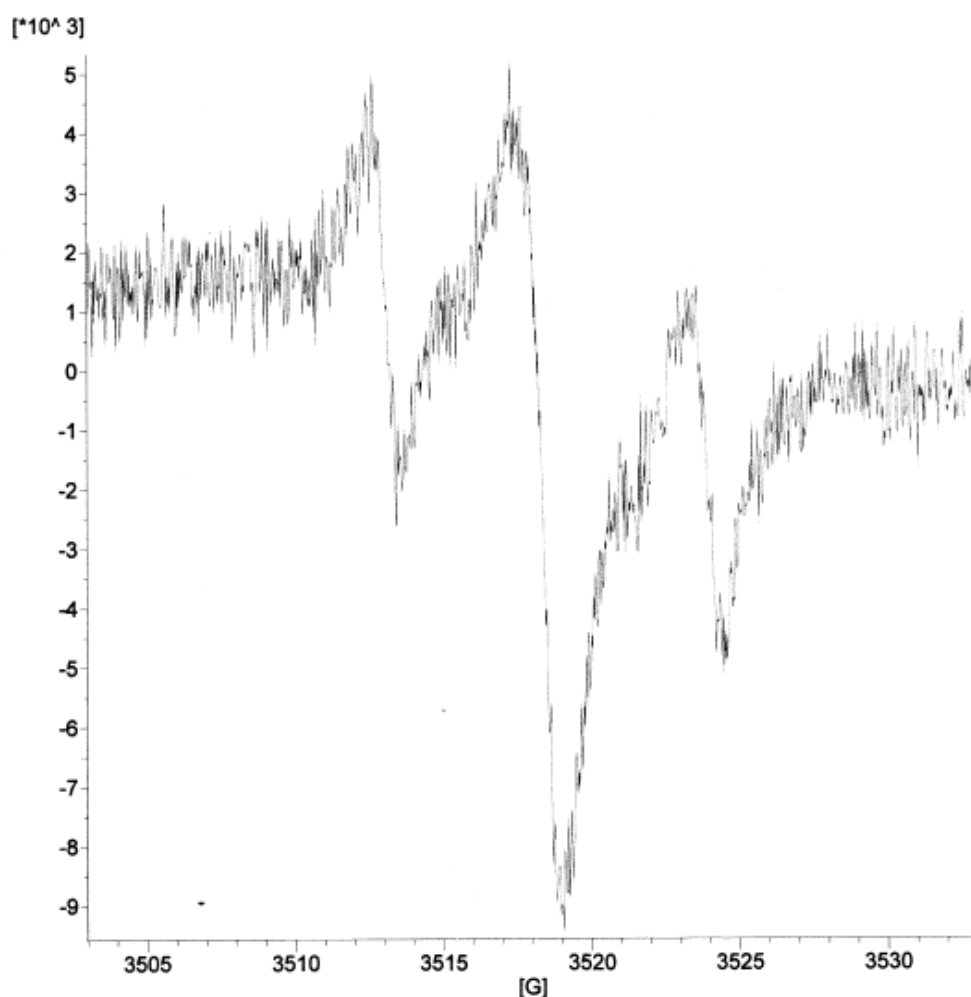


**Figure 6.6:** ESR spectrum of s-PMMA electrospun fibers containing  $^{14}\text{N}@C_{70}$  vertically aligned within quartz tube.

## 6.5 Conclusions

The use of ESR to study the induced orientation in materials produced by the alignment templates discussed in early chapters was analyzed. Unfortunately, the stability of the  $^{14}\text{N}$  ion seemed to be jeopardized as there were no evident peaks in the ESR of the fullerene star solution. This result is not surprising as endohedral fullerenes has been shown to undergo reactions in most chemical procedures. This concludes that this method of alignment is not suited for aligning systems containing  $^{14}\text{N}$  ions.

Better results were seen in the samples prepared using the electrospinning method as the typical three peak pattern was seen in all the samples analyzed. The samples were analyzed by controlling the orientation of the fibers with respect to the applied magnetic field. There was no appearance of additional splitting in the peaks in the aligned fibers which would suggest a defined orientation. However, this could be due to the lack of strain induced on the fullerene cage that led to the asymmetrical behavior as seen in previous work [64]. Despite the lack of splitting seen in the ESR spectra, there were noticeable changes in the peak width between the vertically and horizontally aligned samples which could suggest

## CHAPTER 7

### CONCLUSIONS AND FUTURE WORK

#### 7.1 Conclusions

The goal of this research was to create functional nanomaterials by incorporating fullerenes into self-assembling systems by using interactions with other molecules. One potential application of these materials would be for quantum computing which would utilize the ability to manipulate the spin behavior of the endohedral element. A high degree of alignment is needed between the fullerenes in order to allow the spins to undergo the entanglement phenomena. Previous techniques used to align fullerenes have been proven ineffective in the ability to create the desired materials. The three techniques analyzed in this work were the incorporation of fullerenes into electrospun fibers, supramolecular polymer formation with cyclodextrins, and inclusion of within block copolymers after polymer grafting to the cage.

##### 7.1.1 Electrospinning of Fullerene Encapsulated Fibers

- Electrospun fibers were shown to contain encapsulated fullerene within the helical forming s-PMMA fiber by DSC. The melting transition due to the fullerene encapsulation was evident upon the first heating step but did not appear during the second heating cycle due to loss of encapsulation.
- The formation of the encapsulated complex with s-PMMA is much more favorable than using carbon nanotubes. The inclusion of fullerenes into carbon nanotubes requires use of either high temperature or an ionic liquid

which limits the type of endohedral fullerene can be used in that system. The synthetic procedure used in formation of the aligned s-PMMA fibers is much more advantageous for the nitrogen containing endohedral fullerenes.

- SEM confirmed uniform fiber formation and showed the high degree of macro-scale orientation seen in the fibers when collected using the split electrode method.
- WAXS results showed that high orientation factors are reached when the s-PMMA due to increased rigidity from the encapsulation of the fullerene.
- The C<sub>60</sub> fibers contained a greater degree of orientation compared to the C<sub>70</sub> fibers probably due to the higher concentration of C<sub>60</sub> encapsulated.
- The alignment achieved in these fibers could potentially create useful materials for use in quantum computing.

### **7.1.2 Supramolecular Cyclodextrin:Fullerene Complex**

- The reversible inclusion complex that facilitates the supramolecular assembly is formed at room temperature through non-covalent interactions. Formation under these inert conditions makes this method of self-assembly an ideal candidate for use with less stable endohedral fullerenes.
- The inclusion complex of C<sub>60</sub> with a  $\beta$ -CD dimer was analyzed which showed an increase in the viscosity of dilute solutions. The complex size

in solution was measured with LS which determined the  $R_h$  of the complex to be ~220 nm.

- From the TEM images, the supramolecular chains are believed to aggregate into micron sized bundled structures. The formation of these structures was only evident after inclusion of fullerene as the cyclodextrin dimer did not show any chain formation resulting from self-aggregation.
- Due to the 1:1 molar concentration of the fullerene and cyclodextrin dimer in the supramolecular polymer, this alignment approach offers a higher weight percent of fullerene (~23%) when compared to other approaches. Another positive for using this method is that the inclusion complex forms at room temperature under rather inert conditions.

### **7.1.3 Synthesis and Inclusion of Fullerene Stars into a Polymer Matrix**

- These fullerene stars showed improved solubility in common organic solvents and PS films. The WAXS studies on pure fullerenes began to aggregate at weight concentrations exceeding 1wt% in PS however; the fullerene stars did not show aggregation in the PS matrix up to 50 wt%.
- Light scattering results of the fullerene star in solution provided a size of  $12 \pm 1$  nm for the  $R_h$ . The results found in that experiment matched well with the calculated values of the  $R_g$  for a PS star polymer.
- The neutron scattering results on the block copolymer/fullerene thin films showed that the fullerene stars were confined to the PS block in the symmetric block copolymer. The formation of uniform layers was found

to be dependent on both size and concentration of fullerene star. At higher concentrations of the fullerene stars, the surface roughness between the blocks became more evident. At the highest concentrations of the fullerenes star, segregation of the fullerenes stars to the middle of the PS layer was concluded due to the dip seen in the SLD profile.

- Inclusion of fullerene stars proved to be a good method of confining the fullerene to specific regions within a material. This approach would be useful were unique architectures of fullerene based materials are needed. However, due to the dilution of the fullerene with the polymer arm, only low concentrated materials could be made.

#### **7.1.4 ESR Studies on Endohedral Fullerenes Using Templating Methods**

- ESR was used to study the  $^{14}\text{N}$  and  $^{15}\text{N}$  endohedral fullerenes that were aligned using the approaches discussed.
- Unfortunately, the stability of the  $^{14}\text{N}$  ions were jeopardized during the anionic reaction of the grafting of PS arms on the cage. The ESR spectrum of a solution of the fullerene stars revealed no characteristic peak associated with the unpaired electrons in the nitrogen atom.
- Electrospun fibers containing  $^{14}\text{N}@C_{60}$  and  $^{14}\text{N}@C_{70}$  were prepared and the signal due to the endohedral element was still apparent after the fibers were aligned. The spectra showed slight differences in the peak width between the vertically and horizontally aligned fibers which could suggest some orientation dependence on the fibers.

## **7.2 Recommendations for Future Work**

### **7.2.1 Electrospinning of Fullerene Encapsulated Fibers**

- One method to improve the concentration of fullerenes with the polymer chains would be to synthesize s-PMMA chains that had a higher degree of syndiotactic content. Commercially available s-PMMA polymers only contain a maximum concentration of 85% syndiotactic content. Some polymerization techniques will allow for a higher syndiotactic content to be acquired in the PMMA [180, 181].
- One issue with this method is that inclusion of fullerene dimers with the helix of the PMMA is not seen. A method to try and incorporate alignment in systems containing fullerenes dimers would be to electrospin using a polyamide. Research has shown that photochromic molecules that have a high aspect ratio have been shown to orient when embedded in electrospun nylon fibers [182, 183]. The fullerene dimers also have a high aspect ratio so the inclusion and alignment of these molecules in nylon fibers can be studied.

### **7.2.2 Supramolecular Cyclodextrin:Fullerene Complex**

- The supramolecular chain formation found between the cyclodextrin and fullerene is quite intriguing. A study on the control of the length formed by these molecules would prove useful in determining the aspect ratio of the chains. By adding in varying amounts of the unmodified  $\beta$ -CD, the length of the supramolecular complex can be controlled. Shorter chains

may behave more rod-like which would allow for greater alignment within a liquid crystalline material.

- Another study could be on the use of a  $\gamma$ -CD dimer which should have a higher association constant with the fullerene [184]. The increases association should lead to longer chains being formed compared with those formed with the bis  $\beta$ -CD.

### **7.2.3 Synthesis and Inclusion of Fullerene Stars into a Polymer Matrix**

- A method to increase the concentration of the fullerene in the star molecules would be to reduce the amount of arms attached to the surface. This is controlled by the stoichiometric ratio of addition of the PS arms to the fullerenes in solution. By only double the amount of PS compared to the fullerenes should make fullerenes stars with 1-3 arms. A larger distribution in the average number of PS chains attached to the cage would result, but the overall fullerene concentration could be tripled. The behavior of these fullerene stars with fewer amounts of PS arms would be interesting to measure in the block copolymers. If too much of the fullerene cage is exposed then it can possibly aggregate together with other molecules decreasing the control over the alignment of the fullerenes.

#### **7.2.4 ESR Studies on Endohedral Fullerenes using Templating Methods**

- The interesting results seen in the peak width of ESR spectra for the vertically and horizontally aligned fibers merit more detailed analysis. By having more endohedral sample to work with would allow for greater concentration of signal to be detected in the sample. This increased signal would allow for higher resolution of the spectra. Continued work on modeling the spectra through simulations may prove useful in understanding any impact the alignment has on the signal of the endohedral nitrogen molecules.

## APPENDIX A

### s-PMMA:FULLERENE COMPLEX CALCULATIONS

Yields:

Starting materials: 110 mg C<sub>60</sub>, 100 mg s-PMMA, 5 mL 1,2-dichlorobenzene, 5 mL toluene

Recovered C<sub>60</sub> after gelation from washes with toluene: 85.8 mg

Remaining C<sub>60</sub> in gel: 110 mg - 85.8 mg = 24.2 mg

Calculation of weight % of C<sub>60</sub> in the gel:

$$\frac{24.2 \text{ mg C}_{60}}{123.4 \text{ mg gel}} = 19.6\% \text{ C}_{60}$$

Starting materials: 30.5 mg C<sub>70</sub>, 27.7 mg s-PMMA, 1.4 mL 1,2-dichlorobenzene, 1.4 mL toluene

Recovered C<sub>70</sub> after gelation from washes with toluene: 25.7 mg

Remaining C<sub>70</sub> in gel: 30.5 mg - 25.7 mg = 4.8 mg

Calculation of weight % of C<sub>70</sub> in the gel:

$$\frac{4.8 \text{ mg C}_{70}}{32.7 \text{ mg gel}} = 14.7\% \text{ C}_{70}$$

% of s-PMMA Helical Space Filled with C<sub>60</sub>

Using 19.6 weight % C<sub>60</sub> in encapsulated fiber complex

Out of 10 mg of sample:

8.04 mg is s-PMMA

1.96 mg is C<sub>60</sub>

Using molecular weight of each molecule:

$$\frac{8.04 \text{ mg s-PMMA}}{50 \text{ kg/mol}} = 0.16 \text{ } \mu\text{mol s-PMMA}$$

$$\frac{1.96 \text{ mg C}_{60}}{720 \text{ g/mol}} = 2.7 \text{ } \mu\text{mol C}_{60}$$

Using molecular weight of monomer unit:

$$\frac{8.04 \text{ mg s-PMMA}}{100 \text{ g/mol}} = 8.04 \times 10^1 \text{ } \mu\text{mol repeat units of PMMA}$$

Assuming 100% of the helical space filled:

$$(85\% \text{ syndiotactic content}) * (8.04 \times 10^1 \text{ } \mu\text{mol repeat unit of PMMA}) \\ = 6.8 \times 10^1 \text{ } \mu\text{mol syndiotactic repeating units in PMMA}$$

Length of molecules:

C<sub>60</sub>: 1.034 nm

One helical turn (18.5 monomer units): 0.947 nm

Number of helical turns per C<sub>60</sub>:

$$\frac{0.947 \text{ nm}}{1.034 \text{ nm}} = 0.915 \text{ helical turns per C}_{60}$$

Number of monomer units per C<sub>60</sub>:

$$\frac{18.5 \text{ monomer units per helical turn}}{0.915 \text{ helical turns per C}_{60}} = 20.2 \text{ monomers per C}_{60}$$

Using 20.2:1 ratio of PMMA monomer units per C<sub>60</sub>:

$$\frac{(6.8 \times 10^1 \text{ } \mu\text{mol syndiotactic repeating units in PMMA})}{20.2 \text{ s-PMMA monomer units/C}_{60}} = 3.4 \text{ } \mu\text{mol C}_{60}$$

Comparing actual concentration to 100% filled:

$$\frac{2.8 \text{ } \mu\text{mol C}_{60}}{3.4 \text{ } \mu\text{mol C}_{60}} = 0.82$$

82% of the helical space is filled in the electrospun fibers with C<sub>60</sub>

% of s-PMMA Helical Space Filled with C<sub>70</sub>

Using 14.7 weight % C<sub>70</sub> in encapsulated fiber complex

Out of 10 mg of sample:

8.53 mg is s-PMMA

1.47 mg is C<sub>70</sub>

Using molecular weight of each molecule:

$$\frac{8.53 \text{ mg s-PMMA}}{50 \text{ kg/mol}} = 0.17 \text{ } \mu\text{mol s-PMMA}$$

$$\frac{1.47 \text{ mg C}_{70}}{840 \text{ g/mol}} = 1.8 \text{ } \mu\text{mol C}_{70}$$

Using molecular weight of monomer unit:

$$\frac{8.53 \text{ mg s-PMMA}}{100 \text{ g/mol}} = 8.53 \times 10^1 \text{ } \mu\text{mol repeat units of PMMA}$$

Assuming 100% of the helical space filled:

$$(85\% \text{ syndiotactic content}) * (8.53 \times 10^1 \text{ } \mu\text{mol repeat unit of PMMA}) \\ = 7.3 \times 10^1 \text{ } \mu\text{mol syndiotactic repeating units in PMMA}$$

Length of molecules:

C<sub>70</sub>: 1.13 nm (longer diameter), 1.05 nm (shorter diameter)

One helical turn (18.5 monomer units): 0.947 nm

Number of helical turns per C<sub>70</sub>:

$$\frac{0.947 \text{ nm}}{1.13 \text{ nm}} = 0.838 \text{ helical turns per C}_{70}$$

Number of monomer units per C<sub>70</sub>:

$$\frac{18.5 \text{ monomer units per helical turn}}{0.838 \text{ helical turns per C}_{70}} = 22.1 \text{ monomers per C}_{70}$$

Using 20.2:1 ratio of PMMA monomer units per C<sub>70</sub>:

$$\frac{(7.3 \times 10^1 \text{ } \mu\text{mol syndiotactic repeating units in PMMA})}{22.1 \text{ s-PMMA monomer units/C}_{70}} = 3.3 \text{ } \mu\text{mol C}_{70}$$

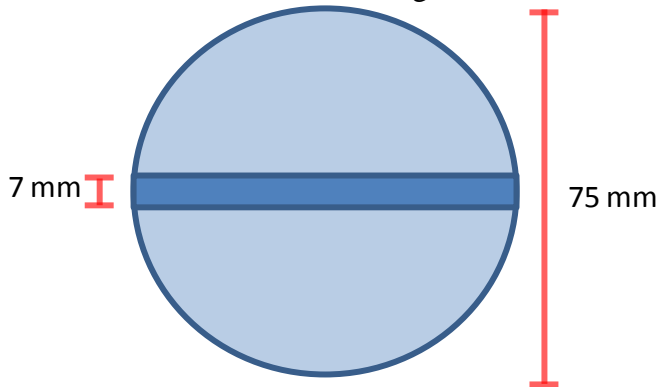
Comparing actual concentration to 100% filled:

$$\frac{1.8 \text{ } \mu\text{mol C}_{70}}{3.3 \text{ } \mu\text{mol C}_{70}} = 0.55$$

55% of the helical space is filled in the electrospun fibers with C<sub>70</sub>

Calculation of the % electrospun fibers collected in the void or aligned area

Calculation assumes the following dimensions:



Area of circle(unaligned fibers):

$$\pi(75 \text{ mm})^2 = 1.7 \times 10^4 \text{ mm}^2$$

Area of void (aligned fibers):

$$(7 \text{ mm}) \times (75 \text{ mm}) = 525 \text{ mm}^2$$

Ratio of unaligned to aligned:

$$\frac{525 \text{ mm}^2}{1.7 \times 10^4 \text{ mm}^2} = 3\% \text{ of spun fibers collected in void region}$$

Weight determination of the % electrospun fibers collected in the void or aligned area using two-plate method

$$\frac{10.5 \text{ mg aligned fiber}}{778 \text{ mg unaligned fiber} + 10.5 \text{ mg aligned fiber}} = 1.3\% \text{ spun fibers collected in void region}$$

Weight determination of the % electrospun fibers collected in the void or aligned area using multi-void comb plate

$$\frac{30.4 \text{ mg aligned fiber}}{71.6 \text{ mg unaligned fiber} + 30.4 \text{ mg aligned fiber}} = 29.8\% \text{ spun fibers collected in void region}$$



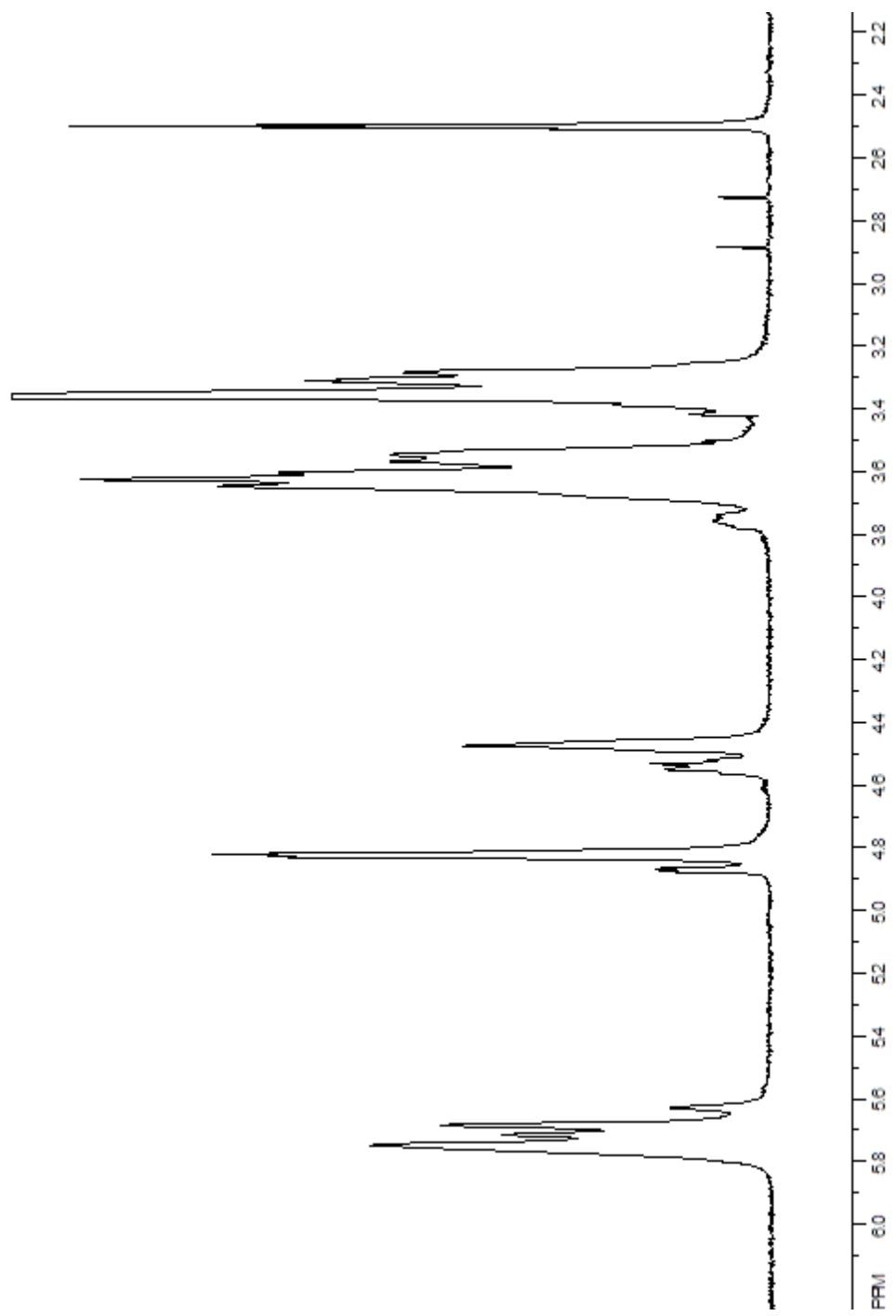


**Figure B2:** <sup>1</sup>H NMR of mono-amino-β-CD.

## APPENDIX C

### MASS SPECTRA OF CYCLODEXTRIN INTERMEDIATES

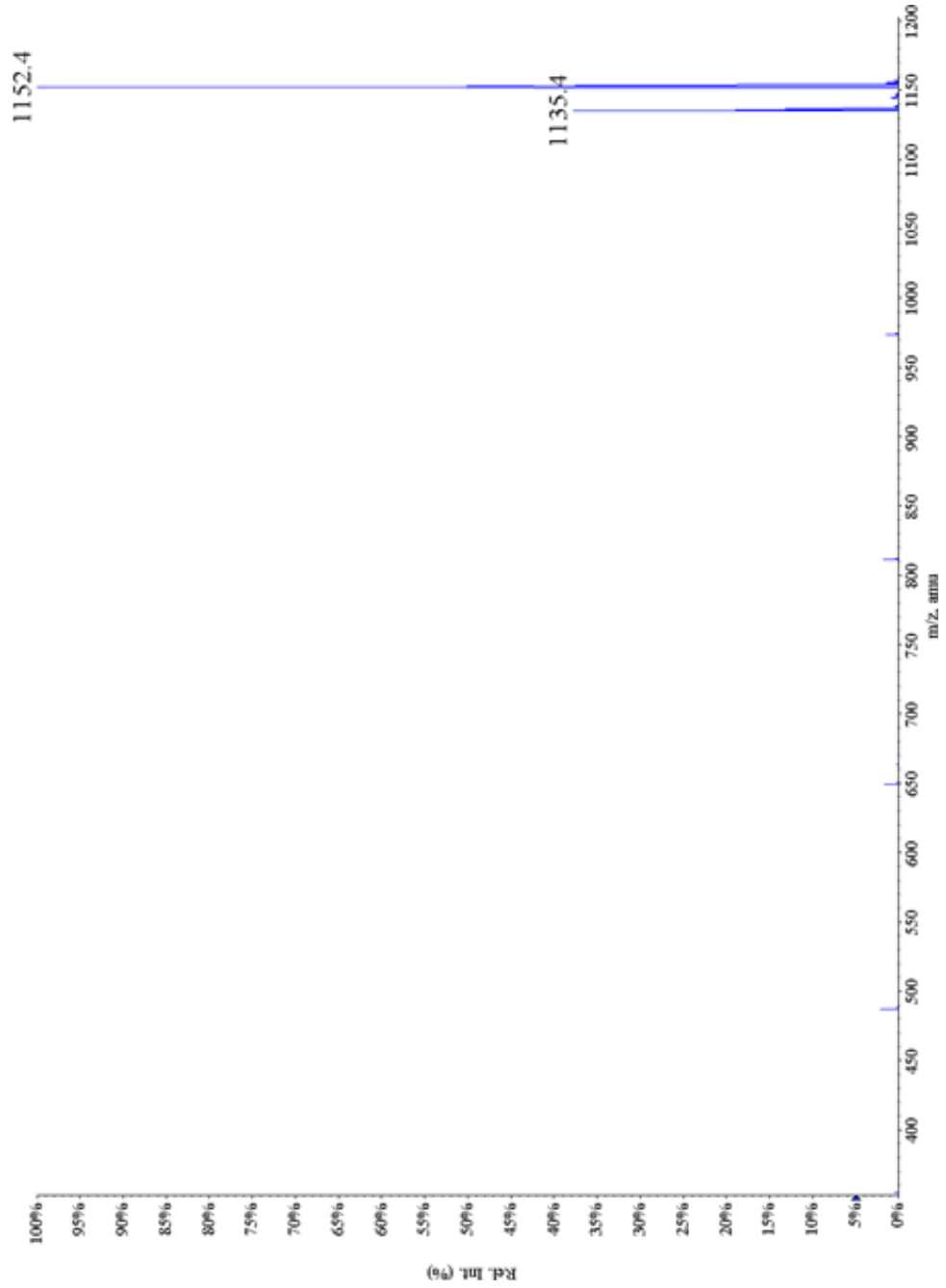


**Figure C1:** Mass spectrum of  $\beta$ -CD

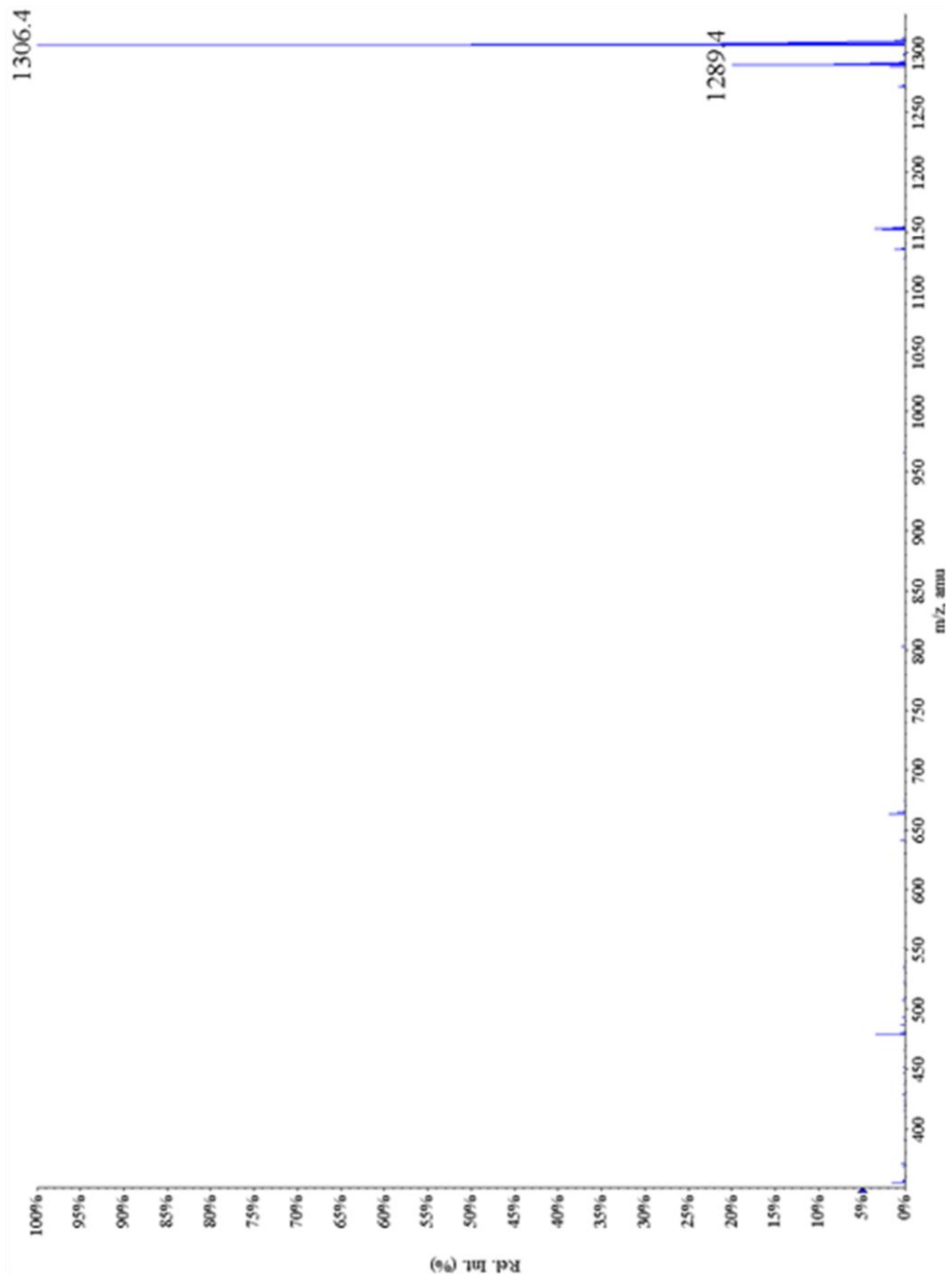


**Figure C2:** Mass spectrum of mono-tos- $\beta$ -CD.

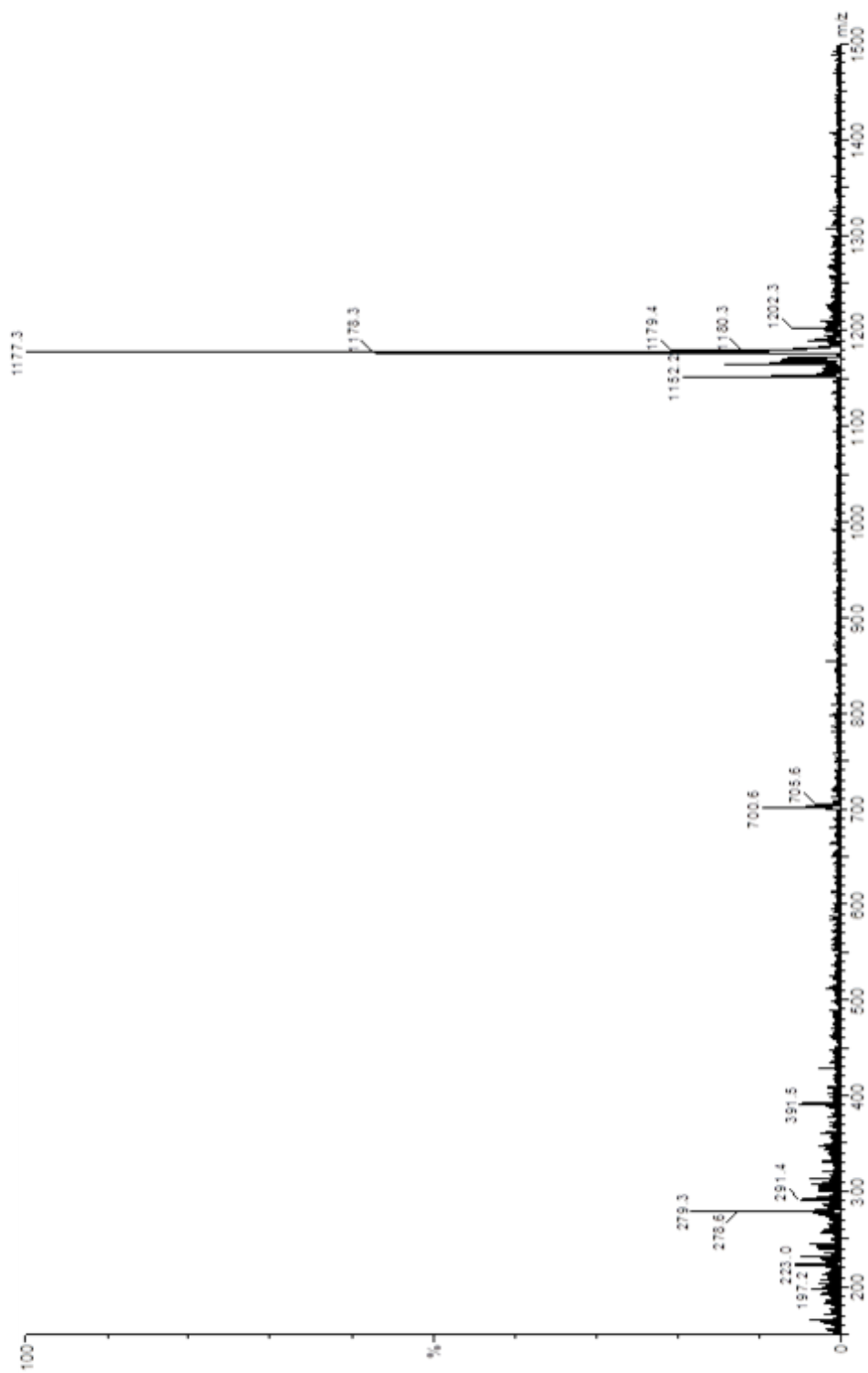


**Figure C3:** Mass Spectrum of mono-amino- $\beta$ -CD

## **APPENDIX D**

### **EXPERIMENTAL USE OF DIFFERENT GAUGE NEEDLES** **DURING ELECTROSPINNING**

In order to look at minimizing the diameter of the electrospun fibers, experiments were carried out to look at the possibility of using a smaller gauge needle. The needle used in the experiments discussed in Chapter 3 was an 18 gauge with an inner diameter of 0.838 mm. During these experiments we looked at using a 21 gauge (0.514 mm) and 23 gauge (0.337 mm) needles which have decreased inner diameters. The decreased inner diameter would decrease the initial size of the Taylor cone resulting in reduced sizes in the final fiber. However, due to the gelation behavior of the complex, the solution quickly cools and easily clogs the needle. For these experiments, 35, 52, 78, and 120 kg/mol PMMA solutions were made containing 23 – 30 wt. % polymer concentration in the [1:1:1] toluene, dichlorobenzene, and DMF solvent mixture. The solutions were then heated to 58, 75, and 115°C and tested to determine if the solutions could be drawn in and out of the needle. From these experiments it was determined that the 23 gauge needle was too small and easily clogged for the solutions. The 21 gauge needle had limited success at the lower temperatures; however, most of the solutions did not clog the needle at the elevated 115°C temperature. To use the needle during the electrospinning process a new glass heating jacket would need to be made since the length of the needles shortens as the gauge is decreased. It would be interesting to look at the effects on the alignment as the shortened needle would provide less time the polymer solution

undergoes shear stress. However, the magnitude of the shearing stress is increased due to the narrowed diameter of the needle.

**APPENDIX E**

**DILUTE SOLUTION VISCOMETRY OF**

**CYCLODEXTRIN:FULLERENE COMPLEX DURING**

**FORMATION**

The study of an equimolar solution of C<sub>60</sub> and bis-β-cyclodextrin for indication of supramolecular chain formation was analyzed by capillary dilute solution viscometry. These experiments were performed in a two solvent mixture which differs from the dilute solution viscometry measurements discussed in Chapter 4 which were only measured of solutions in DMSO. In the two solvent mixture, both molecules stay in solution since each is soluble in either DMF or toluene. Over a period of three weeks of mixing, the time for the solution to flow through the thin capillary of a viscometer was seen to supramolecular complex formation since the efflux time did not increase as much when the β-CD monomer was mixed with C<sub>60</sub>. The increase over time may suggest further lateral aggregation which is seen in other results discussed in Chapter 4.

**Table E1:** Dilute solution viscometry data from two-solvent mixture studies.

Solution	Efflux Time (sec.)	% Increase
1:1 DMF/toluene	87.0 ± 0.3	-
0.5% β-CD in DMF/toluene	89.6 ± 0.2	3.0
0.5% β-CD dimer in DMF/toluene	89.7 ± 0.1	3.1
0.5% [2:1] β-CD:C <sub>60</sub> in DMF/toluene	89.9 ± 0.3	3.3
0.5% [1:1] β-CD dimer:C <sub>60</sub> in DMF/toluene after three weeks	112.9 ± 0.5	29.7

## APPENDIX F

### CALCULATIONS OF FULLERENE STAR $R_g$ 'S

For a star:

$$\langle R_g^2 \rangle = \left[ \frac{(N/f)b^2}{f} \right] \left( 3 - \frac{2}{f} \right)$$

where N = number of monomers in arm

b = Kuhn length (for PS, b = 1.8nm)

f = number of arms (6 for this study)

repeat unit of PS: 104 g/mol

MW of C<sub>60</sub>: 720 g/mol

For the 40 kg/mol C<sub>60</sub>-PS<sub>6</sub> star:

$$\begin{aligned} \langle R_g^2 \rangle &= \left[ \frac{(378) \cdot (1.8 \text{ nm})^2}{6} \right] \left( 3 - \frac{2}{6} \right) \\ &= [(63) \cdot (.54 \text{ nm}^2)](2.667) \\ &= 90.7 \text{ nm}^2 \\ \langle R_g \rangle &= 9.5 \text{ nm} \end{aligned}$$

For the 11.5 kg/mol C<sub>60</sub>-PS<sub>6</sub> star:

$$\begin{aligned} \langle R_g^2 \rangle &= \left[ \frac{(104) \cdot (1.8 \text{ nm})^2}{6} \right] \left( 3 - \frac{2}{6} \right) \\ &= [(17.2) \cdot (.54 \text{ nm}^2)](2.667) \\ &= 24.8 \text{ nm}^2 \\ \langle R_g \rangle &= 5.0 \text{ nm} \end{aligned}$$

For the 6.1 kg/mol C<sub>60</sub>-PS<sub>6</sub> star:

$$\begin{aligned} \langle R_g^2 \rangle &= \left[ \frac{(52) \cdot (1.8 \text{ nm})^2}{6} \right] \left( 3 - \frac{2}{6} \right) \\ &= [(8.6) \cdot (.54 \text{ nm}^2)](2.667) \\ &= 12.4 \text{ nm}^2 \\ \langle R_g \rangle &= 3.5 \text{ nm} \end{aligned}$$

## APPENDIX G

### DIFFUSION NMR OF FULLERENE STARS

Diffusion is the term used to describe random, Brownian motion of a solute in solution. This motion of molecules is characterized by the coefficient of lateral diffusion,  $D$ , which is critically dependent on sample temperature, solvent viscosity, molecular shape, and molecular size. We analyzed NMR data to determine the diffusion coefficient of the fullerene stars in a deuterated chloroform solution. As seen in Figure G1, the log of the  $D$  for the PS standards and fullerene stars are plotted according to the molecules weights of the samples measured. The PS standards have a smaller molecule weight which results in a smaller  $D$  since the materials behave similarly in solution. The use of diffusion NMR allow for better size characterization in solution then the light scattering since the fullerene is known to absorb some of the laser light during the scattering experiment. An interesting trend was seen in the data that could not be explained as the results would show deviation from linear increase with molecular weight. This may result from increased aggregation in the smallest star (5.5 kg/mol) due to the decreased concentration of PS in the molecule. This fullerene star has a larger  $D$  when comparing with the PS standard of a similar MW which could be justified due to the decreased mobility of the fullerene. However further, experiments with more samples would help justify this behavior.

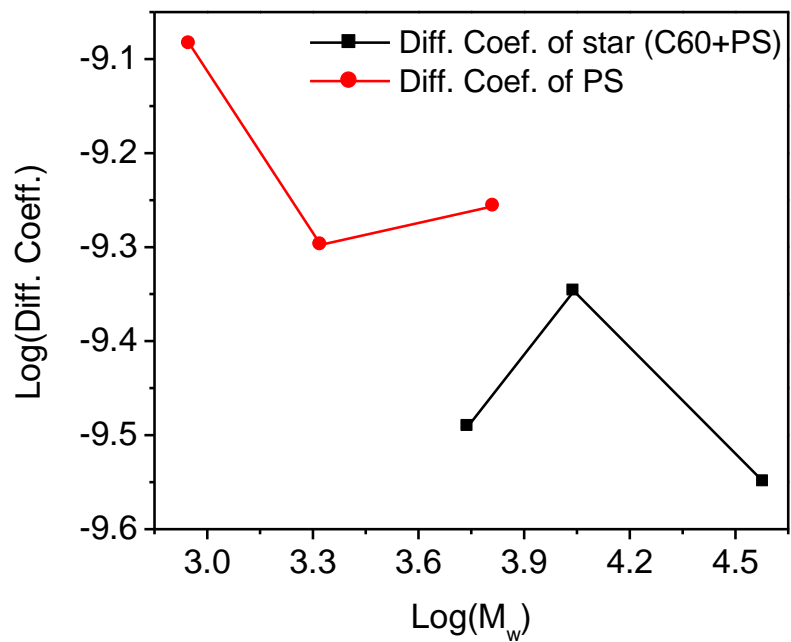


**Figure G1:** Diffusion coefficients of PS standards (●) and fullerene stars (■).

## APPENDIX H

### FURTHER LIGHT SCATTERING ANALYSIS OF FULLERENE STARS

Dynamic light scattering allowed analysis of the supramolecular structure in solution, allowing an estimate of the size and polydispersity of the complex to be made. These measurements were also performed in DMSO to limit the interaction between the CD molecules. In DLS of a dilute solution the electric field correlation function can be expressed as a product of exponential powers of cumulants,

$$g_1(q, \tau) = e^{-K_1\tau + K_2\tau^2 - K_3\tau^3 + \dots}$$

$K_1 = \langle \gamma \rangle = \langle D \rangle q^2$ , the first cumulant, defines the relaxation frequency of diffusion of the particles in terms of their average diffusion coefficient and the scattering wave vector,  $q$ . Higher-order cumulants correspond to variance (polydispersity) in second order, skewness in third, etc. For particles as polydisperse as these, the higher-order terms contribute in the form of a bias in the measured mean size. However, these effects can be avoided by using only the very short-time correlation function values to extract  $\gamma$ . By plotting the linear fit of decay rate,  $\gamma$ , to the wave vector,  $q^2$ , the mean diffusion coefficient can be calculated from the slope. From this diffusion coefficient, hydrodynamic radius (the radius of a sphere with equivalent drag) can be calculated for the structures in solution via the Stokes-Einstein equation,

$$R_h = k_B T / 6\pi\eta D$$

The scattering of the 12 kg/mol and 5.5 kg/mol did not result in reliable data being obtained. This is believed to be due to the fullerene absorbing some of the light which results lower scattering intensities thereby increasing the error associated with those measurements. In Figures H1 and H2, the data obtained from these two stars are shown. From the graphs, the decay rates show less change as the size is decreased which causes the data obtained to not be accurate for determination of the size.

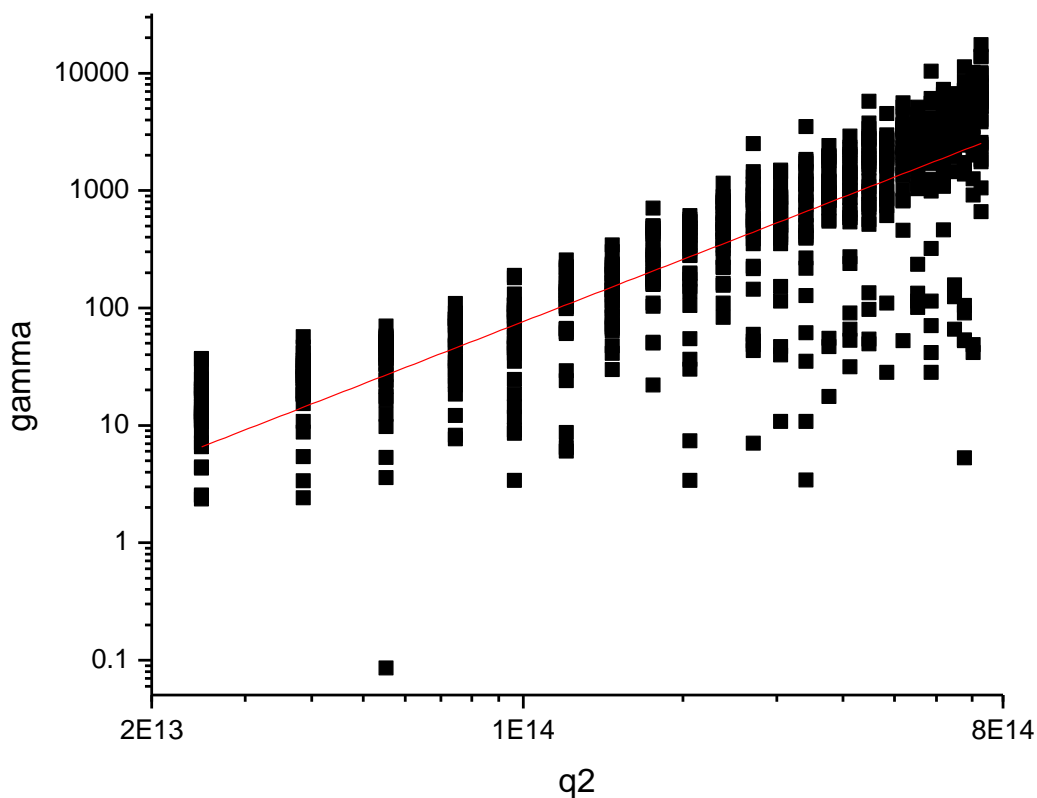


**Figure H1:** Dynamic light scattering of 12 kg/mol fullerene star in THF.

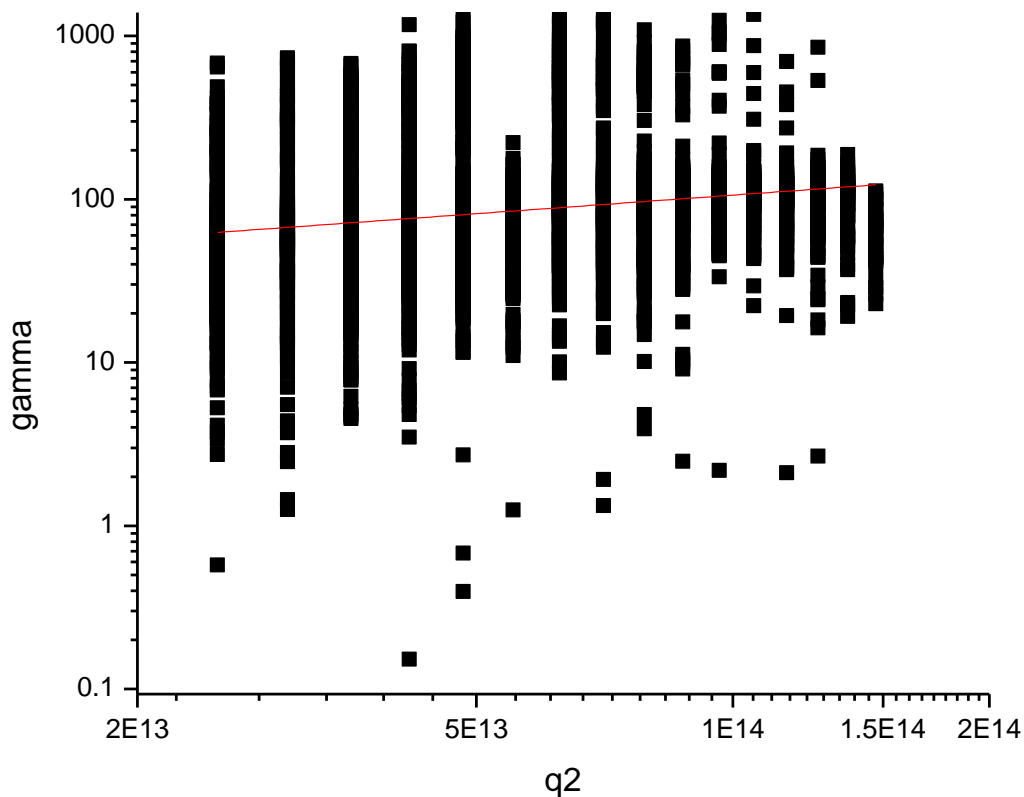


**Figure H2:** Dynamic light scattering of 5.5 kg/mol fullerene star in THF.

An alternate method to analyze the dynamics is to directly obtain the size distribution by numerical reverse Laplace transform of the correlation function. This gives a size distribution with some width about a mean radius. Measurement of the radius and width of this distribution are shown in Figures H3 and H4. The reverse Laplace transform is an ill-posed problem and requires some prior knowledge about the system parameters to guide the integration. It also shows a dependence on  $q$ . The average size from this analysis is  $200 \pm 32$  nm with a polydispersity of  $23 \pm 2\%$ .

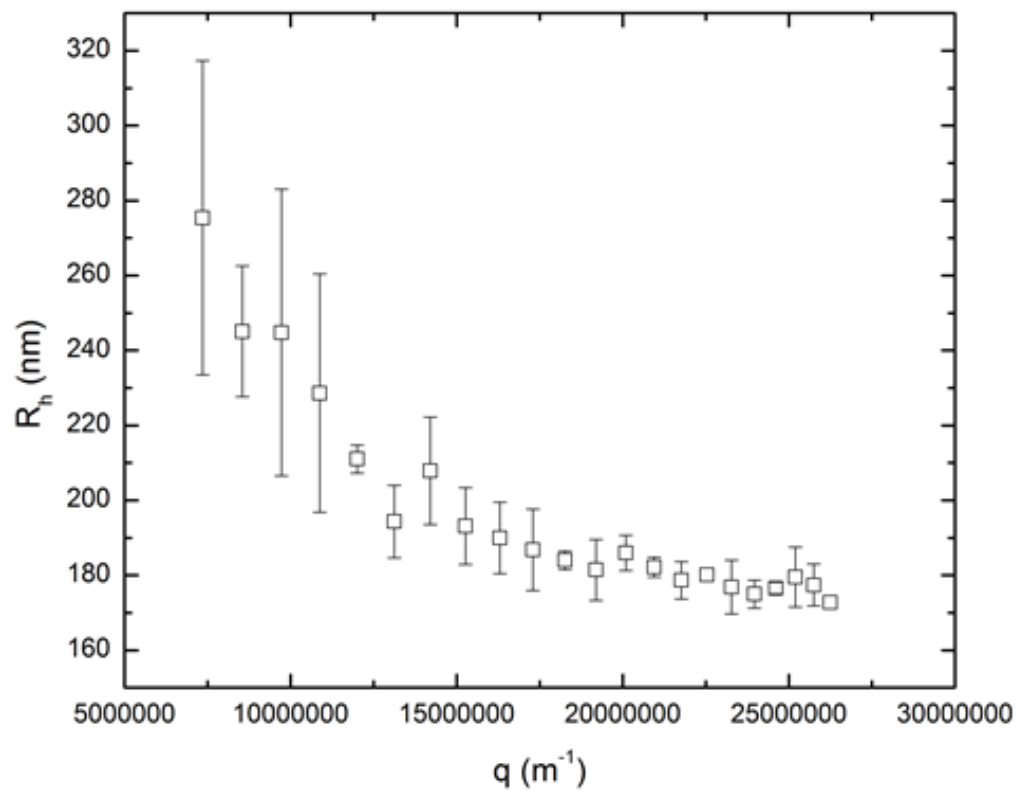


**Figure H3:** Hydrodynamic radius analysis obtained from CONTIN analysis of light scattering data.

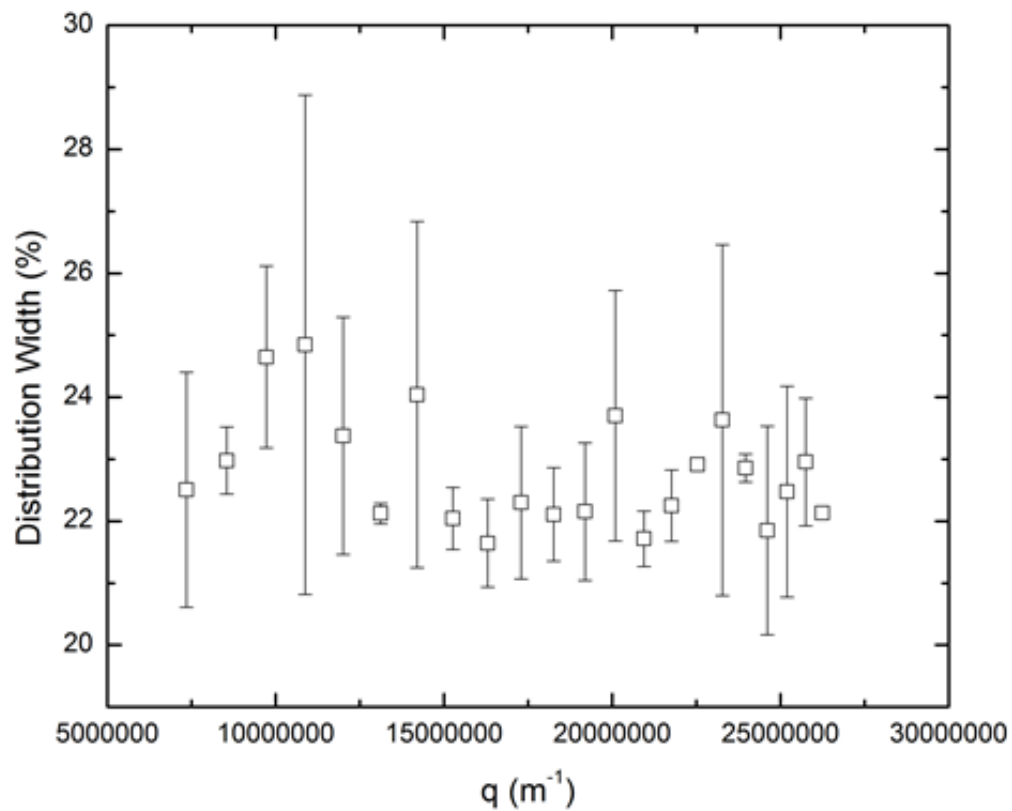


**Figure H4:** Polydispersity analysis obtained from CONTIN analysis of light scattering data.

## REFERENCES

1. Kroto, H.W., *et al.*, *C-60 - BUCKMINSTERFULLERENE*. Nature, 1985. **318**(6042): p. 162-163.
2. Kratschmer, W., *et al.*, *Solid C-60 - a New Form of Carbon*. Nature, 1990. **347**(6291): p. 354-358.
3. Chatterjee, K., *et al.*, *Fast One-Step Separation and Purification of Buckminsterfullerene, C-60, from Carbon Soot*. Journal of Organic Chemistry, 1992. **57**(11): p. 3253-3254.
4. Bezmelnitsin, V.N., *et al.*, *Isolation and characterisation of C700*. Journal of the Chemical Society-Perkin Transactions 2, 1997(4): p. 683-686.
5. Langa, F. and J.-F. Nierengarten, *Fullerenes : principles and applications*. RSC nanoscience & nanotechnology.2007, Cambridge: Royal Society of Chemistry. xii, 398 p.
6. dos Santos, L.J., *et al.*, *Fullerene C(60): Chemistry and Applications*. Quimica Nova, 2010. **33**(3): p. 680-693.
7. Nakanishi, T., S.S. Babu, and H. Mohwald, *Recent progress in morphology control of supramolecular fullerene assemblies and its applications*. Chemical Society Reviews, 2010. **39**(11): p. 4021-4035.
8. Conyers, J.L. and R. Partha, *Biomedical applications of functionalized fullerene-based nanomaterials*. International Journal of Nanomedicine, 2009. **4**: p. 261-275.
9. Darwish, A.D., *et al.*, *Improved Chromatographic-Separation of C-60 and C-70*. Journal of the Chemical Society-Chemical Communications, 1994(1): p. 15-16.
10. Hirsch, A. and M. Brettreich, *Fullerenes : chemistry and reactions*2005, Weinheim ; Great Britain: Wiley-VCH. xvii, 423 p.
11. Qiao, R., *et al.*, *Translocation of C-60 and its derivatives across a lipid bilayer*. Nano Letters, 2007. **7**(3): p. 614-619.
12. Yannoni, C.S., *et al.*, *NMR DETERMINATION OF THE BOND LENGTHS IN C60*. Journal of the American Chemical Society, 1991. **113**(8): p. 3190-3192.

13. David, W.I.F., *et al.*, *CRYSTAL-STRUCTURE AND BONDING OF ORDERED C60*. Nature, 1991. **353**(6340): p. 147-149.
14. Dresselhaus, M.S., G. Dresselhaus, and P.C. Eklund, *Science of fullerenes and carbon nanotubes* 1996, San Diego: Academic Press. xviii, 965 p.
15. Burgi, H.B., *et al.*, *The Crystal-Structure of C706(S8) at 100-K*. Helvetica Chimica Acta, 1993. **76**(5): p. 2155-2159.
16. Boo, W.O.J., *AN INTRODUCTION TO FULLERENE STRUCTURES - GEOMETRY AND SYMMETRY*. Journal of Chemical Education, 1992. **69**(8): p. 605-609.
17. Langa, F., J.-F. Nierengarten, and Royal Society of Chemistry (Great Britain), *Fullerenes : principles and applications*. RSC nanoscience & nanotechnology 2007, Cambridge: Royal Society of Chemistry. xii, 398 p.
18. Ruoff, R.S., *et al.*, *ANOMALOUS SOLUBILITY BEHAVIOR OF C60*. Nature, 1993. **362**(6416): p. 140-141.
19. Ruoff, R.S., *et al.*, *SOLUBILITY OF C-60 IN A VARIETY OF SOLVENTS*. Journal of Physical Chemistry, 1993. **97**(13): p. 3379-3383.
20. Diederich, F., *et al.*, *THE HIGHER FULLERENES - ISOLATION AND CHARACTERIZATION OF C76, C84, C90, C94, AND C700, AN OXIDE OF D5H-C70*. Science, 1991. **252**(5005): p. 548-551.
21. Ettl, R., *et al.*, *ISOLATION OF C76, A CHIRAL (D2) ALLOTROPE OF CARBON*. Nature, 1991. **353**(6340): p. 149-153.
22. Guo, T., R.E. Smalley, and G.E. Scuseria, *Abinitio Theoretical Predictions of C28, C28h4, C28f4, (Ti at C28)H4, and M at C28 (M=Mg, Al, Si, S, Ca, Sc, Ti, Ge, Zr, and Sn)*. Journal of Chemical Physics, 1993. **99**(1): p. 352-359.
23. Yamada, M., *et al.*, *Spectroscopic and theoretical study of endohedral dimetallofullerene having a Non-IPR fullerene cage: Ce-2@C-72*. Journal of Physical Chemistry A, 2008. **112**(33): p. 7627-7631.
24. Kadish, K.M. and R.S. Ruoff, *Fullerenes : chemistry, physics, and technology* 2000, New York: Wiley-Interscience. ix, 968 p.
25. Cataldo, F., *On the Solubility Parameter of C60 and Higher Fullerenes*. Fullerenes Nanotubes and Carbon Nanostructures, 2009. **17**(2): p. 79-84.

26. Ruoff, R.S., et al., *Solubility Properties of C60*. Advanced Materials '93, I - a & B, 1994. **14**(A & B): p. 1193-1196.
27. Sivaraman, N., et al., *Solubility of C-70 in Organic-Solvents*. Fullerene Science and Technology, 1994. **2**(3): p. 233-246.
28. Aihara, J., *LACK OF SUPERAROMATICITY IN CARBON NANOTUBES*. Journal of Physical Chemistry, 1994. **98**(39): p. 9773-9776.
29. Aihara, J., *IS SUPERAROMATICITY A FACT OR AN ARTIFACT - THE KEKULENE PROBLEM*. Journal of the American Chemical Society, 1992. **114**(3): p. 865-868.
30. Yakobson, B.I. and P. Avouris, *Mechanical properties of carbon nanotubes*. Carbon Nanotubes, 2001. **80**: p. 287-327.
31. Fomenko, L.S., et al., *Mechanical properties of C-60 single crystals*. Materials Science and Engineering a-Structural Materials Properties Microstructure and Processing, 2005. **400**: p. 320-324.
32. Stetzer, M.R., et al., *Thermal stability of solid C-60*. Physical Review B, 1997. **55**(1): p. 127-131.
33. Arndt, M., et al., *Wave-particle duality of C-60 molecules*. Nature, 1999. **401**(6754): p. 680-682.
34. Nairz, O., M. Arndt, and A. Zeilinger, *Quantum interference experiments with large molecules*. American Journal of Physics, 2003. **71**(4): p. 319-325.
35. Shinohara, H., *Endohedral metallofullerenes*. Reports on Progress in Physics, 2000. **63**(6): p. 843-892.
36. Bethune, D.S., et al., *ATOMS IN CARBON CAGES - THE STRUCTURE AND PROPERTIES OF ENDOHEDRAL FULLERENES*. Nature, 1993. **366**(6451): p. 123-128.
37. Saunders, M., et al., *Noble gas atoms inside fullerenes*. Science, 1996. **271**(5256): p. 1693-1697.
38. Wilson, L.J., et al., *Metallofullerene drug design*. Coordination Chemistry Reviews, 1999. **192**: p. 199-207.

39. Macfarlane, R.M., et al., *Measurement of pair interactions and 1.5  $\mu$  m emission from Er<sup>3+</sup> ions in a C-82 fullerene cage*. Physical Review Letters, 1997. **79**(7): p. 1397-1400.
40. Toth, E., et al., *Water-soluble gadofullerenes: Toward high-relaxivity, pH-responsive MRI contrast agents*. Journal of the American Chemical Society, 2005. **127**(2): p. 799-805.
41. Meyer, C., et al., *Experimental steps towards the realisation of a fullerene quantum computer*. Physica Status Solidi B-Basic Research, 2002. **233**(3): p. 462-466.
42. Ross, M.M., et al., *PRODUCTION AND CHARACTERIZATION OF METALLOFULLERENES*. Journal of Physical Chemistry, 1992. **96**(13): p. 5231-5234.
43. Weidinger, A., et al., *Atomic nitrogen in C-60 : N@C-60*. Applied Physics a-Materials Science & Processing, 1998. **66**(3): p. 287-292.
44. Harneit, W., *Fullerene-based electron-spin quantum computer*. Physical Review A, 2002. **65**(3).
45. *Endohedral Fullerenes*. 2008; Available from: [http://homepage.mac.com/jschrier/endofullerenes\\_table.html](http://homepage.mac.com/jschrier/endofullerenes_table.html).
46. Hingston, T.J., *Synthesis of Endohedral Fullerenes and Novel Fullerene Dimers, Part II Thesis*, in University of Oxford 2006.
47. Prato, M., *60 Fullerene chemistry for materials science applications*. Journal of Materials Chemistry, 1997. **7**(7): p. 1097-1109.
48. Benjamin, S.C., et al., *Towards a fullerene-based quantum computer*. Journal of Physics-Condensed Matter, 2006. **18**(21): p. S867-S883.
49. Steane, A., *Quantum computing*. Reports on Progress in Physics, 1998. **61**(2): p. 117-173.
50. Hingston, T.J., et al., *Synthesis of an asymmetric fullerene dimer via sequential cycloadditions*. Tetrahedron Letters, 2006. **47**(48): p. 8595-8597.
51. Schaller, R.R., *Moore's Law: Past, present, and future*. Ieee Spectrum, 1997. **34**(6): p. 52-&.

52. Haddon, R.C., et al., *C-60 THIN-FILM TRANSISTORS*. Applied Physics Letters, 1995. **67**(1): p. 121-123.
53. Spanggaard, H. and F.C. Krebs, *A brief history of the development of organic and polymeric photovoltaics*. Solar Energy Materials and Solar Cells, 2004. **83**(2-3): p. 125-146.
54. Wang, C.C., et al., *Polymers containing fullerene or carbon nanotube structures*. Progress in Polymer Science, 2004. **29**(11): p. 1079-1141.
55. Thompson, B.C. and J.M.J. Frechet, *Organic photovoltaics - Polymer-fullerene composite solar cells*. Angewandte Chemie-International Edition, 2008. **47**(1): p. 58-77.
56. Hoppe, H. and N.S. Sariciftci, *Organic solar cells: An overview*. Journal of Materials Research, 2004. **19**(7): p. 1924-1945.
57. Niyogi, S., et al., *Chemistry of single-walled carbon nanotubes*. Accounts of Chemical Research, 2002. **35**(12): p. 1105-1113.
58. Giacalone, F. and N. Martin, *Fullerene polymers: Synthesis and properties*. Chemical Reviews, 2006. **106**(12): p. 5136-5190.
59. Smith, B.W., M. Monthieux, and D.E. Luzzi, *Encapsulated C-60 in carbon nanotubes*. Nature, 1998. **396**(6709): p. 323-324.
60. Khlobystov, A.N., et al., *Observation of ordered phases of fullerenes in carbon nanotubes*. Physical Review Letters, 2004. **92**(24).
61. Iwasiewicz-Wabnig, A., et al., *Investigations of N@C-60 and N@C-70 stability under high pressure and high temperature conditions*. Physica Status Solidi B-Basic Solid State Physics, 2009. **246**(11-12): p. 2767-2770.
62. Waiblinger, M., et al., *Thermal stability of the endohedral fullerenes N@C-60, N@C-70, and P@C-60 (vol B 63, art. no. 045421, 2001)*. Physical Review B, 2001. **6415**(15).
63. Matsuo, Y., et al., *Stacking of molecules possessing a fullerene apex and a cup-shaped cavity connected by a silicon connection*. Journal of the American Chemical Society, 2004. **126**(2): p. 432-433.
64. Meyer, C., et al., *Alignment of the endohedral fullerenes N@C-60 and N@C-70 in a liquid-crystal matrix*. Physical Review A, 2002. **65**(6).

65. Nishimura, T., et al., *A helical array of pendant fullerenes on an optically active polyphenylacetylene*. *Angewandte Chemie-International Edition*, 2002. **41**(19): p. 3602-3604.
66. Yashima, E., et al., *Synthesis and Conformational Study of Optically-Active Poly(Phenylacetylene) Derivatives Bearing a Bulky Substituent*. *Macromolecules*, 1995. **28**(12): p. 4184-4193.
67. Yashima, E., K. Maeda, and Y. Furusho, *Single- and double-stranded helical polymers: Synthesis, structures, and functions*. *Accounts of Chemical Research*, 2008. **41**(9): p. 1166-1180.
68. Nishimura, T., et al., *Helical arrays of pendant fullerenes on optically active poly(phenylacetylene)s*. *Chemistry-a European Journal*, 2005. **11**(4): p. 1181-1190.
69. Nishimura, T., et al., *A helical array of pendant fullerenes on a helical poly(phenylacetylene) induced by non-covalent chiral interactions*. *Chemical Communications*, 2004(6): p. 646-647.
70. Cassell, A.M., W.A. Scrivens, and J.M. Tour, *Assembly of DNA/fullerene hybrid materials*. *Angewandte Chemie-International Edition*, 1998. **37**(11): p. 1528-1531.
71. Onouchi, H., et al., *Helicity induction on poly(phenylacetylene)s bearing phosphonic acid pendants with chiral amines and memory of the macromolecular helicity assisted by interaction with achiral amines in dimethyl sulfoxide*. *Macromolecules*, 2004. **37**(15): p. 5495-5503.
72. Kawauchi, T., et al., *Encapsulation of fullerenes in a helical PMMA cavity leading to a robust processable complex with a macromolecular helicity memory*. *Angewandte Chemie-International Edition*, 2008. **47**(3): p. 515-519.
73. Kusuyama, H., et al., *Structural-Change of St-Pmma on Drawing, Absorption and Desorption of Solvents*. *Polymer*, 1982. **23**(9): p. 1256-1258.
74. Kumaki, J., et al., *Supramolecular helical structure of the stereocomplex composed of complementary isotactic and syndiotactic poly(methyl methacrylate)s as revealed by atomic force microscopy*. *Angewandte Chemie-International Edition*, 2007. **46**(28): p. 5348-5351.

75. Bailey, A.G., *Electrostatic spraying of liquids*. Electronic & electrical engineering research studies 1988, Taunton, Somerset, England: Research Studies Press; John Wiley & Sons. 197 p.
76. Taylor, G., *Disintegration of Water Drops in Electric Field*. Proceedings of the Royal Society of London Series a-Mathematical and Physical Sciences, 1964. **280**(1380): p. 383.
77. Shin, Y.M., et al., *Electrospinning: A whipping fluid jet generates submicron polymer fibers*. Applied Physics Letters, 2001. **78**(8): p. 1149-1151.
78. Dzenis, Y., *Spinning continuous fibers for nanotechnology*. Science, 2004. **304**(5679): p. 1917-1919.
79. Li, D. and Y.N. Xia, *Electrospinning of nanofibers: Reinventing the wheel?* Advanced Materials, 2004. **16**(14): p. 1151-1170.
80. Zong, X.H., et al., *Electrospun fine-textured scaffolds for heart tissue constructs*. Biomaterials, 2005. **26**(26): p. 5330-5338.
81. Fenn, J.B., et al., *Electrospray Ionization for Mass-Spectrometry of Large Biomolecules*. Science, 1989. **246**(4926): p. 64-71.
82. Salata, O.V., *Tools of nanotechnology: Electrospray*. Current Nanoscience, 2005. **1**(1): p. 25-33.
83. Crne, M., J.O. Park, and M. Srinivasarao, *Electrospinning Physical Gels: The Case of Stereocomplex PMMA*. Macromolecules, 2009. **42**(13): p. 4353-4355.
84. Fox, T.G., et al., *Crystalline Polymers of Methyl Methacrylate*. Journal of the American Chemical Society, 1958. **80**(7): p. 1768-1769.
85. Kumaki, J., et al., *Molecular weight recognition in the multiple-stranded helix of a synthetic polymer without specific monomer-monomer interaction*. Journal of the American Chemical Society, 2008. **130**(20): p. 6373-6380.
86. Buchko, C.J., et al., *Processing and microstructural characterization of porous biocompatible protein polymer thin films*. Polymer, 1999. **40**(26): p. 7397-7407.
87. Shenoy, S.L., et al., *Role of chain entanglements on fiber formation during electrospinning of polymer solutions: good solvent, non-specific polymer-polymer interaction limit*. Polymer, 2005. **46**(10): p. 3372-3384.

88. Kameoka, J., et al., *A scanning tip electrospinning source for deposition of oriented nanofibres*. *Nanotechnology*, 2003. **14**(10): p. 1124-1129.
89. Jarusuwannapoom, T., et al., *Effect of solvents on electro-spinnability of polystyrene solutions and morphological appearance of resulting electrospun polystyrene fibers*. *European Polymer Journal*, 2005. **41**(3): p. 409-421.
90. Megelski, S., et al., *Micro- and nanostructured surface morphology on electrospun polymer fibers*. *Macromolecules*, 2002. **35**(22): p. 8456-8466.
91. Fong, H., I. Chun, and D.H. Reneker, *Beaded nanofibers formed during electrospinning*. *Polymer*, 1999. **40**(16): p. 4585-4592.
92. Son, W.K., et al., *The effects of solution properties and polyelectrolyte on electrospinning of ultrafine poly(ethylene oxide) fibers*. *Polymer*, 2004. **45**(9): p. 2959-2966.
93. Lee, K.H., et al., *The change of bead morphology formed on electrospun polystyrene fibers*. *Polymer*, 2003. **44**(14): p. 4029-4034.
94. Flick, E.W., *Industrial solvents handbook*. 5th ed1998, Westwood, N.J.: Noyes Data Corp. xxxi, 963 p.
95. Smallwood, I., *Handbook of organic solvent properties*1996, New York: Arnold; Halsted Press. xxi, 306 p.
96. Deitzel, J.M., et al., *The effect of processing variables on the morphology of electrospun nanofibers and textiles*. *Polymer*, 2001. **42**(1): p. 261-272.
97. Hohman, M.M., et al., *Electrospinning and electrically forced jets. I. Stability theory*. *Physics of Fluids*, 2001. **13**(8): p. 2201-2220.
98. Katta, P., et al., *Continuous electrospinning of aligned polymer nanofibers onto a wire drum collector*. *Nano Letters*, 2004. **4**(11): p. 2215-2218.
99. Boland, E.D., et al., *Tailoring tissue engineering scaffolds using electrostatic processing techniques: A study of poly(glycolic acid) electrospinning*. *Journal of Macromolecular Science-Pure and Applied Chemistry*, 2001. **38**(12): p. 1231-1243.
100. Sundaray, B., et al., *Electrospinning of continuous aligned polymer fibers*. *Applied Physics Letters*, 2004. **84**(7): p. 1222-1224.

101. Theron, S.A., E. Zussman, and A.L. Yarin, *Experimental investigation of the governing parameters in the electrospinning of polymer solutions*. *Polymer*, 2004. **45**(6): p. 2017-2030.
102. Li, D., Y.L. Wang, and Y.N. Xia, *Electrospinning nanofibers as uniaxially aligned arrays and layer-by-layer stacked films*. *Advanced Materials*, 2004. **16**(4): p. 361-366.
103. Schlenk, H. and D.M. Sand, *Association of Alpha- and Beta-Cyclodextrins with Organic Acids*. *Journal of the American Chemical Society*, 1961. **83**(10): p. 2312-&.
104. Rekharsky, M.V. and Y. Inoue, *Complexation thermodynamics of cyclodextrins*. *Chemical Reviews*, 1998. **98**(5): p. 1875-1917.
105. Wenz, G., *CYCLODEXTRINS AS BUILDING-BLOCKS FOR SUPRAMOLECULAR STRUCTURES AND FUNCTIONAL UNITS*. *Angewandte Chemie-International Edition in English*, 1994. **33**(8): p. 803-822.
106. Loftsson, T. and M.E. Brewster, *Pharmaceutical applications of cyclodextrins .I. Drug solubilization and stabilization*. *Journal of Pharmaceutical Sciences*, 1996. **85**(10): p. 1017-1025.
107. Lehn, J.M., *SUPRAMOLECULAR CHEMISTRY - SCOPE AND PERSPECTIVES MOLECULES, SUPERMOLECULES, AND MOLECULAR DEVICES*. *Angewandte Chemie-International Edition in English*, 1988. **27**(1): p. 89-112.
108. Kawase, T., et al., *Supramolecular dynamics of cyclic [6]paraphenyeneacetylene complexes with [60]- and [70]fullerene derivatives: Electronic and structural effects on complexation*. *Angewandte Chemie-International Edition*, 2004. **43**(38): p. 5060-5062.
109. Sun, D.Y., et al., *Porphyrin-fullerene host-guest chemistry*. *Journal of the American Chemical Society*, 2000. **122**(43): p. 10704-10705.
110. Diederich, F. and M. Gomez-Lopez, *Supramolecular fullerene chemistry*. *Chemical Society Reviews*, 1999. **28**(5): p. 263-277.
111. Yoshida, Z.I., et al., *Molecular Recognition of C-60 with Gamma-Cyclodextrin*. *Angewandte Chemie-International Edition in English*, 1994. **33**(15-16): p. 1597-1599.

112. Haino, T., M. Yanase, and Y. Fukazawa, *Self-inclusion properties of C-60-linked calix[5]arene*. Tetrahedron Letters, 2005. **46**(9): p. 1411-1414.
113. Hisada, K., et al., *Preparation of supramolecular assembled films of fullerene C-60 on the aqueous solution of water-soluble azocalixarene*. Composite Interfaces, 2004. **11**(4): p. 315-324.
114. Andersson, T., et al., *C-60 Embedded in Gamma-Cyclodextrin - a Water-Soluble Fullerene*. Journal of the Chemical Society-Chemical Communications, 1992(8): p. 604-606.
115. Gil-Ramirez, G., et al., *A Cyclic Porphyrin Trimer as a Receptor for Fullerenes*. Organic Letters, 2010. **12**(15): p. 3544-3547.
116. Priyadarsini, K.I., et al., *Inclusion Complex of Gamma-Cyclodextrin-C-60 - Formation, Characterization, and Photophysical Properties in Aqueous-Solutions*. Journal of Physical Chemistry, 1994. **98**(17): p. 4756-4759.
117. Murthy, C.N. and K.E. Geckeler, *Stability studies on the water-soluble beta-cyclodextrin [60]fullerene inclusion complex*. Fullerenes Nanotubes and Carbon Nanostructures, 2002. **10**(2): p. 91-98.
118. Haino, T., Y. Matsumoto, and Y. Fukazawa, *Supramolecular nano networks formed by molecular-recognition-directed self-assembly of ditopic calix[5]arene and dumbbell [60]fullerene*. Journal of the American Chemical Society, 2005. **127**(25): p. 8936-8937.
119. Kawase, T. and H. Kurata, *Ball-, bowl-, and belt-shaped conjugated systems and their complexing abilities: Exploration of the concave-convex pi-pi interaction*. Chemical Reviews, 2006. **106**(12): p. 5250-5273.
120. Campbell, K., et al., *Role of Conformation in pi-pi Interactions and Polymer/Fullerene Miscibility*. Journal of Physical Chemistry B, 2011. **115**(29): p. 8989-8995.
121. Bonini, M., et al., *Self-assembly of beta-cyclodextrin in water. Part 1: Cryo-TEM and dynamic and static light scattering*. Langmuir, 2006. **22**(4): p. 1478-1484.
122. Coleman, A.W., et al., *Aggregation of Cyclodextrins - an Explanation of the Abnormal Solubility of Beta-Cyclodextrin*. Journal of Inclusion Phenomena and Molecular Recognition in Chemistry, 1992. **13**(2): p. 139-143.

123. Polarz, S., et al., *From cyclodextrin assemblies to porous materials by silica templating*. *Angewandte Chemie-International Edition*, 2001. **40**(23): p. 4417-+.
124. Girardeau, T.E., et al., *Solid inclusion complexes of alpha-cyclodextrin and perdeuterated poly(oxyethylene)*. *Macromolecules*, 2005. **38**(6): p. 2261-2270.
125. Benesi, H.A. and J.H. Hildebrand, *A Spectrophotometric Investigation of the Interaction of Iodine with Aromatic Hydrocarbons*. *Journal of the American Chemical Society*, 1949. **71**(8): p. 2703-2707.
126. Fielding, L., *Determination of association constants (K-a) from solution NMR data*. *Tetrahedron*, 2000. **56**(34): p. 6151-6170.
127. Giacalone, F. and N. Martin, *New Concepts and Applications in the Macromolecular Chemistry of Fullerenes*. *Advanced Materials*, 2010. **22**(38): p. 4220-4248.
128. Brunsveld, L., et al., *Supramolecular polymers*. *Chemical Reviews*, 2001. **101**(12): p. 4071-4097.
129. Ciferri, A., *Supramolecular polymers*. 2nd ed2005, Boca Raton: Taylor & Francis. xiii, 761 p.
130. Easton, C.J. and S.F. Lincoln, *Modified cyclodextrins : scaffolds and templates for supramolecular chemistry*1999, River Edge, N.J.: Imperial College Press. ix, 293 p.
131. Petter, R.C., et al., *Cooperative Binding by Aggregated Mono-6-(Alkylamino)-Beta-Cyclodextrins*. *Journal of the American Chemical Society*, 1990. **112**(10): p. 3860-3868.
132. Trotta, F., et al., *Recent advances in the synthesis of cyclodextrin derivatives under microwaves and power ultrasound*. *Journal of Inclusion Phenomena and Macrocyclic Chemistry*, 2007. **57**(1-4): p. 3-7.
133. Mourer, M., et al., *Click chemistry as an efficient tool to access beta-cyclodextrin dimers*. *Tetrahedron*, 2008. **64**(30-31): p. 7159-7163.
134. Kolb, H.C., M.G. Finn, and K.B. Sharpless, *Click chemistry: Diverse chemical function from a few good reactions*. *Angewandte Chemie-International Edition*, 2001. **40**(11): p. 2004.

135. Liu, Y., et al., *Water-soluble supramolecular fullerene assembly mediated by metallobridged beta-cyclodextrins*. *Angewandte Chemie-International Edition*, 2004. **43**(20): p. 2690-2694.
136. Liu, Y., et al., *Bundle-shaped cyclodextrin-Tb nano-supramolecular assembly mediated by C-60: Intramolecular energy transfer*. *Nano Letters*, 2006. **6**(10): p. 2196-2200.
137. Arrighi, V., et al., *Characterization of a main-chain semiflexible liquid crystalline polymer: Degree of orientational order*. *Polymer*, 1996. **37**(1): p. 141-148.
138. Jeong, U.Y., et al., *Asymmetric block copolymers homopolymers: Routes to multiple length scale nanostructures*. *Advanced Materials*, 2002. **14**(4): p. 274.
139. Bates, F.S., *POLYMER-POLYMER PHASE-BEHAVIOR*. *Science*, 1991. **251**(4996): p. 898-905.
140. Thompson, R.B., et al., *Block copolymer-directed assembly of nanoparticles: Forming mesoscopically ordered hybrid materials*. *Macromolecules*, 2002. **35**(3): p. 1060-1071.
141. Schmaltz, B., M. Brinkmann, and C. Mathis, *Nanoscale organization of fullerenes by self-assembly in a diblock copolymer host matrix*. *Macromolecules*, 2004. **37**(24): p. 9056-9063.
142. Hamley, I.W., *The physics of block copolymers*. Oxford science publications 1998, Oxford ; New York: Oxford University Press. viii, 424 p.
143. Jeong, U.Y., et al., *Precise control of nanopore size in thin film using mixtures of asymmetric block copolymer and homopolymer*. *Macromolecules*, 2003. **36**(26): p. 10126-10129.
144. Hansen, C.M. and A.L. Smith, *Using Hansen solubility parameters to correlate solubility of C-60 fullerene in organic solvents and in polymers*. *Carbon*, 2004. **42**(8-9): p. 1591-1597.
145. Waller, J.H., et al., *C-60 fullerene inclusions in low-molecular-weight polystyrene-poly(dimethylsiloxane) diblock copolymers*. *Polymer*, 2009. **50**(17): p. 4199-4204.
146. Samulski, E.T., et al., *Flagellenes - Nanophase-Separated, Polymer-Substituted Fullerenes*. *Chemistry of Materials*, 1992. **4**(6): p. 1153-1157.

147. Ederle, Y. and C. Mathis, *Grafting of anionic polymers onto C-60 in polar and nonpolar solvents*. *Macromolecules*, 1997. **30**(9): p. 2546-2555.
148. Mathis, C., B. Schmaltz, and M. Brinkmann, *Controlled grafting of polymer chains onto C-60 and thermal stability of the obtained materials*. *Comptes Rendus Chimie*, 2006. **9**(7-8): p. 1075-1084.
149. Cao, T. and S.E. Webber, *Free radical copolymerization of styrene and C-60*. *Macromolecules*, 1996. **29**(11): p. 3826-3830.
150. Okamura, H., et al., *Solubility characteristics of C-60 fullerenes with two well-defined polystyrene arms in a polystyrene matrix*. *Macromolecular Rapid Communications*, 1999. **20**(2): p. 37-40.
151. Ederle, Y. and C. Mathis, *Control of the addition of various carbanions onto C-60 in polar and non polar solvents*. *Synthetic Metals*, 1997. **86**(1-3): p. 2275-2276.
152. Pham, Q.T., *Proton and carbon NMR spectra of polymers*. 5th ed2003, Chichester, West Sussex, England ; New York: Wiley. xviii, 507 p.
153. Fazeli, N., N. Mohammadi, and F.A. Taromi, *A relationship between hydrodynamic and static properties of star-shaped polymers*. *Polymer Testing*, 2004. **23**(4): p. 431-435.
154. Okumoto, M., et al., *Excluded-volume effects in star polymer solutions: Four-arm star polystyrene in cyclohexane near the Theta temperature*. *Macromolecules*, 1997. **30**(24): p. 7493-7499.
155. Shida, K., et al., *Dimensional and hydrodynamic factors for flexible star polymers in the good solvent limit*. *Macromolecules*, 1998. **31**(7): p. 2343-2348.
156. Mayes, A.M., Russell, T.P., Deline, V.R., Satija, S.K., Majkrzak, C.F., *Block Copolymer Mixtures As Revealed by Neutron Reflectivity*. *Macromolecules*, 1994. **27**: p. 7447-7453.
157. Jeong, U., Ryu, D.Y., Kho, D.H., Lee, D.H, Kim, J.K., *Phase Behavior of Mixtures of Block Copolymer and Homopolymers in Thin Films and Bulk*. *Macromolecules*, 2003. **36**: p. 3626-3634.
158. Peng, J., Gao, X., Wei, Y., Wang, H., Li, B., Han, Y., *Controlling the size of nanostructures in thin films via blending of block copolymers and homopolymers*. *J. Chem. Phys.*, 2005. **122**: p. 114706.

159. Likhtman, A.E., Semenor, A.N., *Theory of Microphase Separation in Block Copolymer/Homopolymer Mixtures*. *Macromolecules*, 1997. **30**: p. 7273-7278.
160. Holoubek, J., Baldrian, J., Lednicky, F., Malkova, S., Lal, J., *Self-assembled Structures in Blends of Block Copolymer A-block-B with Homopolymer A: SAXS and SANS Study*. *Macromol. Chem. Phys.*, 2006. **207**: p. 1834-1841.
161. Matsen, M.W., *Phase Behavior of Block Copolymer/Homopolymer Blends*. *Macromolecules*, 1995. **28**: p. 5765-5773.
162. Orso, K.A., Green, P.F., *Phase Behavior of Thin Film Blends of Block Copolymers and Homopolymers: Changes in Domain Dimensions*. *Macromolecules*, 1999. **32**: p. 1087-1092.
163. Hamley, I.W., *Ordering in thin films of block copolymers: Fundamentals to potential applications*. *Progress in Polymer Science*, 2009. **34**(11): p. 1161-1210.
164. Weng, C.-C., Wei, K.-H., *Selective Distribution of Surface-Modified TiO<sub>2</sub> Nanoparticles in PS-*b*-PMMA Diblock Copolymer*. *Chem. Mater.*, 2003. **15**: p. 2936-2941.
165. Tsutsumi, K., Funaki, Y., Hirokawa, Y., Hashimoto, T., *Selective Incorporation of Palladium Nanoparticles into Microphase-Separated Domains of Poly(2-vinylpyridine)-block-Polyisoprene*. *Langmuir*, 1999. **15**(5200-5203).
166. Lazzari, M., Lopez-Quintela, M.A., *Block Copolymer for Nanomaterial Fabrication*. *Adv. Mater.*, 2003. **15**(19): p. 1583.
167. Lauter-Pasyuk, V., Lauter, H.J., Ausserre, D., Gallot, Y., Cabuil, V., Hamdoun, B., Kornilov, E.I., *Neutron Reflectivity studies of composite nanoparticle-copolymer thin films*. *Physica B*, 1998. **248**: p. 243-245.
168. Lauter-Pasyuk, V., Lauter, H.J., Ausserre, D., Gallot, Y., Cabuil, V., Kornilov, E.I., Hamdoun, B., *Effect of nanoparticle size on the internal structure of copolymer-nanoparticles composite thin films studies by neutron reflection*. *Physica B*, 1998. **241-243**: p. 1092-1094.
169. Kim, B.J., Bang, J., Hawker, C.J., Kramer, E.J., *Effect of Areal Chain Density on the Location of Polymer-Modified Gold Nanoparticles in a Block Copolymer Template*. *Macromolecules*, 2006. **39**: p. 4108-4114

170. Hamley, I.W., *Nanotechnology with Soft Materials*. Angew. Chem. Int. Ed., 2003. **42**: p. 1652-1712.
171. Darling, S.B., *Directing the self-assembly of block copolymers*. Progress in Polymer Science, 2007. **32**: p. 1152-1204.
172. Chiu, J.J., Kim, B.J., Kramer, E.J., Pine, D.J., *Control of Nanoparticle Location in Block Copolymers*. Journal of the American Chemical Society, 2005. **127**: p. 5036-5037.
173. Buckstaller, M.R., Mickiewicz, R.A., Thomas, E.L., *Block Copolymer Nanocomposites: Perspectives for Tailored Functional Materials*. Adv. Mater., 2005. **17**: p. 1331-1349.
174. Laiho, A., Ras, R.H.A., Valkama, S., Ruokolainen, J., Sterbacka, R., Ikkala, O., *Control of Self-Assembly by Charge-Transfer Complexation between C<sub>60</sub> Fullerene and Electron Donating Units of Block Copolymers*. Macromolecules, 2006. **39**(22): p. 7648-7653.
175. Schmaltz, B., Brinkmann, M., Mathis, C., *Nanoscale Organization of Fullerenes by Self-Assembly in a Diblock Copolymer Host Matrix*. Macromolecules, 2004. **37**: p. 9056-9063.
176. Seifert, G., et al., *Electron spin resonance spectra: geometrical and electronic structure of endohedral fullerenes*. Applied Physics a-Materials Science & Processing, 1998. **66**(3): p. 265-271.
177. Atherton, N.M., *Principles of electron spin resonance*. Ellis Horwood series in physical chemistry 1993, Chichester: Ellis Horwood. 585 p.
178. Knapp, C., et al., *Fourier transform EPR study of N@C-60 in solution*. Chemical Physics Letters, 1997. **272**(5-6): p. 433-437.
179. Dietel, E., et al., *Atomic nitrogen encapsulated in fullerenes: Effects of cage variations*. Journal of the American Chemical Society, 1999. **121**(11): p. 2432-2437.
180. Ning, Y. and E.Y.X. Chen, *Metallocene-catalyzed polymerization of methacrylates to highly syndiotactic polymers at high temperatures*. Journal of the American Chemical Society, 2008. **130**(8): p. 2463-2465.

181. Kawauchi, T., M. Kawauchi, and T. Takeichi, *Facile Synthesis of Highly Syndiotactic and Isotactic Polymethacrylates via Esterification of Stereoregular Poly(methacrylic acid)s*. *Macromolecules*, 2011. **44**(4): p. 1066-1071.
182. Bianco, A., et al., *Strong orientation of polymer chains and small photochromic molecules in polyamide 6 electrospun fibers*. *Chemphyschem*, 2007. **8**(4): p. 510-514.
183. Lagerwall, J.P.F., et al., *Coaxial electrospinning of microfibrils with liquid crystal in the core*. *Chemical Communications*, 2008(42): p. 5420-5422.
184. Harada, T., et al., *Cooperative Binding and Stabilization of the Medicinal Pigment Curcumin by Diamide Linked gamma-Cyclodextrin Dimers: A Spectroscopic Characterization*. *Journal of Physical Chemistry B*, 2011. **115**(5): p. 1268-1274.